Title

Investigating the Source of Particulate Matter Toxicity: Kinetics of Reactive Oxygen Species from Biomass Burning Components in Lung Lining Fluids and Characterization of Toxic Components

Author

Gonzalez-Martinez, David Hilario

Publication Date

2019

Peer reviewed|Thesis/dissertation

UNIVERSITY OF CALIFORNIA

Los Angeles

Investigating the Source of Particulate Matter Toxicity:

Kinetics of Reactive Oxygen Species from Biomass Burning Components in Lung Lining Fluids and Characterization of Toxic Components

A dissertation submitted in partial satisfaction of the requirements for the degree Doctor of Philosophy in Atmospheric and Oceanic Sciences

by

David Hilario Gonzalez-Martinez

2019

ABSTRACT OF THE DISSERTATION

Investigating the Source of Particulate Matter Toxicity: Kinetics of Reactive Oxygen Species from Biomass Burning Components in Lung Lining Fluids and Characterization of Toxic Components

by

David Hilario Gonzalez-Martinez

Doctor of Philosophy in Atmospheric and Oceanic Sciences

University of California, Los Angeles 2019

Professor Suzanne E. Paulson, Chair

Epidemiological studies have shown that inhalation of particulate matter (PM) is associated with increased cardiovascular diseases, respiratory diseases, asthma and cancer. However, the underlying biological mechanisms and PM components responsible for adverse health outcomes are poorly understood. Induction of oxidative stress mediated by an overproduction of reactive oxygen species (ROS) is one hypothesis for PM induced health effects. The PM components responsible for ROS generation and under conditions relevant to the lung are not well known. Inhalation of PM containing of water-soluble like substances (HULIS) are thought to disrupt cellular iron homeostasis, contributing to the development of pulmonary inflammation and disease. Cigarette smoke and wood smoke contain significant amounts of HULIS, but there is scant literature characterizing HULIS in these particles. Malondialdehyde (MDA) is a toxic aldehyde traditionally measured in biological systems as a marker for oxidative stress. Interestingly, a handful of literature suggests that MDA may be present in ambient PM,

potentially adding to the toxicity of inhaled PM. However, no study has quantified MDA in ambient PM.

In this work we apply the terephthalate probe, thermodynamic modeling and chemical kinetics modeling to elucidate mechanisms of OH generation from HULIS-Fe interactions in simulated lung fluids (SLF) and human bronchoalveolar lavage fluids (BALF). We employ fluorescence and infrared spectroscopy to characterize HULIS isolated from the water-soluble fraction of cigarette smoke condensate and wood smoke particles. We apply the 2-thiobarbituric acid method on biomass burning and urban $PM_{2.5}$ to quantify ambient particle phase MDA for the first time.

We use Suwannee River Fulvic Acid (SRFA) as a surrogate for HULIS and investigate its impact on OH generation from Fe(II) in SLF and BALF. Model and experimental results are used to find best-fit rate coefficients for key reactions. In SLF, modeling results indicate SRFA strongly chelates Fe species and enhances Fe-mediated reduction of O_2 to O_2^- to 5.1 ± 1.5 M^{-1} s^{-1} and destruction of H_2O_2 to $(4.3 \pm 1.4) \times 10^3$ M^{-1} s^{-1}. In BALF, the dominant Fe binding protein is albumin but the impact of albumin-Fe complexes on ROS generation has never been defined. Using a rate limiting approximation and experiments measuring OH generation, we estimate that the rate constant for albumin-Fe mediated O_2 to O_2^- reduction is (1.8 ± 0.1) M^{-1} s^{-1}. We also estimate the rate constant for SRFA-Fe(II) mediated O_2 to O_2^- reduction to be 2.7 ± 0.3 M^{-1} s^{-1}.

Fluorescence and Fourier transform infrared (FTIR) spectroscopy is used on HULIS isolated from cigarette smoke condensate and wood smoke particles. Fluorescence spectra indicate that HULIS in both cigarette smoke condensate and wood smoke contains fluorophores that closely resemble those of SRFA. FTIR spectroscopy further indicates that isolated HULIS

contain similar organic functional groups as SRFA, but with higher aliphatic, ether, primary alcohol, organonitrogen character. Using the 2-thiobarbiutric acid assay, we estimate ambient malondialdehyde concentrations to be 40.7 ng/m^3 – 75.3 ng/m^3 in biomass burning and urban $PM_{2.5}$ extracts, making up an average of (1.37 ± 0.12) $\times 10^{-2}$ % of total $PM_{2.5}$ mass. These concentrations are comparable to previous field measurements of particle phase methylglyoxal and malonic acid, two similar atmospheric carbonyls.

The dissertation of David Hilario Gonzalez-Martinez is approved.

Jochen Peter Stutz

Tina Irene Treude

Yifang Zhu

Suzanne E. Paulson, Committee Chair

University of California, Los Angeles

2019

Table of Contents

List of Figures

List of Tables

Acknowledgements

I would like to first thank my advisor, Dr. Suzanne Paulson for her support throughout my undergraduate and graduate studies. Her guidance, immense knowledge and encouragement helped me thrive during my PhD research. Her patience during my involvement in science-policy training and diversity outreach efforts allowed me to grow as an educator, advocate and scientist. I could not have asked for a better graduate advisor. I would like to thank my committee members, Dr. Jochen Stutz, Dr. Tina Treude and Dr. Yifang Zhu for their insightful comments and encouragement. My sincere thanks to Dr. Andrew Ghio (MD) for essentially acting as a second advisor, assisting me in understanding biological concepts and for providing the lung lavage fluids that provided the foundation for chapter 4 of this work. I thank my fellow Paulson lab members Michelle Kuang, Jiaqi Shen and Angie Chen who aided in this work and who have shared with me moments of failures, doubt, surprises and successes. I would like to thank our undergraduate assistants, Keegan Cala, Qiaoyun Peng, Joshua Baumann and David Diaz for assisting in lab maintenance, experiments and data analysis throughout the years. I thank my fellow graduate students in atmospheric and oceanic sciences and the Organization for Cultural Diversity in Science (OCDS) for their personal and scientific support. To my siblings Joe, Gina and Sammy, thanks for a lifetime of mentoring, support, encouragement and tough love, it got me through graduate school. To my mother, Dolores, thank you for the unconditional love and warmth that is unmatched on this earth—you made me the man I am today.

Finally, this work is dedicated to the memory of my father, Jose Gonzalez. You always encouraged me to remember our roots, keep family close, work hard and shoot for the stars. Because of your guiding light, I pushed myself to accomplish my childhood dream of becoming a scientist. Not a day goes by where we don’t think of you.

Vita

David Hilario Gonzalez-Martinez

SUMMARY

PhD candidate interested in the interface atmospheric chemistry and human health. I currently investigate the impact of organic-iron mediated reactive oxygen species generation in simulated and human lung fluids.

EDUCATION

M.S. Atmospheric and Oceanic Sciences - University of California, Los Angeles

03/2017

B.S. Chemistry, Physical Chemistry Specialization - University of California, Los Angeles

12/2012

A.S. Chemistry, Physics & Astrophysics – Moorpark College

05/2010

SKILLS

Technical

-MS Office

Research

- Analytical techniques including, High Performance Liquid Chromatography (HPLC), Fluorescence Spectroscopy, UV-Vis Spectroscopy, FTIR Spectroscopy, Gas Chromatography, Liquid Waveguide Capillary Cell (LWCC). Aerosol Characterization and Sampling: Scanning Mobility Particle Sizer, Condensation Particle Counter, Polar Nephelometer. Modeling: Chemical Kinetics (FACSIMILE) and Thermodynamic (MINTEQ, PHREEQ).

LANGUAGE

- Fluent in English

-Conversant in Spanish

EXPERIENCE

Laboratory experience UCLA

06/2012 – Present

- Quantified reactive oxygen species (ROS) formation by ambient particulate matter extracts and particle components under atmospheric and physiologically relevant conditions.

- Developed a chemical kinetics model and experimental methods to confirm a crucial parameter for hydroxyl radical quantification (Terephthalate Probe).

- Analyzed iron speciation using Liquid Waveguide Capillary Cell with UV-Vis spectroscopy (Ferrozine Assay).

- Ran and assisted with secondary organic aerosol chamber experiments.

- Developed and performed model calculations of aqueous chemistry under atmospheric and physiological conditions using FACSIMILE.

- Coordinated with undergraduate students, graduate students, postdoctoral scholars, and visiting scholars, training them on basic and advanced conceptual information, laboratory techniques, sample analysis and data analysis.

- Managed laboratory supplies and hazardous waste management.

Field Experience

- Conducted two field campaigns, in the summer 2012 (Claremont, CA) and one in winter 2013 (Fresno, CA) each for approximately 21 days.

- Extensively participated in preparation for the field campaigns, including experiment planning, chemical reagents, laboratory supplies, and filter preparation.

Teaching Assistant, Atmospheric and Oceanic Sciences

06/2012 – Present

- Conducted discussion sections and office hours over 100 students during five separate quarters of instruction. Assisted with exam grading and maintaining student records. Instructed in courses including air and water pollution, chemical oceanography and climate change.

PUBLICATIONS

Paulson, S. E.; Gallimore, P. J.; Kuang, X. M.; Chen, J. R.; Kalberer, M.; Gonzalez, D. H., A light-driven burst of hydroxyl radicals dominates oxidation chemistry in newly activated cloud droplets. Science Advances 2019, 5, (5), eaav7689.

Gonzalez, D. H., Kuang, X. M., Scott, J. A., Rocha, G. O., & Paulson, S. E. (2018). Terephthalate Probe for Hydroxyl Radicals: Yield of 2-Hydroxyterephthalic Acid and Transition Metal Interference. Analytical Letters, 51(15), 2488-2497.

Gonzalez, D. H., Cala, C. K., Peng, Q., & Paulson, S. E. (2017). HULIS enhancement of hydroxyl radical formation from Fe (II): Kinetics of fulvic acid–Fe (II) complexes in the presence of lung antioxidants. Environmental science & technology, 51(13), 7676-7685.

1. Introduction

1.1 Background

Epidemiological studies have shown that particulate matter (PM) inhalation is associated with increased mortality, cancer, cardiovascular diseases, cardiopulmonary diseases, respiratory diseases and emergency room visits.[1-6] However, the chemical components and biological mechanisms that underlie PM induced diseases have yet to be determined.[7, 8] One hypothesis that has received much attention is the induction of oxidative stress and inflammation due to an overproduction of reactive oxygen species (ROS) from inhaled PM.[7-10] ROS are a class of highly reactive oxygen bearing species that include superoxide (O_2^-), hydrogen peroxide (H_2O_2) and the hydroxyl radical (OH).

1.2 Health Impacts of Particulate Matter and ROS

1.2.1 Health Impacts of Fine Particulate Matter

In the 1980's and 1990's, epidemiological studies determined that exposure to total suspended particles were associated with increased morbidity and mortality, suggesting a strong causal link between particle inhalation and adverse health outcomes.[11] Further studies suggested an association with fine particulate matter ($PM_{2.5}$) specifically.[11] Famously, the Harvard Six Cities Study investigated mortality risk as a function of $PM_{2.5}$ concentrations for cities with differing particle concentrations.[1] The results of the Harvard Six Cities Study, which have been confirmed by several metanalyses, revealed a decrease in life expectancy by roughly two years in the most polluted city compared to the cleanest city.[1, 2, 12] The growing amount of epidemiological evidence for $PM_{2.5}$ induced health effects ultimately led to the U.S. Environmental Protection Agency to regulate particulate matter in 1997.[11, 13] At the time, the

association of $PM_{2.5}$ exposure and health outcomes were not supported by toxicological and clinical studies. At the present time, the underlying mechanisms of particle induced diseases are still not well defined.

1.2.2 Endogenous and Exogenous ROS

Endogenous ROS primarily arises from the mitochondria during normal cellular metabolism and signaling.[14, 15] ROS can also be generated as a macrophage response to foreign bodies, initiated by O_2 reduction by NADPH.[16] These processes are crucial to maintain cellular homeostasis and viability. Exogenous ROS refers to species produced from external ROS active components entering physiological systems, such as inhaled particles. An overproduction of ROS is thought to overwhelm antioxidant defense systems, induce oxidative stress and initiate pulmonary and systemic inflammation.[7, 8] Inflammation is generally characterized by transcription factor activation,[17] cytokine/chemokine production[18] and oxidative damage to DNA, proteins, lipids[19] and cell death.[20] Inflammation is a common underlying condition in the myriad of detrimental health effects associated with $PM_{2.5}$ inhalation. Of all $PM_{2.5}$ components, soluble transition metal ions[21-27] and quinones[25, 26, 28-31] are most commonly identified as important contributors to ROS in surrogate lung fluids (SLF), broncholaveolar lavage fluids (BALF) and other aqueous solutions.[21-24] The focus of this work in on the role of Fe mediated ROS generation in SLF and BALF.

1.3 Mimicking the Lung

1.3.1 Surrogate Lung Fluids (SLF)

Inhaled $PM_{2.5}$ deposited in the alveoli first contacts the alveolar lining fluid. Thus, to investigate $PM_{2.5}$ mediated ROS chemistry relevant to the lung, a representative solution must be used. Many studies have adopted surrogate lung fluids (SLF) to mimic physiological conditions as much as possible.[32-36] The composition of SLF varies greatly among studies but several components are commonly used.[35, 36] SLF usually includes a combination of inorganic salts, antioxidants that may include ascorbate (Asc), glutathione (GSH), uric acid (UA), α-tocopherol and various organic acids. The solutions are usually buffered at pH 7.2-7.4 with an ionic strength that mimics lung lining fluid.[35, 36] Asc, GSH, UA and α-tocopherol are naturally occurring lung antioxidants and reducing agents,[37] while the organic acids mimic metal-binding proteins.[35, 36] Common organic acids used are citrate (Cit), acetate, pyruvate, lactate, glycine or L-cysteine used singly or in combination.[35] However, many studies use these organic acids at varying concentrations without rigorous justification.[24] While these organic acids are convenient, they do not represent the true metal binding proteins that impact ROS chemistry in the lung. For example, Cit has been shown to enhance ROS formation from Fe[34] whereas metal binding proteins are thought to inhibit Fe mediated ROS formation.[38, 39]

Few studies have employed SLF with phospholipids and proteins that better reflect lung lining fluid,[24, 35, 36, 40, 41] with Asc, GSH, UA, albumin and dipalmitoylphosphatidylcholine being the most common bio molecules used. Among these studies, investigators use different concentrations of antioxidants, phospholipids and proteins. This is partially due to a wide range of reported concentrations and varying methodologies for measuring antioxidants, phospholipids

and proteins in lung lining fluid.[41] Furthermore, the pH of SLF and physiological lung lining fluid has a significant impact on ROS chemistry and protein-metal binding. While most reported SLF have pH of 7.2-7.4,[35] recent *in vivo* measurements of alveolar lining fluid indicate a pH range of 6.6-6.9.[42, 43] Thus, while SLF are convenient to use, there is reason to adopt solutions more representative of human lung lining fluids to understand mechanisms and variability of ROS generation.

1.3.2 Bronchoalveolar Lavage Fluids (BALF)

Bronchoalveolar lavage fluids (BALF) are the supernatant collected from bronchoalveolar lavage procedure performed on humans and are a good representation of alveolar lining fluid.[41] BALF composition is dominated by inorganic salts, phospholipids and proteins.[35, 41] The lipid fraction is mostly phosphatidylcholine while the protein mass fraction is dominated by albumin (50%), non-metal binding proteins (43%) and transferrin (7%).[41] A limitation of BALF is that it is 50 to 200-fold diluted compared to true physiological conditions; thus, the concentration of lipids, proteins and antioxidants are significantly diminished.[41] Furthermore, the composition and pH of BALF varies among patients. Despite this, investigators have been able to correct for this dilution and estimate concentrations of alveolar lung lining fluid components.[41] Although BALF are mostly used for compositional information, some studies have used them for particle extractions to investigate ROS formation.[24]

1.4 Role of transition metals in ROS formation

Of all $PM_{2.5}$ components, soluble transition metal ions are most commonly identified as important contributors to OH formation by particles extracted in SLF, BALF and other aqueous solutions.[21-27] The redox active transitions metals Fe, Cu and Mn can form OH via similar

reactions shown in R1.1-R1.4. Under some physiological conditions, the biological reducing agent Asc reduces oxidized metal species (R1.4) and catalytically forms OH radicals:[32]

$$Fe(II) + O_2 \rightarrow O_2^- + Fe(III) \quad \text{R1.1}$$

$$Fe(II) + O_2^- + 2H^+ \rightarrow H_2O_2 + Fe(III) \quad \text{R1.2}$$

$$Fe(II) + H_2O_2 \rightarrow Fe(III) + OH^- + OH \quad \text{R1.3}$$

$$HAsc^- + Fe(III) \rightarrow HAsc^{\cdot} + Fe(II) \quad \text{R1.4}$$

Where $HAsc^-$ represents the singly protonated ascorbate molecule that is dominant in SLF and BALF. There is evidence that chelators such as Cit can complex Fe(II) and catalyze R1.1 and R1.3,[44-46] increasing its rate coefficient by almost two orders of magnitude (R1.5-R1.6) and effectively acting as a prooxidant.

$$Cit\text{-}Fe(II) + O_2 \rightarrow O_2^- + Cit\text{-}Fe(III) \quad \text{R1.5}$$

$$Cit\text{-}Fe(II) + H_2O_2 \rightarrow Cit\text{-}Fe(III) + OH^- + OH \quad \text{R1.6}$$

Conversely, Charrier et al. (2011)[32] has shown that the Cit-Cu(II) complex is less ROS active relative to Cu(II) and Asc dissolved in pH 7.4 phosphate buffer, indicating an antioxidant effect from Cit-Cu(II). Thus, the presence of organic chelating agents significantly alters transition metal mediated ROS generation.

1.5 Influence of Organic Chelators and BALF Proteins on Fe Mediated ROS Generation

1.5.1 Influence of Organic Chelating Agents on Fe mediated ROS Generation

The inorganic Fe(III)/Fe(II) couple has a relatively high reduction potential (+.770 V), and produces OH relatively slowly at physiological pH.[34, 47, 48] Organic chelating agents can alter

the reduction potential of the Fe(III)/Fe(II) and may either enhance or diminish oxidation by O_2 and H_2O_2, impacting Fe mediated ROS generation.[41, 47, 49] Fe(II) stabilizing ligands such as 1,10-phenanthroline, tend to inhibit ROS generation by increasing the Fe(III)/Fe(II) reduction potential (+1.14 V), such that Fe(II) oxidation is inhibited.[49] Many naturally occurring Fe(III) stabilizing ligands are carboxylates, which tend to lower the reduction potential of the Fe(III)/Fe(II) redox couple, making the complex thermodynamically favored to oxidation.[47] Some proteins are such strong Fe(III) stabilizing ligands that they reduce the reduction potential outside of the range accessible of biological reductants, which inhibits ROS generation by R1.1-R1.4.[41]

Electrochemical studies have revealed that Cit commonly used in SLF can significantly reduce the reduction potential of the Fe(III)/Fe(II) redox couple, making Fe(II) more susceptible to oxidation by O_2 and H_2O_2.[50, 51] In this work we investigate the kinetics of ROS generation from Cit-Fe complexes due to their presence in SLF. However, the use of Cit in SLF does not represent the role of iron binding proteins and their physiological relevance of Fe mediated ROS chemistry in lung lining fluid.

1.5.2 Influence of Fe Binding Lung Proteins on ROS Generation

In contrast to SLF, the Fe chelators in BALF are dominated by the Alb and Tf.[41] Alb and Tf are thought to exhibit antioxidant properties by chelating Fe species.[39, 52] Alb is thought to weakly and non-specifically chelate Fe(II), forming complexes that inhibit ROS generation while also scavenging ROS and sparing damage to more crucial biomolecules.[52, 53] Much of this evidence is based on non-specific ROS assays with varying protocols that fail to reveal fundamental ROS reactions or Fe speciation.[54-57] In contrast, Xu et al. (2008)[58] observed that

bovine serum albumin complexes Fe(III) and enhances Fe(II) oxidation by O_2, potentially indicating an enhancement of ROS dur to bovine serum albumin. Furthermore, there is a lack of literature on binding constants between inorganic Fe(II) and Alb. Along with the conflicting literature regarding the antioxidant nature of Alb, we could find no studies investigating ROS formation kinetics arising from the interactions of Alb and inorganic Fe(II). While Alb-Fe interactions are poorly defined, the interactions of Tf and Fe are better characterized.

Tf has two pH dependent Fe(III) binding sites located at the N-terminal and C-terminal of the protein.[59, 60] Both binding sites are considered to be independent, since Fe(III) binding on one site does not affect binding on the second site.[60] Electrochemical studies have revealed the Tf -Fe binding significantly reduces the redox potential of the Fe(III)/Fe(II) outside of the range accessible by biological reducing agents.[39, 59, 61, 62] This would inhibit the Tf-$(Fe(III))_2$ complex from being reduced by Asc or O_2^-, thereby inhibiting OH generation through R1.1-R1.4. The mobilization of Fe from Tf by external organic chelators have been associated with Fe toxicity, oxidative stress and inflammation.[63-65]

1.6 Role of Atmospheric Humic-Like Substances in ROS and Health Effects

1.6.1 Humic-Like Substances (HULIS)

Atmospheric humic-like substances (HULIS) are water soluble, polyacidic, low molecular weight compounds typically associated with biomass burning,[66-69] although secondary formation of HULIS has been reported.[70] HULIS derives its name due to its physical and chemical similarities to soil derived humic acids and fulvic acid, and often fulvic acids and humic acids are used as HULIS surrogates. In general, the humic acid fraction of soil is soluble at alkaline pH (pH ~8) whereas the fulvic acid fraction is soluble at all pH and contains lower

molecular weight, aromaticity and higher oxygenated groups than the humic acid fraction.[71] Both HULIS and humic substances contain similar organic functional groups such as quinone moieties, phenols, ketones, and carboxylates.[71, 72] However, HULIS has been shown to generally have lower molecular weight, aromaticity and weaker acid characteristics.[71, 72]

1.6.2 Isolation of HULIS

Isolation of HULIS from PM has been achieved through extraction with aqueous alkaline[73-76] and organic solvents.[77, 78] Using alkaline extraction methods allow for separation of a humic acid-like and fulvic acid-like fraction of HULIS. The most common methods for HULIS separation include individual or combinations of ion change chromatography, size exclusion chromatography, and reversed phase liquid chromatography.[71] Spectroscopic characterization has revealed that the water-soluble fraction of HULIS is most similar to fulvic acids.[71]

1.6.3. Spectroscopic Characterization of HULIS

To chemically characterize HULIS UV-Vis, fluorescence, Fourier transform infrared (FTIR) and nuclear magnetic resonance (NMR) spectroscopy have been used. Fluorescence and FTIR characterization with be discussed in detail in chapter 6. UV-Vis characterization of HULIS have shown similarities to UV-Vis spectra of humic acid and fulvic acid, characterized by high UV absorption that decreases into the visible with featureless spectra.[72] Multiple authors measure absorbance of aqueous HULIS extracts to obtain some chemical information about the sample,[75, 79-81] although this form of characterization is very limited due to featureless UV-Vis spectra of HULIS. The ratio of absorbance at 250 nm to 350 nm, known as the E_2/E_3 ratio, has been associated with HULIS molecular size and aromaticity.[78, 79, 82] Higher E_2/E_3 ratios have

been observed in summer HULIS relative to autumn HULIS collected from the same region, possibly due to combustion of lignin material in the autumn.[77]

Both ^{1}H-NMR and ^{13}C-NMR have been employed to characterize HULIS functional groups.[75-77, 83] Decesari et al. (2000)[83] used ^{1}H-NMR on aerosol extracts and fog water and determined the presence of polyphenols, alcohols, ethers, aliphatic and hydroxylated carboxylic acids. This characterization is consistent with SRFA and FTIR characterizations of HULIS isolated from atmospheric aerosols. Havers et al. (1998)[75] used ^{1}H-NMR and assigned H atoms from HULIS to polysaccharides, aliphatic and aromatic structures and noted the lower aromatic character of HULIS relative to humic acid and fulvic acid. A drawback of ^{1}H-NMR is that HULIS extractions are mixtures and thus ^{1}H signals from separate neighboring molecules interfere with resultant ^{1}H-NMR spectra.[72] ^{13}C-NMR analysis on HULIS extracts have revealed the presence of mostly aliphatic and aromatic carbon similar to HA and FA.[76] Duarte et al. (2005)[77] analyzed summer and autumn HULIS extracts that revealed saturated aliphatics, C-O bonds, C-N bonds, ethers, esters and carboxyl groups. Duarte et al. (2005)[77] also noted that autumn samples were higher in aromatic content due to contributions from biomass burning.

1.6.4 HULIS-Fe Mediated ROS Generation

Atmospheric HULIS contains quinone, carboxylic, and phenolic functional groups that are associated with ROS activity.[72, 84, 85] Redox cycling of quinone moieties by imidazole groups on HULIS have been shown to produce ROS.[85] The carboxylate and phenolic groups make HULIS a strong Fe chelator that tends to enhance Fe mediated ROS formation.[72] Little attention has been given to HULIS-Fe in a physiological context, but recent studies have shown HULIS to form ROS in physiologically relevant systems.[86-88] HULIS and HULIS-transition metal complexes

have been shown to catalyze DTT consumption at physiological pH, indicating ROS generation under physiologically relevant conditions.[86] The 2-deoxy-D-ribose (2-DR) assay has been applied on human lung tissues exposed to HULIS derived from coal and cigarette smoke.[87, 88] These studies have shown that HULIS-Fe interactions were associated with 2-DR oxidation products indicating OH generation, Fe accumulation and collagen deposition in human lung tissues. These studies suggest that HULIS-Fe plays a role in lung injury induced by cigarette smoke and coal dust exposure.

Because no standard HULIS material exists, multiple studies have used fulvic acids as a surrogate for HULIS.[71, 72] Multiple studies investigating fulvic acid have shown that it is capable of chelating Fe species and enhancing Fe mediated O_2 and H_2O_2 reduction.[89-91]

$$FA + Fe(II) \leftrightharpoons SRFA\text{-}Fe(II) \quad \text{R1.7}$$

$$FA\text{-}Fe(II) + O_2 \rightarrow SRFA\text{-}Fe(III) + O_2^- \quad \text{R1.8}$$

$$FA\text{-}Fe(II) + H_2O_2 \rightarrow SRFA\text{-}Fe(III) + OH^- + OH \quad \text{R1.9}$$

A recent study has shown that binding of Fe(II) by Suwannee River Fulvic Acid (SRFA) enhances Fe(II) mediated O_2 reduction and H_2O_2 decomposition by two to three orders of magnitude when compared to inorganic Fe.[91] In this work we use SRFA as a substitute for atmospheric HULIS and investigate its impact on Fe mediated OH generation in SLF and BALF.

1.7 ROS Measurement Methods

There exists a wide variety of acellular and cellular assays to monitor ROS formation *in vitro* and *in vivo*. For decades, the 2-thiobarbituric acid (TBA) assay to quantify

malondialdehyde (MDA) has been used in biological systems.[92-95] Under acidic and heated conditions, two TBA molecules react with MDA to form an absorbing and fluorescent TBA_2-MDA adduct. MDA is a product of lipid peroxidation and has been used as a marker for ROS and oxidative stress.[92-95] However, due to the presence of non-MDA interfering chromophores, authors often use the signal from this assay for analysis, calling these products thiobarbituric acid reactive substances (TBARS).[96, 97] Preparation of biological samples for the TBA assay introduces several problems due to precipitation of material under acidic conditions (pH ~3) and MDA binding with proteins, requiring a deproteinization step.[98, 99] The heating phase of the TBA assay can cause MDA precursors to form MDA during the assay, a behavior that can be reduced by adding a radical scavenger.[100] Such interferences on the TBA assay are improved by using HPLC fluorescence and mass spectrometry methods.[98, 99]

MDA is also a product OH induced 2-DR oxidation and thus 2-DR has been added to aqueous and biological systems as a marker of OH generation.[101, 102] However, the 2-DR assay does not reveal fundamental reactions that lead to OH generation of 2-DR degradation and is not useful for quantifying fundamental ROS. Interestingly, there is some evidence that MDA forms in the atmosphere, but it has not yet been quantified in either the gas or particle phase.[103-105] In this work we will use the TBA assay on atmospheric extracts to attempt to quantify MDA in atmospheric aerosols.

Two common assays used to investigate PM mediated ROS generation under physiological conditions are the DTT and dichlorofluorescein diacetate ($DCFH_2$-DA). In the DTT assay, particle components have been shown to catalyze the formation of disulfide bonds in the DTT molecules and thus ROS generation is correlated with DTT consumption.[106, 107] It is not

clear what ROS the DTT assay is sensitive to nor what its physiological relevance is. DTT consumption has shown correlations with redox active components in PM.[106, 108, 109] $DCFH_2$-DA forms a fluorescent product with multiple ROS including OH, H_2O_2, organic peroxides and peroxynitrates.[110] However, the non-specificity of the $DCFH_2$-DA assay limits its use in mechanistic and kinetic studies.

In order to understand fundamental ROS reactions that lead to OH generation, this work employs the terephthalate probe for OH radicals. Of all probes available for OH radicals, the terephthalate probe is the most sensitive and forms only a single ring retaining fluorescent product.[111, 112] In order to accurately quantify OH radicals using the terephthalate probe, it is crucial that an accurate percent yield be calculated. There is evidence that the percent yield of this reaction has a pH dependence.[111, 112] However, the two studies investigating the pH dependences of the terephthalate probe report yield values that differ by a factor of two. The use of the terephthalate probe will be the foundation for the bulk of this work.

In this work we have four main goals (1) To develop a method using experiments and kinetic modeling to determine the yield of the terephthalate + OH reaction. (2) Apply the terephthalate probe, kinetic and thermodynamic modeling to understand HULIS-Fe mediated OH generation in SLF and BALF. (3) Use spectroscopic methods to characterize HULIS from wood smoke and cigarette smoke condensate. (4) Apply the TBA assay to quantify MDA in atmospheric aerosols.

2. Determination 2-Hydroxy Terephthalic Acid Yield for Hydroxyl Radical Quantification

2.1 Introduction

·OH plays an important role in various atmospheric and surface water processes. Aerosol aging by ·OH can modify chemical composition[113] cloud condensation nuclei (CCN) activity[114] hygroscopic properties,[115] and optical properties of aerosols.[116] Hydroxyl radical also plays an important role in the chemistry of surface waters,[117, 118] degradation of drugs after release into the environment,[119] in oxidative stress in marine organisms,[120] and in waste water treatment.[121] Inhalation of fine particulate matter has shown correlation with adverse health impacts, including asthma, cardiovascular diseases, pulmonary inflammation, lung cancer and mortality.[122, 123] While the mechanism(s) by which ambient particles impact health is not yet completely understood, a hypothesized cause under active investigation is oxidative stress, mediated by reactive oxygen species (ROS).[124]

A direct measurement of hydroxyl radicals in aqueous solutions is difficult due to its low concentrations, short lifetime and chemical and physical similarity to the aqueous solvent. Chemical probes such as benzene,[125] nitrobenzene,[126] benzoate,[127] and terephthalate (TA)[112, 128-132] have been used to quantify OH. These methods depend on fluorescence (2-hydroxyterephthalic acid) or UV absorption (benzene derivatives) of oxidation products. Additional approaches, such as electron paramagnetic resonance, are also available.[133]

Of the hydroxyl radical probes, terephthalate has several advantages. Due to its symmetric configuration, the ·OH reaction with terephthalate results in only one ring- preserving product, 2-hydroxyterephthalic acid (hTA, Fig. 2.1). Furthermore, 2-hydroxyterephthalic acid is strongly fluorescent [134] facilitating detection limits as low as ~2 nM (Tab. 2.1), compared to 30

nM for benzoate.[135] Further, TA is more soluble, has a more stable fluorescent product and is less susceptible to pH changes compared to several other ·OH probes.[136]

Table 2.1. Excitation/emission wavelengths and detection limits for OH detection using terephthalic acid.

Excitation (nm)	Emission (nm)	hTA Detection Limit	OH generation System	Ref.
320	420	1.4 nM	Fenton Reaction	This
315	435	$5x10^{-7}$ M	Microdialysis	137
309	412	5nM	Fenton reaction	138
320	420	*	Photolysis of Nitrate/H_2O_2	139
323	435	50nM	Radiolysis	140
240/310	435	‡	Photolysis of Nitrate	141

‡Detection limit of formation of hTA. These authors state hTA can be detected at "sub-nM levels, but do not provide a number or limit of detection determination methodology.

*****These authors reported detection limits as rates ($5x10^{-12}$ M/s) but did not report the integration times, so detection limits in absolute terms are not known.

Accurate quantification of ·OH with the terephthalate probe requires knowledge of the yield of the fluorescent product, hTA, per molecule of ·OH reacted. A handful of prior studies have quantified the ·OH formation yield, each with a different source of hydroxyl radicals: Matthews (1980)[111] used radiolysis; Charbouillot et al. (2011)[112] used photolysis of nitrate and H_2O_2 (Fig. 2.2), Page et al. (2010)[141] used photolysis of nitrite and Mark et al. (1998)[142] used sonication of water but did not show data or indicate a pH for their measurements. The Matthews (1980)[111] (30.5 – 35% increasing as pH increased from 2 - 9), Mark et al. (1998)[142] and Page et al. (2010)[141] (both 35% at unspecified pH) measurements are nearly double those of Charbouillot et al. (2011)[112] (14 – 23% increasing as pH increased from 4 – 7.5). As both the high[27, 136, 143, 144] and low[145-148] values have been taken up in the literature we attempt to address the discrepancy.

The hTA yield has also been found to depend on the O_2 concentration in the sample;[111, 140] all yields discussed here are for aqueous solutions in equilibrium with air at one atmosphere. Charbouillot et al. (2011)[112] found that the hTA yield is not influenced by ionic strength, ammonium or sulfate ions within the 0.25 – 2 mM range studied, but that the yield has a fairly strong temperature dependence; the yield increases by about a factor of 2 between 278 and 303 K at pH 5.4.

The discrepancy between the measurements of Matthews (1980),[111] Page et al. (2010),[141] and Charbouillot et al. (2011)[112] were suggested by Page et al. (2012)[149] to be due to the photolysis light source used by Charbouillot et al. (2011)[112] also photolyzing hTA, reducing its apparent yield.

Here, we report a new measurement of the hTA yield, using a different source of OH. Because of the substantial discrepancy between the published datasets, and because there is little data available for the yield of hTA under acidic conditions relevant to water in the atmosphere, such as cloud, fog and rain water[150] we measure Y_{hTA} at pH 3.5 using a dark ferrous Fenton system to generate OH.

2.2 Materials and Methods

2.2.1 Materials

Disodium terephthalate (TA) was purchased from TCI America. 2-hydroxy terephthalic acid (hTA) was purchased from Apollo Sci. Methanol (HPLC grade) and sulfuric acid (reagent grade), Chelex® 100 sodium form (50-100 dry mesh), uric acid (>99%), sodium Citrate tribasic dihydrate (>99%), L-ascorbic acid (BioXtra, >99%), L-glutathione reduced (>98%), ethylenediaminetetraacetic acid (EDTA), horseradish peroxidase type II, para-hydroxyphenyl

acetic acid, potassium hydrogen phthalate, H_2O_2 (30%) and $FeSO_4$ (>98%) were purchased from Sigma-Aldrich. Sodium phosphate dibasic and potassium phosphate monobasic were purchased from Acros Organics. Ferrozine (4,4'-[3-(2-pyridinyl)-1,2,4-triazine-5,6-diyl] dibenzenesulfonate) was purchased from Fluka Analytic. Hydrophilic Lipophilic Balance cartridges were purchased from Waters (Oasis, 10mg). All materials were used as received.

A rigorous cleaning process was followed for all glass and Teflon containers. After each use, the glass/plastic ware was washed with warm water and soap, then rinsed in deionized (18 MΩ DI) water (3×), ethanol (3×), and finally DI water (3×). The vessels were then soaked in a 1 M nitric acid bath overnight, rinsed with DI water (3×) and air dried. Nitric acid baths were replaced after being used twice.

Stock solutions were prepared with 18 MΩ DI water after further purification by passing through a Chelex column to remove trace metals. pH was measured with a bench top pH meter (HANNA instruments, HI 3220), calibrated daily. Stock solutions of hTA (10^{-3} M) and Fe(II) (5.1 mM) were wrapped in foil; hTA was kept refrigerated for a few months and Fe(II) was prepared daily and refrigerated. Dissolved oxygen was present in all solutions as solutions were in contact with air and were not degassed.

2.2.2 Fluorescence Spectroscopy and Quantification of hTA

hTA fluorescence intensity was measured in single wavelength mode at excitation/emission wavelengths of 320/420 nm with a Lumina Fluorescence Spectrometer (Thermo Scientific). For the purposes of the measurements carried out here, hTA calibration curves were prepared in pH 3.5 solutions at hTA concentrations of 50, 100, 500 and 800 nM. An A 10^{-3} M Stock solution of hTA in milli-Q water (18 MΩ) was prepared using an acid cleaned

Teflon bottle which was wrapped in aluminum and stored in the refrigerator. A 5-point calibration was performed prior to each experiment.

2.2.3 Quantification of Fe(II)

Fe(II) was quantified with the ferrozine method[151] using a liquid waveguide capillary cell (LWCC-3100, World Precision Instruments Inc.), a UV-Vis light source (AvaLight-DHS, Avantes) and UV-Vis spectrometer (AvaSpec 2048L, Avantes). The Fe(II)-ferrozine complex has a maximum absorbance at 562 nm (A_{562}). To account for instrument drift and solution turbidity, the absorbance at 700 nm (A_{700}) was subtracted from A_{562}. Aliquots were analyzed by adding 10 µL of 5.1 mM ferrozine to 2.0 mL aliquots. Fe(II) calibration curves are made by preparing a stock solution of 2 mM Iron Sulfate (Sigma-Aldrich) at pH 3.5 and diluting to between 0.012 and 0.75 µM Fe(II).

2.2.4 Quantification of H_2O_2

Quantification of aqueous H_2O_2 was performed using a High Performance Liquid Chromatograph equipped with a fluorescence detector (Shimadzu RF-10AXL detector).[152] The eluent, water with 0.1 mM EDTA adjusted to pH 3.5 with 0.1 N sulfuric acid, was delivered at 0.6 mL/min to a C18 guard column. H_2O_2 elutes at 0.5 min, after which it is mixed with a fluorescent reagent containing horseradish peroxidase and para-hydroxyphenyl acetic acid (POHPAA). The peroxidase enzyme catalyzes a reaction between H_2O_2 and POHPAA to form a fluorescent dimer, which is detected at the $\lambda_{ex}/\lambda_{em}$ 320/400 nm. The solution is mixed with ammonium hydroxide (30%) to increase its fluorescence intensity prior to detection. The HPLC was calibrated at least weekly with 10^{-8} to 10^{-6} M standards prepared from a 0.3% stock solution, titrated with sodium thiosulfate to determine the concentration.

2.2.5 Oxidation of TA via a Ferrous Fenton System

Experiments to derive hTA yields were carried out as follows. Triplicate samples of 4.44-4.77 µM $FeSO_4$ and 5.38-6.00 µM H_2O_2 (Tab. 2.2) were mixed with excess terephthalate (~500 µM, 100-fold excess) in 60 mL Teflon bottles and allowed to react in the dark with gentle shaking (25 rpm, Heidolph Rotamax) at 20°C. $FeSO_4$ was added last as to initiate the Fenton reaction. The resulting solution was monitored in triplicate for H_2O_2, Fe(II) and hTA every 20 minutes for 2 h. Initial concentrations of H_2O_2 and Fe(II) are shown in Table 2.2. Blanks consisted of TA in pH 3.5. Aliquots were diluted by 5 - 10× to fall within the ranges of detection for Fe(II) and H_2O_2. At µM concentrations, the system is sensitive to trace contaminants, including metals and organics, which can change ·OH formation chemistry and/or the ability of terephthalate to scavenge all available OH, thus rigorous cleaning, dust exclusion and high purity reagents were critical for these experiments.

Table 2.2. Initial conditions for hydroxy terephthalic acid (hTA) yield experiments.

Trial	**$[Fe(II)]_o$ µM**	**$[H_2O_2]_o$ µM**
1	4.44 ± 0.16	6.00 ± 0.34
2	4.55 ± 0.22	5.38 ± 0.06
3	4.77 ± 0.06	5.48 ± 0.25

A 54-reaction chemical kinetics model (Tab. 2.3) including reactions describing Fenton chemistry, acid-base equilibria, iron sulfate chemistry and odd oxygen free radical chemistry was

developed to derive hTA yields. Concentrations as a function of time were calculated from initial concentrations using FACSIMILIE (MCPA Software, UK).

Table 2.3. Kinetic Model used to fit to experimental data.

#	Reaction	k_f	k_r	K_{eq}	Ref
	*General Equilibria**				
1	$H_2O \rightleftharpoons H^+ + OH^-$	1.3×10^{-3}	1.3×10^{11}	10^{-14}	[2]
2	$Fe^{3+} + H_2O \rightleftharpoons FeOH^{2+} + H^+$	6.46×10^{7}	10^{10}	6.46×10^{-3}	[3]
3	$Fe^{3+} + 2\ H_2O \rightleftharpoons Fe(OH)_2^{+} + 2H^+$	2.14×10^{3}	10^{10}	2.14×10^{-6}	[3]
4	$2\ Fe^{3+} + 2\ H_2O \rightleftharpoons Fe_2(OH)_2^{4+} + 2H^+$	1.12×10^{7}	10^{10}	1.12×10^{-3}	[3]
5	$Fe^{2+} + H_2O \rightleftharpoons FeOH^{+} + H^+$	3.16	10^{10}	3.16×10^{-10}	[3]
6	$H_2O_2 \rightleftharpoons HO_2^- + H^+$	1.26×10^{-2}	10^{10}	1.26×10^{-12}	[3]
7	$HO_2 \rightleftharpoons O_2^- + H^+$	1.58×10^{5}	10^{10}	1.58×10^{-5}	[3]
8	$Fe^{3+} + H_2O_2 \rightleftharpoons FeHO_2^{2+} + H^+$	5×10^{-3}	1.36	3.65×10^{-3}	[4]
9	$FeOH^{2+} + H_2O_2 \rightleftharpoons Fe(OH)(HO_2)^{+} + H^+$	2×10^{6}	10^{10}	2×10^{-4}	[3]
	Terephthalate Probe				
10	$TA + OH \rightarrow (Y)\ hTA + (1\text{-}Y)\ X$	4.4×10^{9}			[1]

11	$X + OH \rightarrow Z$	10^9	[5]
12	$hTA + OH \rightarrow hTA_{ox}$	6.3×10^9	[1]
	Fe(II)/Fe(III) Reactions		
13	$Fe^{2+} + O_2 \rightarrow Fe^{3+} + O_2^-$	0.111 ± 0.007	[6]
14	$Fe^{2+} + O_2^- + 2H^+ \rightarrow Fe^{3+} + H_2O_2$	10^7	[6]
15	$Fe^{2+} + H_2O_2 \rightarrow Fe^{3+} + OH + OH^-$	76	[3]
16	$FeOH^+ + H_2O_2 \rightarrow Fe^{3+} + OH + 2\ OH^-$	5.9×10^6	[3]
17	$FeHO_2^{2+} \rightarrow HO_2 + Fe^{2+}$	2.3×10^{-3}	[4]
18	$Fe(OH)(HO_2)^+ \rightarrow Fe^{2+} + HO_2 + OH^-$	2.3×10^{-3}	[3]
19	$Fe^{2+} + OH \rightarrow Fe^{3+} + OH^-$	2.7×10^8	[3]
20	$FeOH^+ + OH \rightarrow Fe^{3+} + 2\ OH^-$	2.7×10^8	[7]
21	$Fe^{2+} + HO_2 \rightarrow Fe^{3+} + HO_2^-$	1.2×10^6	[3]
22	$FeOH^+ + HO_2 \rightarrow FeOH^{2+} + HO_2^-$	1.2×10^6	[3]
23	$Fe^{2+} + O_2^- \rightarrow Fe^{3+} + O_2^{2-}$	10^7	[3]
24	$FeOH^+ + O_2^- \rightarrow FeOH^{2+} + O_2^-$	10^7	[3]
25	$Fe^{3+} + HO_2 \rightarrow Fe^{2+} + O_2 + H^+$	3.1×10^3	[7]
26	$FeOH^{2+} + HO_2 \rightarrow FeOH^+ + O_2 + H^+$	2×10^4	[3]

27	$Fe(OH)_2^+ + HO_2 \rightarrow Fe(OH)_2 + O_2 + H^+$	2×10^4			[3]
28	$Fe^{3+} + O_2^- \rightarrow Fe^{2+} + O_2$	5×10^7			[3]
29	$FeOH^{2+} + O_2^- \rightarrow FeOH^+ + O_2$	5×10^7			[3]
30	$Fe(OH)_2^+ + O_2^- \rightarrow Fe(OH)_2 + O_2$	5×10^7			[3]
	ROS Reactions				
31	$H_2O_2 + OH \rightarrow HO_2 + H_2O$	3.3×10^7			[3]
32	$HO_2 + OH \rightarrow O_2 + H_2O$	7.1×10^9			[7]
33	$O_2^- + OH \rightarrow O_2 + OH^-$	10^{10}			[7]
34	$OH + OH \rightarrow H_2O_2$	5.2×10^9			[3]
35	$H_2O_2 + HO_2 \rightarrow OH + O_2 + H_2O$	0.5			[7]
36	$HO_2 + HO_2 \rightarrow H_2O_2 + O_2$	8.3×10^5			[3]
37	$HO_2 + O_2^- \rightarrow HO_2^- + O_2$	9.7×10^7			[3]
38	$O_2^{2-} + H^+ \rightarrow HO_2^-$	10^{10}			[3]
39	$O_2^- + H_2O_2 \rightarrow OH^- + OH + O_2$	10^{-4}			[7]
	Sulfate Equilibria				
40	$H^+ + SO_4^{2-} \rightleftharpoons HSO_4^-$	9.77×10^{11}	10^{10}	97.7	[3]
41	$Fe^{2+} + SO_4^{2-} \rightleftharpoons FeSO_4$	1.78×10^{12}	10^{10}	178	[3]

42	$Fe^{3+} + SO_4^{2-} \rightleftharpoons FeSO_4^+$	8.31×10^{13}	10^{10}	8.31×10^{3}	[3]
43	$Fe^{3+} + 2\ SO_4^{2-} \rightleftharpoons Fe(SO_4)_2^-$	2.63×10^{15}	10^{10}	2.63×10^{5}	[3]
	Sulfate Reactions				
44	$FeSO_4 + H_2O_2 \rightarrow Fe^{3+} + SO_4^{2-} + OH + OH^-$	78			[3]
45	$FeSO_4 + OH \rightarrow Fe^{3+} + SO_4^{2-} + OH^-$	2.7×10^{8}			[3]
46	$FeSO_4 + HO_2 \rightarrow Fe^{3+} + SO_4^{2-} + HO_2^-$	1.2×10^{6}			[3]
47	$FeSO_4 + O_2^- \rightarrow Fe^{3+}\ SO_4^{2-} + O_2^{2-}$	5×10^{8}			[3]
48	$Fe^{2+} + SO_4^- \rightarrow Fe^{3+} + SO_4^{2-}$	3×10^{8}			[3]
49	$FeOH^+ + SO_4^- \rightarrow Fe^{3+} + SO_4^{2-}$	3×10^{8}			[3]
50	$FeSO_4 + SO_4^- \rightarrow Fe^{3+} + 2\ SO_4^{2-}$	3×10^{8}			[3]
51	$FeSO_4^+ + O_2^- \rightarrow Fe^{2+} + SO_4^{2-} + O_2$	10^{3}			[3]
52	$FeSO_4^+ + HO_2 \rightarrow Fe^{2+} + SO_4^{2-} + O_2 + H^+$	10^{3}			[3]
53	$Fe(SO_4)_2^- + HO_2 \rightarrow Fe^{2+} + 2\ SO_4^{2-} + O_2 + H^+$	10^{3}			[3]
54	$Fe(SO_4)_2^- + O_2^- \rightarrow Fe^{2+} + SO_4^{2-} + O_2$	10^{3}			[3]

*Rate constants include the concentration of water [55 M]; model uses a concentration of 1 M for water. [1] Page et al. (2010)[141]; [2] Miller et al. (2012) [89]; [3] De Laat et al. (2005)[153]; values for I ~0; [4] Walling et al. (1973)[154]; [5] Klopffer et al. (1991) [155]: the rate constants of between OH and most organics in aqueous solution are on the order of $10^9\ M^{-1}S^{-1}$, the rate constant of products from the OH reaction with TA other than hTA was estimated based on this. [6] Pham et al. (2008) [156]; [7] Bielski et al. (1985)[157]

2.3 Results

2.3.1 2-Hydroxyterephthalate Yield

Fig. 2.1 shows experimental data (symbols) and model best fit (lines) for the average of three experiments; error bars show the standard deviation of nine measurements at each time point (three replicates from each of three experiments). The model is most sensitive to the rate constant for Fe(II) reacting with H_2O_2 to make $^{\cdot}OH$ and co-products (the Fenton reaction, k_{15} in Tab. 2.3). Most published rates for this reaction fall within the range 55 -76 $M^{-1}s^{-1}$.[158, 159] The best fit between the model and the measured H_2O_2 and Fe(II) was obtained using 76 $M^{-1}s^{-1}$ for the Fenton reaction. This results in mean square errors (MSEs) of 4.3 and 3.1 % for Fe(II) and H_2O_2, respectively (Fig. 2.1). We then adjusted the yield of hTA (Y_{hTA}) to minimize the MSE between the model and the average concentration of hTA and found a best-fit Y_{hTA} = 31.5 ± 7%, with and MSE of 0.24%. Altering Y_{hTA} does not affect the modeled Fe(II) and H_2O_2 concentrations. The error bars for the yield were derived by finding the best fit Y_{hTA} for ± 1 σ of the measured hTA concentrations (Fig. 2.1). At pHs above 4, formation of iron hydroxide and iron sulfate precipitates increase,[158] compromising the utility of the Fe(II)/H_2O_2 system as an $^{\cdot}OH$ source, so we were not able to measure Y_{hTA} at higher pHs.

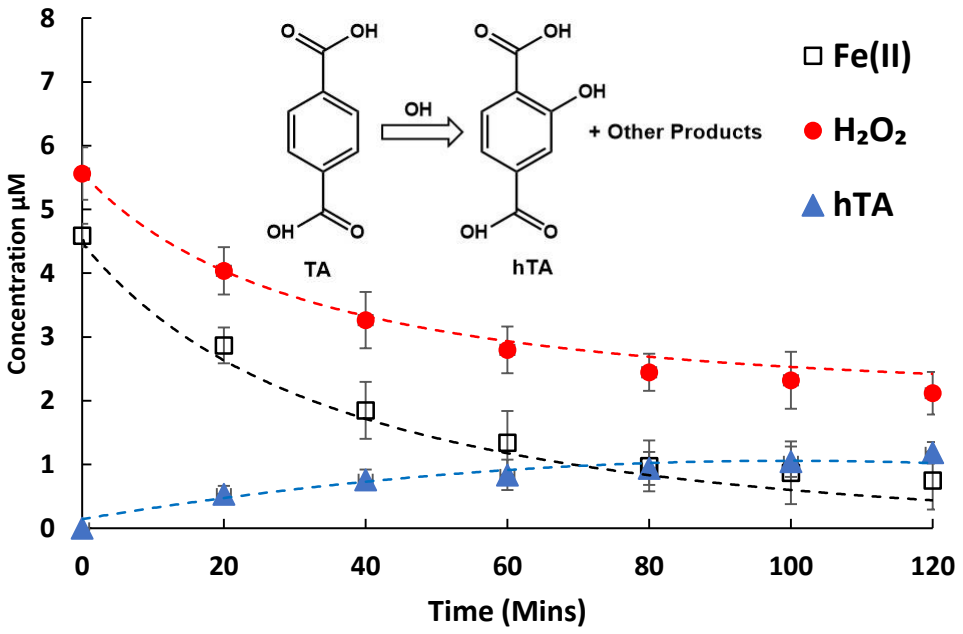

Figure 2.1. Concentration profiles of Fe(II), H_2O_2 and hTA averaged from triplicate measurements of three experimental trials. Error bars represent ± one standard deviation of 9 samples. Dashed lines indicate model fit to experimental data. Average initial concentrations of Fe(II) and H_2O_2 were 4.59 and 5.56 µM, respectively. The yield of hTA is estimated to be 31.5 ±7%.

Fig. 2.2 summarizes reported measurements of hTA yields as a function of pH. Our results are in excellent agreement with the results of Matthews (1980)[111] and about double those of Charbouillot et al. (2011).[112] Some of the difference is explained by the temperature dependence reported by Charbouillot et al. (2011)[112] (above). Differences in the temperature of this work (293 K) and Charbouillot et al. (2011)[112] (288 K) would suggest a difference of about 20% (Matthews et al. (1980)[111] did not report a temperature). To generate ·OH radicals, Matthews (1980)[111] used radiolysis, while Charbouillot et al. (2011)[112] photolyzed either nitrate or H_2O_2 using a 1000 W xenon lamp ($\lambda > 300$ nm). In a separate study, Page et al. (2010)[141] reported that the UV absorption spectrum for hTA contains a weak absorption between 275 - 365 nm, with a slight pH dependence. Wavelengths below 365 nm were observed to cause some

decomposition of hTA, leading the researchers to conclude that nitrate photolysis could not be used to probe hTA formation.[149] Charbouillot et al. (2011)[112] had good agreement between their results using nitrate or H_2O_2 as the ·OH source, but since they used the same lamp, similar degradation of hTA likely occurred. We conclude that the Matthews (1980)[111] yields, together with this work and Page et al. (2010)[141] are correct and recommend a yield of 35% for pHs above 9, decreasing monotonically to 30.5% at pH 2 with the expression Y_{hTA} (%) = 30 + 0.43 × pH, and possibly decreasing more below pH 2.

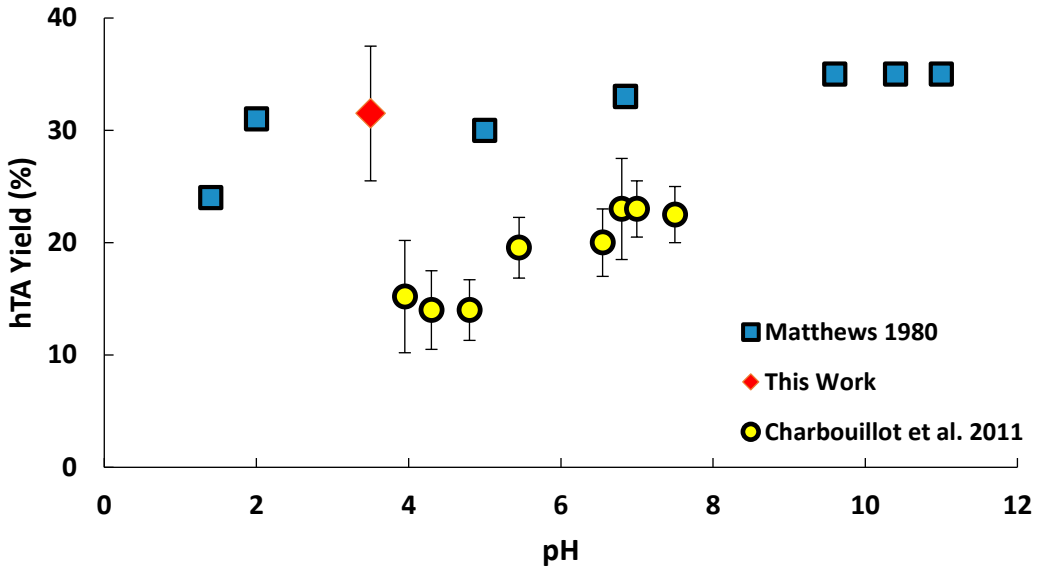

Figure 2.2. hTA yields as a function of pH. Matthews (1980)[111] did not indicate error bars or the experimental temperature; Charbouillot et al. (2011)[112] measurements were performed at 288 K; this work was performed at 293 K. Two other groups[129, 142] report values of 35% at unspecified pH.

2.4 Conclusions

The terephthalate method for quantification of hydroxyl radical is a robust, straightforward method under most conditions, and it can often be used with a stand-alone fluorescence spectrometer without the need for prior separation. To calculate the ·OH concentration, the yield of hTA from the ·OH reaction with TA is required; best estimates off this yield are 35% at pH 9 or above, decreasing monotonically to 30.5% at pH = 2.

3. HULIS Enhancement of Hydroxyl Radicals: Fulvic Acid-Fe(II) Complexes in the Presence of Lung Antioxidants

3.1 Introduction

Epidemiological studies have shown that inhalation of ambient particulate matter (PM) is associated with increased cardiovascular and respiratory diseases and mortality.[2] Inhaled PM may contribute to these health effects by producing an excess of reactive oxygen species (ROS) in the lungs.[7, 8] ROS are a class of reactive oxygen-bearing compounds that include the hydroxyl radical (OH), hydrogen peroxide (H_2O_2) and superoxide (O_2^-). ROS are generated by both PM and by cells as a physiological response to inhaled PM.[22, 44] Antioxidants defend against oxidative damage, but adverse health effects occur when antioxidants are depleted by excess ROS production.[160] Of all ROS species, OH may be the most damaging to the lungs, capable of oxidizing DNA, proteins and lipids.[19]

Due to the complexity and variability in chemical composition, the PM components that contribute to ROS generation are still not well understood. Recently, some studies have adopted surrogate lung fluids (SLF) to mimic physiological conditions as much as possible.[32, 33] Commonly, SLF includes several or all of ascorbate (Asc), glutathione (GSH), uric acid (UA) and citrate (Cit) buffered at pH 7.4 with an ionic strength that mimics lung lining fluid. Asc, GSH and UA are naturally occurring antioxidants and reducing agents[37] while Cit mimics metal-binding proteins.[161, 162] Previous laboratory studies have shown that the presence of these antioxidants has a significant impact on the ability of redox active PM components to produce OH.[32]

Soluble transition metal ions have been identified as important contributors to OH formation by particles extracted in SLF and other aqueous solutions.[21-23] In the presence of Asc, transition metals are capable of producing OH via reactions R14-R16 and R31; note that reactions are numbered per their appearance in Table 3.1:

$$Fe(II) + O_2 \rightarrow O_2^- + Fe(III) \quad \text{R14}$$

$$Fe(II) + O_2^- + 2H^+ \rightarrow H_2O_2 + Fe(III) \quad \text{R15}$$

$$Fe(II) + H_2O_2 \rightarrow Fe(III) + OH^- + OH \quad \text{R16}$$

$$HAsc^- + Fe(III) \rightarrow HAsc^{\cdot} + Fe(II) \quad \text{R31}$$

Where $HAsc^-$ represents the singly protonated ascorbate molecule that is dominant in SLF. There is evidence that Cit can complex Fe(II) and catalyze R3.14 and R3.16[44-46] increasing its rate coefficient by almost two orders of magnitude (Table 3.1).

Humic-like substances (HULIS) is a general term for complex organics common in atmospheric aerosols, including material with a biomass burning source, studied here, and other humic-like substances from soil or formed via secondary reactions as part of SOA formation. Humic and fulvic acids and HULIS share many common functional groups, including polycarboxylates, carbonyls, phenols, quinones, aliphatics and aromatics.[163] Some of these groups chelate transition metals and may be able to participate in redox cycling.[164, 165] Due to the similarities between HULIS and humic substances, fulvic acid (FA) and humic acid (HA) are frequently used as surrogates for HULIS, although there are important chemical and physical differences.[71] FA and HA are found in terrestrial and aquatic environments and result from the biological decomposition of organic matter. Generally, HULIS has been found to have lower

molecular weight, lower aromaticity and weaker acid characteristics compared to FA and HA.[71] Here we use Suwannee River Fulvic Acid (SRFA) as a surrogate for HULIS. SRFA forms Fe(II) complexes that catalyze the decomposition of H_2O_2 by catalyzing R14 and R16,[90, 165] enhancing OH formation in the following manner:

$$\text{SRFA} + \text{Fe(II)} \leftrightharpoons \text{SRFA-Fe(II)} \qquad \text{R51}$$

$$\text{SRFA-Fe(II)} + O_2 \rightarrow \text{SRFA-Fe(III)} + O_2^- \qquad \text{R54}$$

$$\text{SRFA-Fe(II)} + H_2O_2 \rightarrow \text{SRFA-Fe(III)} + OH^- + OH \qquad \text{R56}$$

Previous studies have shown R54 and R56 to be much faster than R14 and R16 respectively.[89, 90] A direct measurement of the reaction of $HAsc^-$ with SRFA-Fe(III) is not available.

Only a handful of studies have analyzed the effect of HULIS in physiologically relevant conditions; some have been carried out under acidic or natural water conditions.[165] Ghio and Quigly (1994)[87] used OH generation in human lung tissue cultures to probe the relationship between Fe, OH formation and HULIS found in coal dusts. Using an indirect assay that measured oxidation products of 2-deoxy-D-ribose (2-DR), they found that addition of the OH scavengers dimethylsulfoxide and dimethylthiourea and the strong metal chelator deferoxamine completely stopped production of 2-DR oxidation products, implicating metal-catalyzed OH formation. The study also observed an increase in both dissolved Fe and oxidation products as coal dust HULIS concentrations were increased. The increases in available Fe and formation of oxidation products were further associated with collagen deposition in the tissue cultures, suggesting HULIS-Fe driven OH formation could play a role in coal-mediated lung damage.[87] In a separate study, Ghio et al. (1994)[88] found that cigarette smoke condensate and HULIS isolated

from lung tissues of smokers had very similar FTIR spectra, and that exposing *in vitro* lung tissue to HULIS isolated from cigarette smoke together with ferric citrate resulted in production of 2-DR oxidation products. The products were also inhibited by the addition of deferoxamine, further supporting the notion that HULIS-Fe redox interactions play a role in lung injury.

HULIS extracted from atmospheric aerosols has been shown to produce ROS in the dithiothreitol (DTT) assay performed in phosphate buffer.[85, 86, 166] Lin and Yu (2011)[85] isolated water-soluble HULIS from $PM_{2.5}$ particles from rural and suburban areas in China during winter, and the extracts averaged 10% Fe by mass. All extracts exhibited strong DTT consumption, activity that was inhibited by 33% upon the addition of the strong iron chelator diethylene triamine pentacetic acid, indicating that DTT oxidation arose from interactions of metals with HULIS.

Few studies have attempted to model "dark" ROS kinetics mediated by Fe(II) in the presence of SRFA, a process complicated by uncertainty of heterogeneity of Fe binding sites on SRFA. Voelker et al. (1996)[165] modeled SRFA-Fe(II) interactions focusing on the behavior of Fe(II) and H_2O_2 at pH 3-5 and without defined SRFA binding to Fe. Miller et al. (2012)[89] measured and modeled OH formation from SRFA-Fe(II) using a two-ligand model for Fe binding at pH = 8.2. Neither study had redox cycling; ROS chemistry was only driven by O_2 reduction (R14), the Fenton reaction (R16) and SRFA interactions (R51, R54, R56).

For thermodynamic modeling, we used Visual MINTEQ 3.1, a model that synthesizes available literature describing aqueous equilibrium reactions relevant to natural waters. The model has available chemistry for SRFA, Cit, inorganic salts and Fe, but it does not have antioxidant chemistry. For SRFA chemistry, a NICA-Donnan model implicit in Visual MINTEQ

3.1 describes binding of metals to FA molecules via carboxylate and phenolic binding sites coupled with Donnan-gel electrostatic interactions.[167, 168]

Here, we investigate SRFA-Fe(II) complexes in SLF, using experiments, and thermodynamic and kinetic modeling. SLF consisted of 100-300 μM Asc, GSH, UA and Cit species that can compete with SRFA or HULIS. Experiments probe OH formation kinetics and cumulative production with and without added H_2O_2. H_2O_2 was added to probe different reactions in the chemical kinetics model. Activity of HULIS extracted from BBA with added Fe is also quantified. A 62 reaction chemical kinetics model developed and combined with a NICA-Donnan thermodynamic model[167, 168] are used to interpret the results, and assess the ability of the models and the underlying chemistry to reproduce the observations.

3.2 Experimental

3.2.1 Materials and Cleaning Protocol

SRFA Standard I (International Humic Substances Society), TA (TCI, 99%), TAOH (Aldrich, 97%), Ferrozine (Aldrich, 97%), $FeSO_4 \bullet 5H_2O$ (Arcos, 99%), NaCl (EMD, 99%), sodium phosphate dibasic (Acros, 99%), potassium phosphate monobasic (Acros, 99%), ascorbate sodium salt (Sigma, 99%), urate sodium salt (Sigma, 99%, L-glutathione reduced (Sigma, 99%) and citrate tribasic sodium salt (Sigma-Aldrich, 99%) and 2,2,2-trifluoroethanol (Arcos, 99%) were used as received. SRFA standard I is a purified material and contains less than 1% inorganic ash and background transition metal contaminants are negligible.

A rigorous cleaning process was followed for vessels. After each use, each vessel was washed with warm water and soap, and then rinsed deionized (18 MΩ DI) water (3×), ethanol (3×), and finally DI water (3×), soaked in a 1 M nitric acid bath overnight, rinsed with DI water and air

dried. Acid baths were replaced after two uses and kept covered to avoid dust deposition. All analytical solutions were prepared with chelex-treated 18 MΩ DI water.

3.2.2 Surrogate Lung Fluid (SLF) and SRFA

SLF was prepared as follows. A buffer solution (pH = 7.2-7.4) consisting of 114 mM NaCl, 7.8 mM Sodium phosphate dibasic and 2.2 mM potassium phosphate monobasic was prepared in DI water (18 MΩ). The buffer was adjusted to pH 7.2-7.4 with a pH meter (HANNA instruments, HI 3220), calibrated daily. The buffer solution was passed through a chromatography column (Chemglass, Coarse filter) filled with Chelex-100 beads (Sodium form, Sigma Life Science) at a rate of 1 drop per 4 seconds to remove trace metals and used within a month of preparation. 200 µM Ascorbate, 100 µM reduced glutathione, 100 µM uric acid sodium salt, and 300 µM citric acid stock solutions were made fresh daily and added to phosphate buffer immediately prior to beginning experiments. 1 mg/mL SRFA stock solutions were prepared in phosphate buffer solution and stored in a refrigerator (4 ^{o}C) for up to a month.

3.2.3 Quantification of OH from SRFA-Fe(II) Complexes Using Terephthalic Acid

Terephthalic acid (TA) reacts with OH to form strongly fluorescent 2-hydroxyterephthalic acid (TAOH) with a yield of 33% at pH 7.4.[111, 169] A 1 mM stock solution of TAOH was prepared in DI water and kept refrigerated in the dark. TAOH solutions in phosphate buffer were used to prepare a 50 – 800 nM daily calibration curve. TAOH fluorescence at was measured at $\lambda_{ex}/\lambda_{em}$ of 320/420 nm with a Lumina fluorescence spectrometer (Lumina Thermo Scientific).

To prepare SRFA-Fe(II) solutions, TA (10 mM) and SRFA (0, 5, 10, 15 or 20 µg/mL) was added to SLF in a Teflon petri dish, and Fe(II) at 0, 100, 250, 500 or 1000 nM was added

immediately prior to analysis. This concentration range of SRFA and Fe(II) corresponds to aqueous BBA and [Fe(II)] observed in ambient PM samples consisting of (25 ± 13) m^3 of ambient urban air extracted in 10 mL (Paulson et al. 2016).[109] To further probe the system, 1 µM H_2O_2 was added to a subset of experiments. Two types of blanks were measured daily: 1) TA and SRFA in SLF and 2) TA in SLF. For kinetic measurements, aliquots were monitored every 30 minutes for two hours; for other samples, OH production was measured only at two hours.

Aqueous SRFA has native fluorescence that interferes with both the excitation and emission wavelengths of TAOH (320 nm and 420 nm), however SRFA has negligible interference with the TAOH assay if [SRFA] = 5 µg/mL (Fig. 3.1). Solutions initially at concentrations > 5 µg/mL were diluted to [SRFA] ≤ 5 µg/mL before measuring TAOH fluorescence.

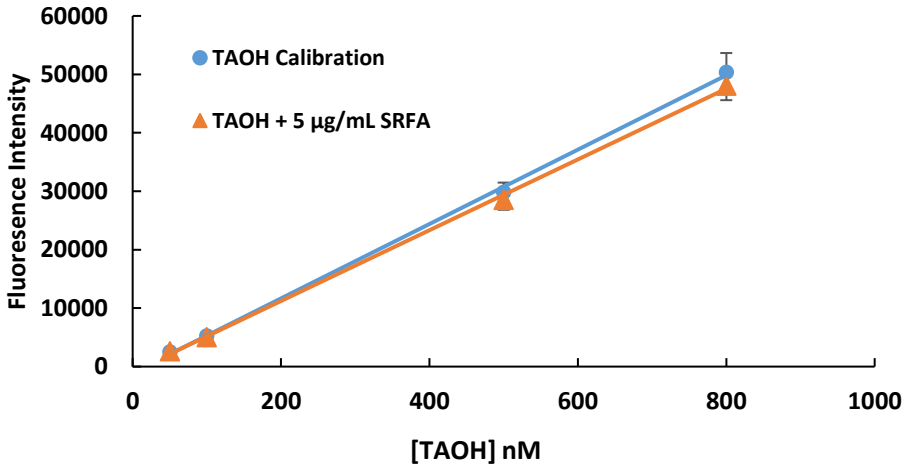

Figure 3.1. Calibration curves for TAOH and TAOH with the addition of 5 µg/mL. Data points represent the average of three measurements and error bars denote ±1σ.

3.2.4 Extraction of Fresno Biomass Burning Aerosol

$PM_{2.5}$ from a biomass burning event near California State University, Fresno (36.82 ^{o}N, 119.74 ^{o}W) was collected from Sept. 10 – 16 2015 on a 406 cm^2 Teflon-coated glass fiber filter (Tisch Environmental, Lot#120618003) using a Hi-volume $PM_{2.5}$ sampler (nominally at 1.13 m^3/min, Tisch Environmental) placed on the roof of one of the University buildings for 143 hours. The sample contained 72.4 μg/cm^2 of aerosol (Ohaus -PA84), and 41.2 μg/cm^2 of BBA (approximately equivalent to HULIS), corresponding to 3.0 and 1.73 μg/m^3 of mass and BBA respectively. BBA was determined using an Optical Transmissometer (Magee Scientific, OT21). The BBA concentration was calculated using an absorption cross section of 9.6 m^2g^{-1} [170] after subjecting to a mass loading correction developed by Jimenez et al. (2007)[171]; more details are available in Paulson et al. (2016).[109] The mass loading is unexpectedly low, possibly due to malfunction of the pump for part or all of the sampling period.

To investigate the effect of atmospheric HULIS on OH production from Fe(II), we extracted two sets of three 1.6 cm^2 punches of the biomass burning sample and filter blanks in 7 mL SLF and measured cumulative OH production at two hours. 20 μL of 2,2,2-Trifluoroethanol was added to filter punches before extraction to improve particle solubility. The HULIS solutions contained 16.7 μg/mL of total aerosol and approximately 9.5 μg/mL HULIS. 500 nM Fe(II) was added to one set of samples. HULIS samples were diluted 2x to avoid the interference of HULIS fluorescence with the TAOH assay. Total soluble Fe (Fe(II) + Fe(III)) was measured at two hours using the ferrozine assay, combined with a strong reducing agent.[151, 172] Briefly, a filtered (0.2 μm polypropylene filter) 2 mL aliquot from the biomass burning sample was mixed with 20 μL of each hydroxylamine (0.6 M) and ferrozine (5.1 mM). Hydroxylamine reduces all soluble

Fe to Fe(II), and ferrozine forms a strongly absorbing complex with Fe(II) (562 nm). Mixtures were allowed to react for 20 minutes at room temperature to ensure complete reduction of Fe(III) species, and absorption was measured with a liquid waveguide capillary cell (LWCC-3100, World precision Inc.).

3.2.5 Chemical Kinetics and Thermodynamic Modeling

The 62-reaction chemical kinetics model (Table 3.1) includes water, H_xO_y, Cl, phosphate, ascorbic, uric and citric acid, glutathione and SRFA chemistry. It is based on several earlier studies (Table 3.1) including a two ligand model for SRFA developed by Miller et al. (2012).[89] Visual MINTEQ 3.1 calculations (not shown) indicate insignificant amounts of free Fe^{3+} due to binding by Cit or SRFA, thus Fe^{3+} precipitation reactions are not important for this system and are not included. Zepp et al. (1992)[173] showed that Fe(II)-phosphate complexes have no effect on OH formation and thus are omitted from the kinetics model (Table 3.1). FACSIMILE v4.2 (MCPA Software Ltd) was used as the solver.

Table 3.1. Kinetic model.

#	Reaction	k_f	k_r	K_{eq}
	General Equilibria			
1[a]	$H_2O \rightleftharpoons H^+ + OH^-$	1.3×10^{-3}	1.3×10^{11}	10^{-14}
2[k]	$H_2O_2 \rightleftharpoons HO_2^- + H^+$	1.26×10^{-2}	10^{10}	1.26×10^{-12}
3[a]	$HO_2 \rightleftharpoons H^+ + O_2^-$	1.14×10^{6}	7.2×10^{10}	1.58×10^{-5}
4[b]	$Fe(II) + Cit^{3-} \rightleftharpoons [Cit\text{-}Fe(II)]^-$	$10^{13.1}$	10^{10}	$10^{3.1}$
5[b]	$Fe(III) + Cit^{3-} \rightleftharpoons Cit\text{-}Fe(III)$	$10^{21.8}$	10^{10}	$10^{11.8}$
6	$H_3PO_4 \rightleftharpoons H_2PO4^- + H^+$	$10^{7.85}$	10^{10}	$10^{-2.15}$
7	$H_2PO_4^- \rightleftharpoons HPO_4^{2-} + H^+$	$10^{2.8}$	10^{10}	$10^{-7.2}$
8[j]	$OH + Cl^- \rightleftharpoons HOCl^-$	4.3×10^{9}	6.1×10^{9}	0.704
9[j]	$HOCl^- + H^+ \rightleftharpoons Cl + H_2O$	2.1×10^{10}	1.3×10^{3}	1.61×10^{7}
10[j]	$Cl + Cl^- \rightleftharpoons Cl_2^-$	2.1×10^{10}	1.1×10^{5}	1.91×10^{5}

	Terephthalate Probe			
11[c]	TA + OH → (Y) TAOH + (1-Y)X	4.4×10^{9}		
12[c]	X + OH → Z	10^{9}		
13[c]	TAOH + OH → $TAOH_{ox}$	6.3×10^{9}		
	Inorganic Fe(II)/Fe(III) Reactions			
14[e]	Fe(II) + O_2 → Fe(III) + O_2^-	8.8×10^{-2}		
15[e]	Fe(II) + O_2^- + $2H^+$ → Fe(III) + H_2O_2	200		
16[k]	Fe(II) + H_2O_2 → Fe(III) + OH + OH^-	55		
17[f]	Fe(III) + H_2O_2 → Fe(II) + HO_2 + H^+	2×10^{-3}		
18[m]	Fe(III) + O_2^- → Fe(II) + O_2	1.5×10^{8}		
19[f]	Fe(III) + HO_2 → Fe(II) + O_2 + H^+	2×10^{3}		
20[f]	Fe(II) + HO_2 → Fe(III) + HO_2^-	1.2×10^{6}		
21[k]	Fe(II) + O_2^- → Fe(III) + O_2^{2-}	10^{7}		
22[f]	Fe(II) + OH → Fe(III) + OH^-	3.2×10^{8}		
23[j]	Fe(II) + Cl → Cl^- + Fe(III)	5.9×10^{6}		
24[j]	Fe(II) + Cl_2^- → Cl + Cl^- + Fe(III)	1.4×10^{7}		
	Citrate Reactions			
25[n]	Cit-Fe(II) + O_2 → Cit-Fe(III) + O_2^-	(3.0 ± 0.7)		
26[m]	Cit-Fe(II) + O_2^- + $2H^+$ → Cit-Fe(III) + H_2O_2	6.0×10^{5}		
27[n]	Cit-Fe(II) + H_2O_2 → Cit-Fe(III) + OH + OH^-	$(4.2 \pm 1.7) \times 10^{3}$		
28[m]	Cit-Fe(III) + O_2^- → Cit-Fe(II) + O_2	4.2×10^{5}		
29[l]	Cit^{3-} + OH → Cit_{ox}	1.1×10^{8}		
	Antioxidant Reactions			
30[h]	$2Asc^{\cdot-}$ + H^+ ⇌ $HAsc^-$ +DHA	1.4×10^{6}	2.8×10^{-9}	5×10^{14}
31[h]	Fe(III) + $HAsc^-$ → Fe(II) + H^+ + $Asc^{\cdot-}$	10^{2}		
32[h]	Cit-Fe(III) + $HAsc^-$ → Cit-Fe(II) + H^+ + $Asc^{\cdot-}$	10^{2}		
33[h]	$HAsc^-$ + OH → $Asc^{\cdot-}$ + H_2O	1.1×10^{10}		
34[h]	$HAsc^-$ + $GSH^{\cdot}$ → $Asc^{\cdot-}$ + GSH	6×10^{8}		
35[h]	$HAsc^-$ + $UA^{\cdot}$ → $Asc^{\cdot-}$ + UA^-	10^{6}		
36[h]	$HAsc^-$ + O_2^- → $Asc^{\cdot-}$ + HO_2	2.7×10^{5}		
37[h]	$HAsc^-$ + HO_2 → $Asc^{\cdot-}$ + H_2O_2	2.7×10^{5}		
38[h]	UA^- + OH → $UA^{\cdot}$	10^{10}		
39[h]	GSH + OH → $GSH^{\cdot}$	1.1×10^{10}		
	ROS Reactions			
40[i]	H_2O_2 + OH → H_2O + HO_2	2.7×10^{7}		
41[g]	O_2^- + H_2O_2 → OH^- + OH + O_2	0.13		
42[a]	OH + OH → H_2O_2	5.5×10^{9}		
43[a]	OH + O_2^- → OH^- + O_2	1.01×10^{10}		
44[m]	O_2^- + O_2^- + $2H^+$ → H_2O_2 + O_2	1.9×10^{5}		
45[a]	H_2O_2 + HO_2 → H_2O + O_2 + OH	3.1		
46[k]	OH + HO_2 → H_2O + O_2	7.1×10^{9}		

47[a]	$HO_2 + HO_2 \rightarrow H_2O_2 + O_2$	8.3×10^5		
48[a]	$HO_2 + O_2^- \rightarrow H_2O_2 + O_2$	9.7×10^7		
49[k]	$HO_2 + O_2^- \rightarrow HO_2^- + O_2$	9.7×10^7		
50[k]	$O_2^{2-} + H^+ \rightarrow HO_2^-$	10^{10}		
	SRFA Reactions			
51[a]	$Fe(II) + SRFA \rightleftharpoons Fe(II)\text{-}SRFA_1$	10^{10}	2.9×10^4	3.5×10^5
52[a]	$Fe(III) + SRFA \rightarrow Fe(III)\text{-}SRFA$	1.3×10^6		
53[a]	$Fe(II)\text{-}SRFA_1 \rightarrow Fe(II)\text{-}SRFA_2$	6.3×10^{-3}		
54[n]	$Fe(II)\text{-}SRFA_1 + O_2 \rightarrow Fe(III)\text{-}SRFA + O_2^-$	(5.1 ± 1.0)		
55[a]	$Fe(II)\text{-}SRFA_1 + O_2^- + 2H^+ \rightarrow Fe(III)\text{-}SRFA + H_2O_2$	2×10^7		
56[n]	$Fe(II)\text{-}SRFA_1 + H_2O_2 \rightarrow Fe(III)\text{-}SRFA + OH + OH^-$	$(4.3 \pm 1.4) \times 10^3$		
57[a]	$Fe(II)\text{-}SRFA_1 + OH \rightarrow Fe(III)\text{-}SRFA + OH^-$	10^{10}		
58[a]	$Fe(II)\text{-}SRFA_2 \rightarrow Fe(III)\text{-}SRFA$	3.1×10^{-3}		
59[a]	$Fe(III)\text{-}SRFA + O2^- \rightarrow Fe(II)\text{-}SRFA_1 + O_2$	2.8×10^5		
60[h]	$Fe(III)\text{-}SRFA + HAsc^- \rightarrow Fe(II)\text{-}SRFA_1 + H^+ + Asc^{\cdot-}$	10^2		
61[a]	$SRFA + OH \rightarrow SRFA_{ox} + O_2^-$	5.3×10^9		
62[a]	$SRFA + O_2^- \rightarrow SRFA_{ox} + H_2O_2$	9×10^3		

Units are in s^{-1} or $M^{-1}s^{-1}$ for first and second order reactions respectively. Fe(II) represents all inorganic Fe(II) species. (a) Miller et al. (2012).[89] Molecular weight of SRFA is 750 g/mol for all calculations. (b) Li et al. (2007).[174] (c) Page et al. (2010).[141] Y represents percent yield of TAOH formation set to 33%. X represents biproducts of TA oxidation and k_{12} is estimated based off rate coefficients for OH oxidation of organics in aqueous solutions (~10^9).[155] (d) Rush et al. (1990).[175] (e) Santana-Casiano et al. (2005).[48] (f) Lewis et al. (2009).[176] (g) Bielski et al. (1985).[157] (h) Buettner et al.[177] Values are for $HAsc^-$ reduction of Fe(II)-EDTA complex. Assumed to be the same for Cit-Fe(III) and Fe(III)-SRFA. DHA represents Dehydroascorbic acid. (i) Christensen et al. (1982).[178] (j) Jayson et al. (1973).[179] (k) De Laat et al. (2005).[153] (l) Monod et al. (2005).[180] Value for Succinic acid. (m) Pham et al. (2008)[46] (n) Indicates rate coefficient fitted to experimental data.

3.3 Results and Discussion

3.3.1 OH Formation from SRFA-Fe(II) Complexes

Figure 3.2 shows OH generation curves from 500 nM Fe(II) as a function of [SRFA] and Figure 3.3 shows the OH production rates. OH production was nearly linear over the first two hours (Fig. 3.2) although it has slight 2nd order behavior (discussed below). The OH production rates increased linearly with [SRFA] until 15 µg/mL but increasing SRFA further to 20 µg/mL resulted in a slight decrease compared to 15 µg/mL (Fig. 3.3, also discussed below). The initial OH production rate for 500 nM Fe(II) in the absence of SRFA was (0.38 ± 0.02) µM/hr, in very

good agreement with 0.34 µM/hr reported by Charrier and Anastasio (2015).[26] Figure 3.4 shows the cumulative quantity of OH produced in two hours as a function of $[Fe(II)]_i$ from (0 – 1000 nM), and SRFA from (0 - 20 µg/mL). As for 500 nM Fe(II) (above), addition of SRFA enhances OH formation until 15 µg/mL. Above this it decreases slightly, especially at higher Fe. For [SRFA] = 0 and 5 µg/mL, OH production increases nearly linearly with $[Fe(II)]_i$. At higher [SRFA], OH production has an increasingly nonlinear dependence on Fe(II).

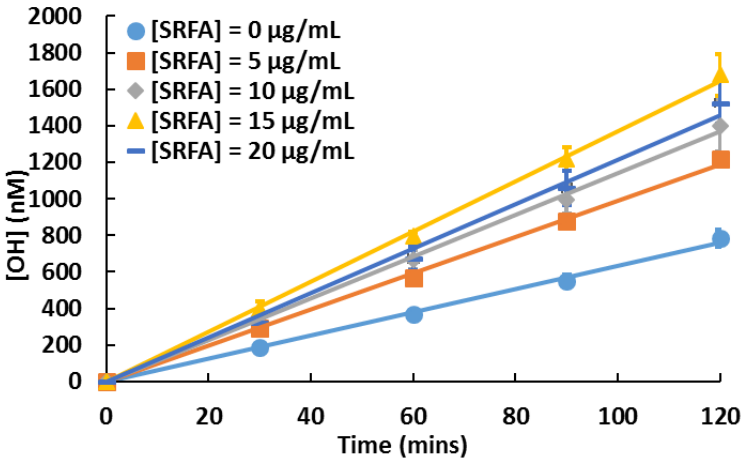

Figure 3.2. Kinetics of OH production from SRFA and 500 nM Fe(II) over two hours. Each point represents the average of three measurements and error bars denote range of data.

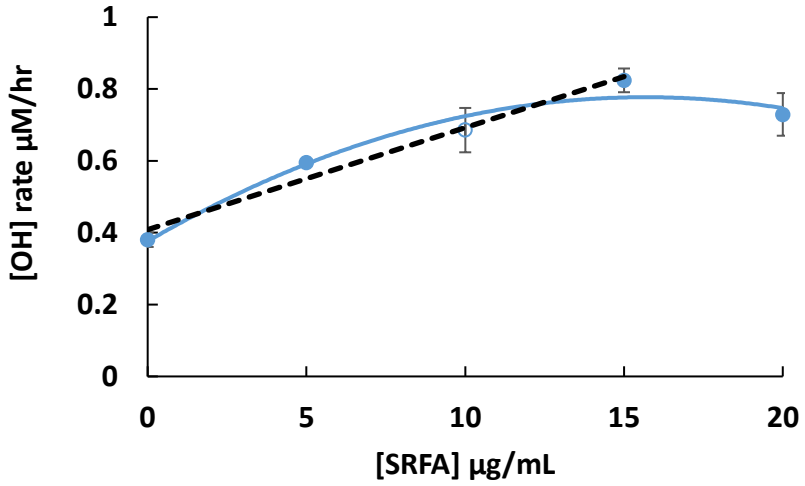

Figure 3.3. Two hour OH production rates from 500 nM Fe(II) as a function of SRFA concentration, calculated data in figure 2. Filled points indicate the average of three measurements while the unfilled point indicates the average of two. Error bars denote ±1σ. The dashed line is a linear fit of the first four points.

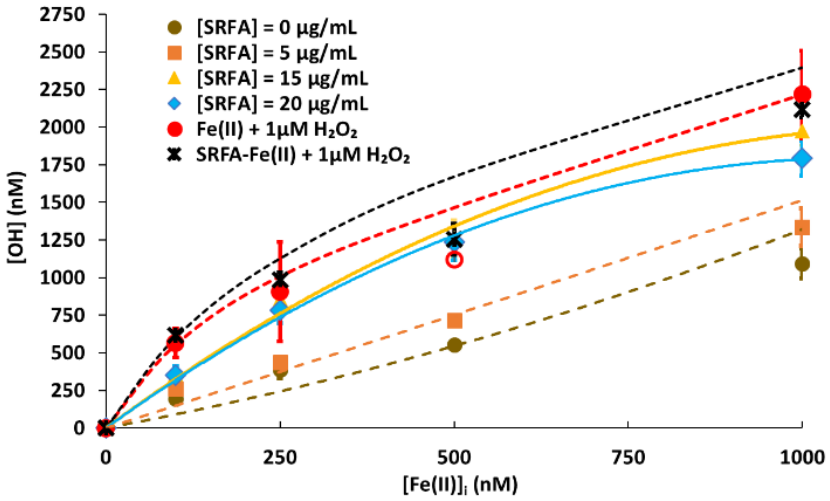

Figure 3.4. OH produced at two hours from Fe(II), SRFA-Fe(II) and Fe(II)/SRFA-Fe(II) + 1 µM H_2O_2. Each filled data point represents the average of three measurements and error bars denote range of data. Open symbols indicate a single measurement. Solid lines denote fit to experimental data. Dashed lines denote model results.

The number of OH molecules produced per Fe(II) after two hours range from a low of 1.9 and 1.1 for $[Fe(II)]_i$ at 100 and 1000 nM respectively and [SRFA] = 0, to a maximum of 3.5

to 2 for $[Fe(II)]_i$ at 100 to 1000 nM and SRFA of 15 μg/mL, respectively (Fig. 3.5). In reasonable agreement with this, Charrier et al. (2011)[32] found 24 – 19 OH produced per initial Fe after 24 hours for $[Fe(II)]_i$ = 500 to 1000 nM, respectively (absent SRFA). Both results for $[OH]/[Fe(II)]_i$ at two and 24 hours are greater than unity, indicating redox cycling of Fe(II). OH production from Fe(II) (R14-R16) requires 3 electrons, allowing the calculation of the number of reduction cycles (Figure 3.6); values range from 2.8 to 9.0 over two hours.

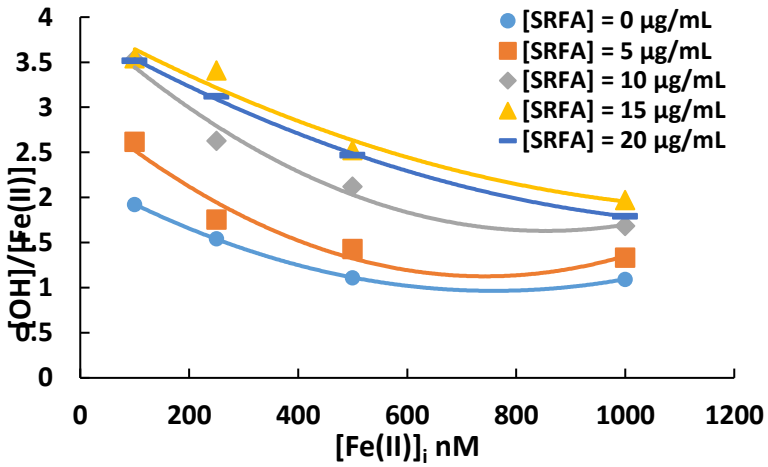

Figure 3.5. Ratio of OH produced at two hours per Fe(II) in solution as a function of [Fe(II)]. Different curves represent differing amounts of SRFA.

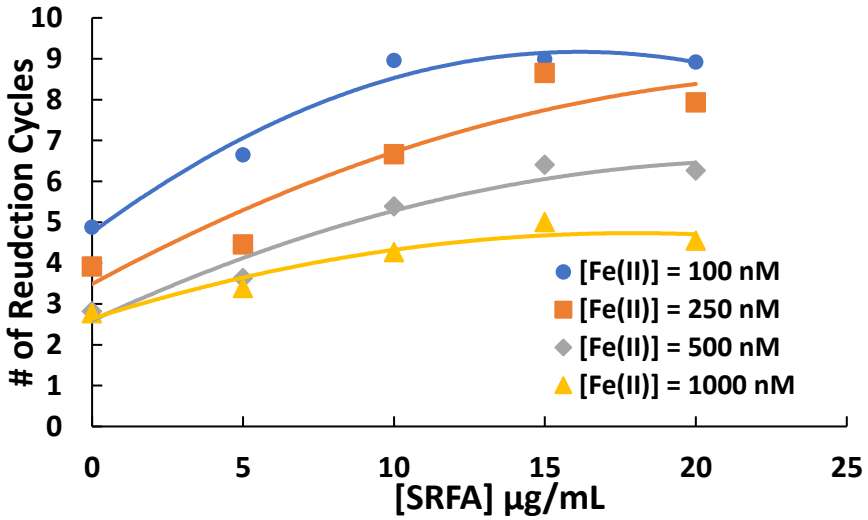

Figure 3.6. Number of reduction cycles in the first two hours as a function of [SRFA]. Data estimated by multiplying [OH]/[Fe(II)] ratio by 3.

There are two possible explanations for the slight decrease in OH production as SRFA is increased from 15 to 20 µg/mL. While scavenging of OH by neighboring groups on the same SRFA molecule near the site of OH production has been proposed,[165] this process would not be expected to depend on [SRFA], as the OH does not escape into solution. This process is different from bimolecular scavenging of OH by SRFA, which would depend on the concentration of SRFA in solution. [SRFA] varies from 5 µg/mL to 20 µg/mL, TA is present in significant excess (10 mM). The ratio of carbon groups on TA to SRFA varies from ~280 to 71, thus even the highest [SRFA] only reduces TA conversion to TAOH by ~1.4%. Two other hypotheses are as follows. A possible concentration-dependent explanation is a reduction in reactivity of TA with OH due to interactions with aromatic groups on SRFA. Lindsey et al. (2000)[181] observed such a phenomenon for the reaction of phenol with OH in the presence of 5-30 µg/mL SRFA in acidic solutions, a phenomenon hypothesized to be due to π-π stacking of aromatic rings with the hydrophobic aromatic regions of SRFA molecules.[181] Another possibility may be the availability

of a set of binding sites on the SRFA molecule that have comparable or higher binding coefficients relative to the sites that enhance Fe reactivity, but have low abundance, and the ability to reduce the reactivity of Fe.

3.3.2 OH from SRFA-Fe(II) with added H_2O_2

OH production in the absence of added H_2O_2 is limited by the reactions that reduce O_2 to form O_2^- (R14, R25, R54), which can then be converted to H_2O_2 and ultimately OH. To test the consistency of the Fenton rate coefficients responsible for converting H_2O_2 to OH, (R27, R56) we added H_2O_2 to some experiments. Figures 3.4, 3.7 and 3.8 show the quantity of OH produced from Fe(II) at two hours after the addition of 1 μM H_2O_2, as a function of $[Fe(II)]_i$ for [SRFA] = 0, 5, 10, and 15 μg/mL. OH produced from Fe(II) without added H_2O_2 is also shown for comparison. In all cases, the addition of 1 μM H_2O_2 enhances OH production from Fe(II), although the magnitude of the enhancement decreases as [SRFA] increases. Model predictions for OH production at two hours are also shown in figure 3.4 and are in very good agreement with experimental data (discussed below).

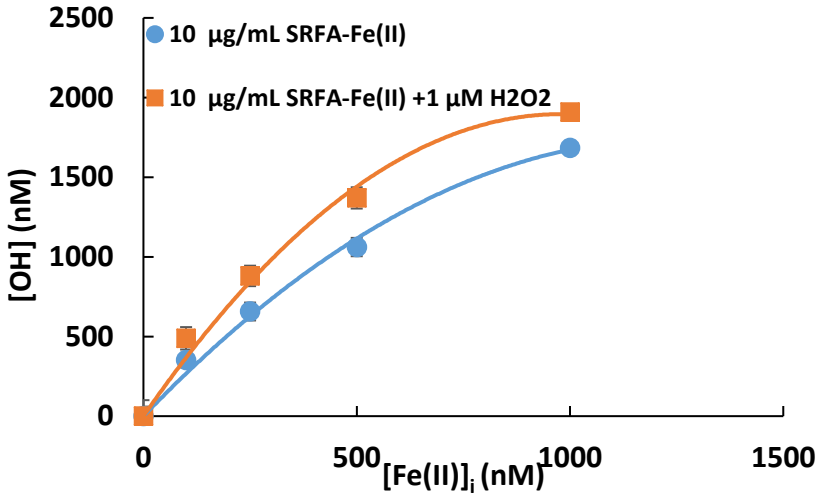

Figure 3.7. OH produced at two hours from 10 µg/mL SRFA mixed with Fe(II) (blue circles) and Fe(II) + 1 µM H_2O_2 (orange circles) as a function of $[Fe(II)]_i$. Each filled data point represents the average of three measurements and error bars denote ±1σ.

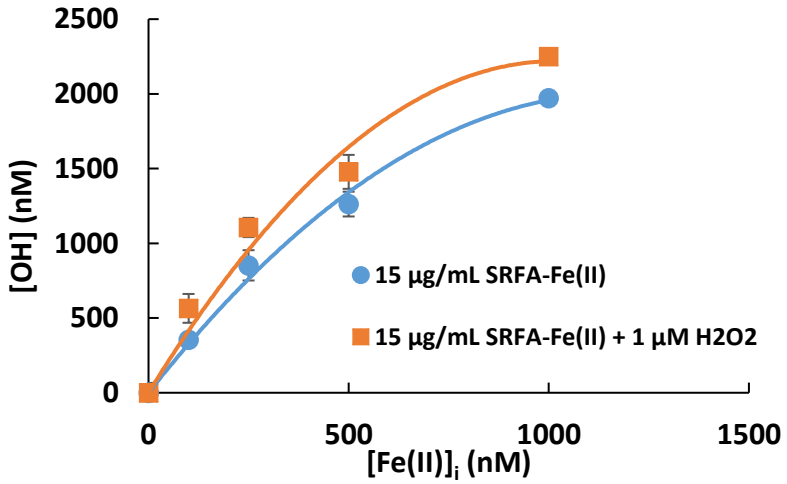

Figure 3.8. OH produced at two hours from 15 µg/mL SRFA mixed with Fe(II) and Fe(II) + 1 µM H_2O_2 as a function of $[Fe(II)]_i$. Each filled data point represents the average of three measurements and error bars denote ±1σ. Lines are best fits of the data.

3.3.3 OH from SRFA-Fe(II) in the absence of Antioxidants

SRFA has been shown to be able to reduce Fe(III) to Fe(II) in pH 3.5 solutions.[165] In separate measurements, OH production at two hours from SRFA-Fe(II) mixtures in phosphate

buffer was measured for [SRFA] between 0 and 20 µg/mL, and $[Fe(II)]_i$ = 500 nM, at two hours. Values fell between -22 nM and 93 nM with no particular trend and averaged 25 ± 38 nM (Figure 3.9), indicating that SRFA on its own has only a minor ability to donate electrons (R31) to promote OH formation. In a similar system at pH = 8.2, Miller et al. (2012)[89] measured OH production using production of 5-hydroxyphthalhydrazide over time. From their data, assuming a yield of 20% for 5-hydroxypthalhydrazide,[182] we can calculate OH production at two hours. Miller et al. (2012)[89] found a modest amount of OH formation from SRFA and a higher concentration of Fe (2 µM); 125 and 250 nM for 10 and 20 µg/mL respectively, in reasonable agreement with our results.

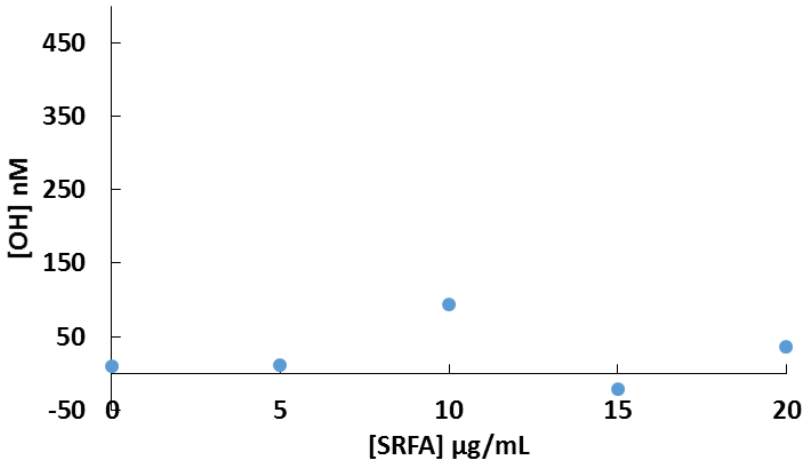

Figure 3.9. OH production at two hours from varying [SRFA] and 500 nM Fe(II) in phosphate buffer (absent from antioxidants).

3.3.4 OH Production from Fresno Biomass Burning Aerosol

Table 3.2 shows OH production from the Fresno winter BBA sample, containing roughly 57% HULIS by mass. Also shown is the same aerosol sample with 500 nM Fe(II) added, and 500 nM Fe(II) alone, all in SLF. The upper limit of the HULIS concentration in solution was 9.5

μg/mL, assuming all HULIS was water soluble. The BBA contained (230 ± 16) nM soluble Fe(II) as measured by the ferrozine assay. The BBA sample mixed with 500 nM Fe(II) produced 49% more OH than the BBA sample alone, and 28% more than the sum of the production from 500 nM Fe(II) and the BBA sample. Although the BBA also likely contained additional redox active transition metals such as Cu and Mn[109] as well as quinones, pyridine and imidazole moieties that may also participate in ROS cycling and contribute to OH formation as well.[85, 166] For example, Cu is known to form a redox couple with Fe species.[183] The results both support the importance of HULIS interactions with transition metals in determining the OH formation and suggest that all binding sites on the HULIS were not already saturated with transition metals. While the results demonstrate that iron activity is enhanced by HULIS, results are limited, since we did not have enough BBA samples to investigate the effect of BBA mass loading on OH formation.

Table 3.2. OH generated at two hours from Fresno BBA and 500 nM Fe(II) extracted in SLF.

System	[OH] Production μM
500 nM Fe(II)	.55 ± .02
BBA*	3.4 ± 0.1
BBA* + 500 nM Fe(II)	5.0 ± 0.1

Errors denote ±1σ of three measurements. *9.5 μg/mL HULIS present in solution (upper limit).

3.3.5 Minteq Chemical Speciation Modeling

Figure 3.10 shows equilibrium speciation in the absence and presence of SRFA for [Fe(II)] = 1000 nM, calculated with Visual MINTEQ 3.1 (Royal Institute of Technology, Sweden) using a NICA-Donnan model for FA binding to Fe(II). Input parameters for MINTEQ are shown in Tables 3.3 and 3.4. No thermodynamic data for Fe(II) binding with UA or GSH could be found, and Charrier and Anastasio (2011)[32] found that Asc does not significantly bind

to Fe(II), thus Asc, UA and GSH were omitted from the calculations. There is evidence that GSH can bind to Fe(II),[184, 185] but the system has not been sufficiently well characterized to put in our model; these interactions merit further study. In the absence of SRFA, only 12% of Fe(II) is free (Fig. 3.10A). The majority of Fe(II) binds to Cit and HPO_4^{2-}, with only a small contribution from $H_2PO_4^-$, in good agreement with similar modeling by Charrier and Anastasio (2011)[32]. Fe speciation was not significantly different for lower $[Fe(II)]_i$. This is likely due to the greater abundance of citrate compared to the range of Fe(II) concentrations.

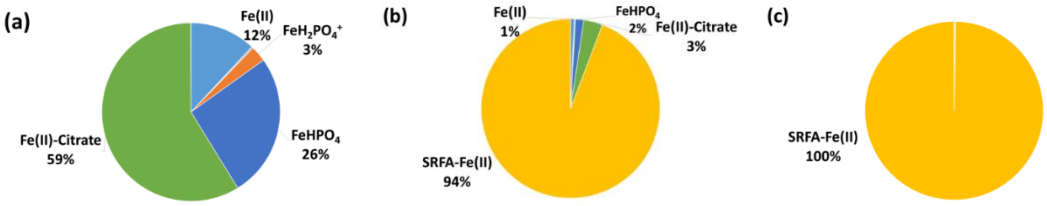

Figure 3.10. Thermodynamic calculations of Fe(II) binding at 1000 nM Fe(II)as a function of [SRFA] at equilibrium using Visual MINTEQ. (A) Fe(II) speciation in SLF. (B) Fe(II) Speciation in SLF with 5 µg/mL SRFA. (C) Fe(II) Speciation in SLF with 10 µg/mL SRFA.

The NICA-Donnan model describes binding of metals to FA molecules via carboxylate and phenolic binding sites coupled with Donnan-gel electrostatic interactions.[167, 168] The concentration of carboxylate (Q_1) and phenolic (Q_2) binding is proportional to the total mass of SRFA (Table 3.4). MINTEQ calculates Q_1 as 29.4 – 118 µM and Q_2 as 9.3 – 37.2 µM for 5 - 20 µg/mL SRFA. For the SRFA system, Fe speciation was the same for lower $[Fe(II)]_i$ with the exception [SRFA] = 5 µg/mL. This is likely due to the greater abundance of SRFA compared to the range of [Fe(II)] (0-1 µM). For 5 µg/mL SRFA and $[Fe(II)]_i$ < 1000 nM, 94% of Fe(II) binds to SRFA with minor contributions from Cit, HPO_4^{2-} and free Fe(II) (Fig. 3.10B). For $[Fe(II)]_i$ = 1000 nM and [SRFA] ≥ 5 µg/mL, 100% of Fe(II) is bound to SRFA (Fig 3.10C). Calculations

predict that Fe(II) is bound to the carboxylate site of SRFA, with no contributions from phenolic binding sites at any of the concentrations tested. This obviously implies that while the model and theoretical framework are able to explain the increased OH production with 5 µg/mL of SRFA, they will not be able to explain increases in OH production as more SRFA is added as Fe binding does not change as [SRFA] is increased.

Table 3.3. Concentration inputs for Visual MINTEQ speciation calculations.

Species	**Concentration (mg/L)**
Cl^-	4041
PO_4^{3-}	950
Citrate	57.6
Na^+	3006
K^+	86.02
Fe^{2+} ($x10^{-2}$)	.558, 1.395, 2.79, 5.58
SRFA	0, .005, .010, .015, .02

pH = 7.4
Ionic Strength set to 0.17 M

Table 3.4. Input parameters for SRFA using NICA-Donnan model.

Species	$logK_1$	n_1	Q_1 (mmol/g)	$logK_2$	n_2	Q_2 (mmol/g)	b	Ratio of DOM to DOC	% active DOM that is FA
Proton	2.34	0.66	5.88	8.6	0.76	1.86	0.57	2	100
Fe	6	0.25		36	0.19				

K-equilibrium constant. Q- Binding site concentration per mass of SRFA. Q_1 and Q_2 indicated carboxylate and phenolic binding sites respectively. n-Non-ideality parameter. b-Donnan volume parameter.

3.3.6 Chemical Kinetics Modeling Results

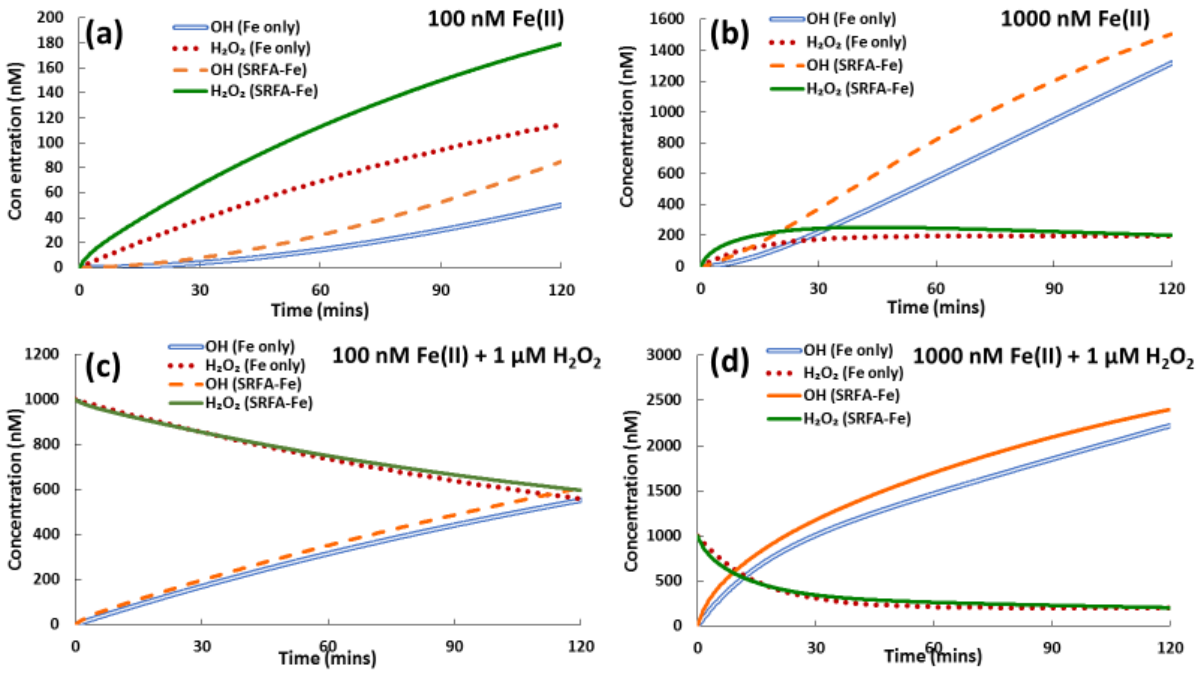

Figure 3.11. Chemical kinetics modeling results for H_2O_2 concentration and the OH produced (cumulative) over two hours from Fe(II) (dashed lines) and SRFA-Fe(II) complexes (solid lines) in SLF. [SRFA] = 5 µg/mL in all cases. (a) 100 nM Fe(II) (b) 1000 nM Fe(II) (c) 100 nM Fe(II) + 1 µM H_2O_2 (d)1000 nM + 1 µM H_2O_2.

Chemical kinetics model results are shown in Figures 3.4 (dashed lines) and 3.11 (all lines). Figure 3.4 shows good agreement between the model and measurement data for OH formation as a function of $[Fe(II)]_i$, with and without 5 µg/mL SRFA and added H_2O_2, including the initially non-linear dependence of this system on Fe(II). For the citrate-Fe system over the range 100 nM – 1000 nM Fe(II) (no SRFA), the kinetic model predicts that 27% of Fe(II) is bound as Cit-Fe(II). This disagrees somewhat with thermodynamic modeling that indicates 59% Fe is bound as Cit-Fe(II) (Figure 3.10A). With SRFA added, the kinetic model predicts 83% - 81% of Fe(II) is bound to SRFA at 5 µg/mL; the remainder is mostly inorganic iron with some Cit-Fe(II). Of the Fe(II) bound to SRFA, ~33 and 67% are bound to the active (type 1) and

inactive (type 2) sites (as defined by Miller et al. (2012),[89] Table 3.1), respectively. This is in reasonable agreement with thermodynamic modeling that predicts 100% and 94 % of Fe bound to SRFA for 100 nM (not shown) and 1000 nM (Figure 3.10B) Fe(II) respectively. The thermodynamic model differentiates carboxylate and phenolic sites, but not active and inactive sites, and places Fe(II) in the carboxylic:phenolic sites at a ratio of 3.2:1. It is not well known which of these sites are more active.

The system of reactions describing the H_yO_x/SRFA/Citrate/Fe chemistry leading to OH formation is very sensitive to the superoxide formation and Fenton rate coefficients (Reactions 25, 27, 54 and/or 56, Table 3.1), depending on whether H_2O_2 was added to the experiment. In the absence of added H_2O_2, OH formation depends ultimately on the initial reduction of O_2 to O_2^- (R25), the rate limiting step in the chain of reactions leading from O_2 to OH via O_2^- and H_2O_2. In the presence of added H_2O_2, the Fenton reaction (R54/56) becomes rate limiting. The rate coefficients for these reactions, including their dependence on pH, T and ionic strength (I) are not well known. The Cit-Fe(II) system, the chemistry is somewhat sensitive to Fe^{2+} (free Fe(II))-mediated formation of O_2^- (k_{14}); SRFA-Fe(II) is less sensitive. While values for k_{14} vary by almost three orders of magnitude in literature (.058 [48] - 13 [186]) $M^{-1}s^{-1}$, many of the studies used very different solutes than those used here. Here we find that the value suggested by Santana-Casiano (2005)[48], 8.8×10^{-2} $M^{-1}s^{-1}$ for I = 0 at pH 6-8.2 and T = (25 ± 0.5) ºC works best. Santana-Casiano (2005)[48], also reports a $k_{14} = 5.8\times10^{-2}$ $M^{-1}s^{-1}$ for I = 0.7 that fits very well with our data. Using k_{14} values higher than 0.3 $M^{-1}s^{-1}$ significantly overshoots observed OH (Fig. 3.12).

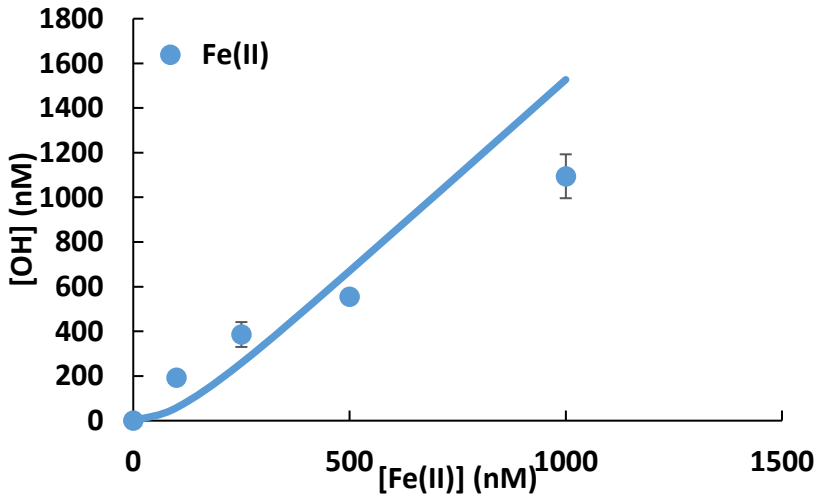

Figure 3.12. OH produced at two hours from Fe(II) and as a function of $[Fe(II)]_i$. Each filled data point represents the average of three measurements and error bars denote ±1σ. Lines are best fits of the data. Solid line indicates model fit with $k_{14} = 0.3\ M^{-1}s^{-1}$.

Best fits for k_{25}, k_{27}, k_{54} and k_{56} were determined by minimizing the cumulative percent error between the four experimental data points and model results as a function of the fitted rate coefficients, except where noted. Error estimates were derived from a 15% departure beyond the minimum error between experimental data and model results.

Reactions 27 and 56, the Cit-Fe(II) and SRFA-Fe(II)-mediated Fenton reactions ($Fe(II) + H_2O_2 \rightarrow Fe(III) + OH + OH^-$) respectively, are dominant for experiments with added 1 µM H_2O_2 and at low $[Fe(II)]_i$. Thus, k_{27} and k_{56} were fitted to experiments with added 1 µM H_2O_2 and low $[Fe(II)]_i$ (100 and 250 nM). For the Fenton reaction mediated by Cit-Fe(II), k_{27} of $(4.2 \pm 1.7) \times 10^3\ M^{-1}s^{-1}$ best fit experimental data. This is in excellent agreement with a k_{27} of $(4.9 \pm 0.3) \times 10^3\ M^{-1}s^{-1}$ reported by Rush et al. (1990)[175] for pH 7.2 and T = 25 °C. Pham et al. (2008)[46] reports a much higher value for k_{27}, $6.7 \times 10^6\ M^{-1}s^{-1}$ (pH = 6-8, I= 0 and T = 25.0 ± 0.6 °C) but noted their study was not very sensitive to this reaction. In the presence of SRFA, data are best fit by

adjusting k_{56} to $(4.3 \pm 1.4) \times 10^3$ $M^{-1}s^{-1}$ (Figs. 2 and 4). For k_{56}, Miller et al. (2012)[187] suggest 1.7×10^3 $M^{-1}s^{-1}$ at pH = 8 and I = 0. Differences in the SRFA-Fe(II) rate coefficients may be due to differences in pH, I and T (which Miller et al. (2012)[187] did not report).

Without added H_2O_2, the model is most sensitive to reactions 25 and 54, reduction of oxygen to superoxide. Thus, k_{25} and k_{54} were fitted to experiments absent external H_2O_2 after fitting k_{27} and k_{56} to the Fe(II)/SRFA-Fe(II) + 1 µM H_2O_2 system. Relative to inorganic Fe(II), chelation of Fe(II) by Cit also enhances the rate of O_2^- formation (k_{25}). We find that a k_{25} of 3.0 ± 0.7 $M^{-1}s^{-1}$ fits best with our experimental data, in very good agreement with two published values for k_{25}; Pham et. al (2008)[46] report $k_{25} = 2.9$ $M^{-1}s^{-1}$ for water at pH 6-8, I = 0 and T = (25 ± 0.6)ºC, and Rose et al. (2003)[188] report $k_{25} = 2.6$ $M^{-1}s^{-1}$ for seawater (pH 8.1, T= 25 ± 0.5 ºC).

The SRFA-enhanced superoxide formation reaction (R54) was investigated by Fuji et al. (2010),[90] using FA isolated from several soil samples, at pH 8.2, I = 0.73 and T = 25 ºC. They report a range for k_{54} from 5.6 – 52 $M^{-1}s^{-1}$. Miller et al. (2009)[189] found a value of 75 $M^{-1}s^{-1}$ for k_{54} for SRFA. Minimizing the k_{54} – dependent error between our modelled and measured values, we find two wells with similar minimum errors, one at 5.1 $M^{-1}s^{-1}$ and the other at 100 $M^{-1}s^{-1}$. The two values are associated with very different steady state H_2O_2 concentrations; ~200 nM (data not shown) and ~1.6 µM. Using the horseradish peroxidase method,[190] we measured H_2O_2 concentrations after two hours for Fe(II) and SRFA-Fe(II) in SLF, and found H_2O_2 to be ~150 nM, in agreement with the lower k_{54} and inconsistent higher value for this reaction (data not shown). The presence of a second minimum for the rate coefficient may possibly explain the high value reported by Miller et al. (2009).[189] The combination of the OH and H_2O_2 results

indicate the best-fit rate coefficient for the SRFA-Fe(II) mediated superoxide formation reaction is 5.1 ± 1.5 $M^{-1}s^{-1}$.

Fe(II) binding by both Cit and SRFA ligands accelerate both O_2^- formation and H_2O_2 destruction relative to Fe(II), interestingly, by very similar amounts; by factors of 34 - 78. As a result, the SRFA has a modest effect when compared to solutions with sufficient Cit to chelate Fe. Furthermore, there is evidence that GSH chelates and cycles Fe(III) to Fe(II),[184, 185] but relevant rate coefficients are not available. However, Charrier et al. (2011)[32] showed Asc and Cit drive OH production from Fe(II) (measured at 24 hours) while GSH had a negligible effect. Thus, it is reasonable to assume that the effect of GSH on Fe cycling is unimportant for our model.

Consistent with the thermodynamic model, the chemical kinetics model also predicts essentially no difference between 5 µg/mL SRFA and higher SRFA concentrations, a behavior that is not consistent with our experimental data. The simplest explanation of this phenomena is that the model does not accurately predict the distribution between active and inactive SRFA binding sites (distributions above). There are a number of sources of such an error, including the assumed $k_{53,}$ the rate of conversion of $SRFA_1$ to $SRFA_2$ (Table 3.1), the form of Fe(II) to which SRFA-Fe(III) is reduced to, and the number of SRFA binding sites, which depends on the assumed SRFA molecular weight; we assume a relatively low molecular weight of SRFA (750 g/mol).[187] Binding site estimates are on a molar basis in the kinetic literature, although as they are on a mass basis in the thermodynamic literature, the assumed molecular weight thus this does not explain the thermodynamic results. Constraining the problem further is worthy of more study.

Figures 3.11a and 3.11b show predicted concentration profiles for OH and H_2O_2 over two hours for 100 and 1000 nM Fe(II) with and without SRFA (without added H_2O_2). For 100 nM Fe(II), OH formation initially has an increasing slope, after which it approaches linearity as H_2O_2 approaches steady state. For 1000 nM Fe(II), H_2O_2 reaches a steady-state concentration within 30 minutes, after which OH production is linear. For both Fe(II) concentrations, H_2O_2 approaches steady-state concentrations of 200 nM and 250 nM for the Cit-Fe(II) and SRFA-Fe(II) system, respectively. For the SRFA-Fe(II) system, H_2O_2 decreases slightly after 60 minutes. The experimental data in Fig. 3.1 are consistent with the model; the slopes, while fit well with linear curves, exhibit slightly increasing slopes with time, and OH production is higher for the SRFA-Fe(II) system.

Figures 3.11c and 3.11d show concentration profiles for OH and H_2O_2 over two hours for 100 and 1000 nM Fe(II), with and without SRFA and with 1 µM added H_2O_2. In all cases with added H_2O_2, OH production is initially fast as there is excess H_2O_2 to be destroyed by Fe(II). OH production then approaches linearity as H_2O_2 reaches steady-state concentrations of 200 nM and 250 nM for the Cit-Fe(II) and SRFA-Fe(II) systems, respectively. H_2O_2 for the SRFA-Fe(II) system begins to slightly decrease after 60 minutes.

In both Cit-Fe(II) and SRFA-Fe(II) systems, H_2O_2 is ultimately limited by the reduction of O_2 to O_2^- (R14, R54). In SLF solutions, Asc is present to efficiently cycle Fe(III) to Fe(II), keeping the Fe(II)/Fe_{total} ratio high throughout (1.0 - 0.97 for Fe(II) and 1 - 0.88 for SRFA-Fe(II)). The system eventually leads to a balance of H_2O_2 production and consumption and consequently a linear OH production rate once the reactions reach steady state.

4. HULIS Enhancement of OH in Human Lung Fluids: Fulvic Acid-Fe(II) Complexes in Bronchoalveolar Lavage Fluids

4.1 Introduction

Particulate matter (PM) inhalation has been associated with increased mortality and the development of asthma, cancer, respiratory and cardiovascular diseases.[2, 191] Despite decades of research, the biological mechanisms associated with particle-induced diseases are still poorly understood. A hypothesized pathway for PM induced pathogenesis is the induction of oxidative stress initiated by an overproduction of reactive oxygen species (ROS).[7, 8] ROS are a class of highly reactive species that include superoxide (O_2^-), hydrogen peroxide (H_2O_2) and the hydroxyl radical (OH). In physiological systems, ROS are naturally formed by metabolic processes and are crucial for cellular signaling and homeostasis.[192] However, an overproduction of ROS can overwhelm antioxidant defenses and initiate oxidative stress.[160, 192] ROS can be generated directly by PM components or by cellular defenses in response to inhaled PM.[22, 26, 34] Of all ROS, OH is the most oxidizing and is capable of damaging proteins, lipids and DNA.[192] Due to the complexity of particle composition and experimental limitations, the mechanisms of OH generation from redox-active particle components under physiological conditions are poorly understood.

Inhaled PM first contacts the epithelial lung lining fluid where particle components can dissolve into the aqueous phase. To mimic physiological conditions of lung lining fluids, numerous studies have used acellular surrogate lung fluids (SLF) that typically contain physiological amounts of ascorbate (Asc), glutathione and uric acid.[32-34] Citrate is commonly added in SLF as a protein mimic, although it is not a component of lung lining fluid. While

convenient to use, the physiological relevance of SLF is limited due to a lack of relevant biomolecules. Only a small subset of studies have used SLF with phospholipids and proteins that better reflect the composition lung lining fluid.[24, 35, 36, 40, 41, 193]

Here we use bronchoalveolar lavage fluids (BALF) to better represent human lung lining fluids.[24] BALF is the supernatant remaining after centrifugal separation of the fluid from the bronchoalveolar lavage procedure.[41] Measurements on concentrated BALF from healthy young adults have suggested that *in vivo* alveolar lung lining fluid contains on average 4.8 mg/mL phospholipids, 14.3 mg/mL proteins, 100-200 μM each of ascorbate, glutathione and uric acid.[35, 41] The lipid fraction is 90% phosphatidylcholine, 9% Phosphatidylglycerol and 1% cholesterol by mass. The protein content on average is composed of 50% Albumin (Alb), 15% immunoglobulins, 7% Transferrin (Tf) and other proteins.[41] Due to the nature of collection, BALF can be 50 to 200 fold diluted compared to true physiological conditions; thus, the concentration of lipids, proteins and antioxidants are significantly diminished compared to *in vivo* lung lining fluid.[41] Furthermore, the protein content, lipid content and pH of BALF varies among patients.

Fe is generally the most abundant transition metal in particulate matter, it actively produces OH in SLF.[26, 32, 34, 194] Soluble Fe is an essential micronutrient crucial for normal cellular function. It is tightly regulated in part by proteins such that ROS formation is controlled or inhibited.[195, 196] In the presence of O_2 and biological reducing agents such as Asc, Fe(II) is capable of redox cycling and producing OH (R4.1-R4.4).[32, 34]

$$Fe(II) + O_2 \rightarrow O_2^- + Fe(III) \qquad R4.1$$

$$Fe(II) + O_2^- + 2\,H^+ \rightarrow H_2O_2 + Fe(III) \qquad R4.2$$

$$Fe(II) + H_2O_2 \rightarrow Fe(III) + OH^- + OH \quad \text{R4.3}$$

$$Asc^- + Fe(III) \rightarrow Asc^{\cdot} + Fe(II) \quad \text{R4.4}$$

Experimental studies utilizing both BALF and SLF have shown that Asc greatly enhances the ability of Fe to produce ROS, consistent with R4.1-R4.4 above, while other antioxidants have a much more minor impacts.[24, 32, 34] Sun et al. (2001)[24] used BALF to extract residual oil fly ash (8.5% transition metals, 50 μg/mL) and investigated ROS production.[24] They measured ROS formation indirectly using an ^{18}O labeling technique on 50 μg/mL residual oil fly ash extracts. Briefly, samples are exposed to $^{18}O_2$, incubated at 37 ºC for 24 hours and the amount ^{18}O incorporated into the sample was measured and used as a marker for ROS. The investigators observed ^{18}O incorporation was significant only when physiological amounts of Asc (284 μM) were added to BALF to account for dilution. No other antioxidants significantly impacted ^{18}O in corporation in BALF.[24] This is consistent with Charrier et al. (2011)[32] who found that Asc was 25 and 145 times as effective at promoting 24 hour OH formation from Fe(II) and Cu(II) respectively. While Asc readily promotes redox cycling of Fe, organic chelators and proteins can significantly alter reduction potential and the rate of ROS formation.[34, 49, 197]

The inorganic Fe(III)/Fe(II) couple has a relatively high reduction potential (+770 mV), and produces OH relatively slowly ($k_{4.1}$ ~0.1 $M^{-1}s^{-1}$, $k_{4.3}$ ~ 55 $M^{-1}s^{-1}$) at physiological pH.[34, 47, 48] Electrochemical studies have revealed that citrate, which is commonly used as a protein mimic in SLF can significantly reduce the reduction potential of the Fe(III)/Fe(II) redox couple, making Fe(II) more susceptible to oxidation by O_2 and H_2O_2.[50, 51] Consistent with this behavior, we previously showed that citrate enhances the rate constants of R4.1 and R4.3 by a factor of 34 and 76 respectively in an SLF at pH 7.2-7.4.[34] However, citrate is not present in physiological lung

fluid. Here we investigate the role of the most abundant iron-binding proteins in BALF, transferrin (Tf) and albumin (Alb).[41]

BALF contains significant amounts of immunoglobulin and other proteins, but since they have no known interactions with Fe, they are not included here. Alb and Tf are thought to inhibit ROS formation by chelating Fe species.[39, 52] Alb is thought to weakly and non-specifically chelate Fe(II), forming complexes that inhibit ROS generation while also scavenging ROS and sparing damage to more crucial biomolecules.[52, 53] Much of this evidence is based on non-specific ROS assays with varying protocols that did not probe fundamental ROS reactions or Fe speciation.[54-57]

Few measurements of binding constants between Fe and albumin are available in the literature. Xu et al. (2008)[58] suggested that bovine serum albumin (BSA) can complex Fe(III) ($\beta_{BSA\text{-}Fe(III)} = 2.9x10^7\ M^{-1}$) and also suggested that BSA enhanced iron redox cycling but did not provide rate constants or binding constants of Alb-Fe(II). To date, one measurement of binding between human serum albumin and inorganic Fe(II) has been reported; Duff et al. (2009)[198] used isothermal titration calorimetry and determined $\beta_{Alb\text{-}Fe} = 2.0 \times 10^4\ M^{-1}$ with a 1:1 stoichiometry (pH 6.4, T = 298 K).[198] Analogous to reactions of Cit-Fe and Fulvic Acid-Fe,[34] these reactions are described as follows:

$$Alb + Fe(II) \leftrightarrow Alb\text{-}Fe(II) \qquad R5.5$$

$$Alb\text{-}Fe(II) + O_2 \rightarrow Alb\text{-}Fe(III) + O_2^- \qquad R5.6$$

$$Alb\text{-}Fe(II) + H_2O_2 \rightarrow Alb\text{-}Fe(III) + OH^- + OH \qquad R5.7$$

We have been unable to find any investigations of OH formation kinetics from the interactions of Alb and inorganic Fe(II).

While Alb-Fe interactions are not well understood, the interactions of Tf and Fe are better characterized. Tf has two homologous pH-dependent Fe(III) binding sites, located at the N and C-terminals of the protein,[59, 60, 199] respectively, and carbonate or bicarbonate anions are necessary for Tf-Fe(III) binding.[60] Although both Fe(III) binding sites on Tf are homologous, experimental studies have shown differences in binding characteristics. The N-terminal binding site does not bind Fe(III) below pH 5.7, and the C-terminal binding site does not significantly bind Fe(III) below pH 4.8; both sites reach maximum iron binding capacity above pH 7.4.[59, 60] Fe(III) appears to bind preferentially to the N-terminal site of unsaturated Tf, especially when incubated at 37ºC.[200] Both binding sites appear to be independent of one another.[60] While the precise molecular dynamics of Tf-Fe(III) binding are not known, recent molecular dynamics simulations suggest pH changes that alter the protonation state of tyrosine residues at the binding site are a critical factor governing Tf-Fe(III) binding.[199, 201] Under endosomal pH (pH 4.5-6.5), protonation of tyrosine residues induces conformational changes that form an "open" Tf, facilitating Fe(III) release.[199, 201]

Electrochemical studies have shown that Tf bonds Fe, significantly reducing the redox potential of the Fe(III)/Fe(II) couple, moving it outside of the range accessible by biological reducing agents (-400 to -500 mV).[39, 59, 61, 62] This inhibits reduction of the Tf-$(Fe(III))_2$ thereby inhibiting OH generation via R4.1-R4.4. Despite Tf's high affinity for Fe, studies have revealed that external chelating agents can compete for Fe binding with Tf and enhance ROS generation.[65, 202] It has been suggested that chelators can mobilize Fe away from Tf, and

depending on the nature of the ligand, promote Fe mediated ROS formation (R4.1-R4.4).[63, 203] In fact, Abdizadeh et al. (2017)[199] performed molecular dynamics simulations that indicate external chelators are necessary for Fe release by Tf.

The Fe species that are not bound to Tf in physiological systems (including that bound by albumin) are commonly referred to as non-transferrin bound iron (NTBI). NTBI have been associated with Fe toxicity, oxidative stress and inflammation.[63-65] It has been suggested that Fe bound to Alb can act as a form of ROS active NTBI, but the impact of Alb and Tf on Fe-mediated OH generation under physiologically relevant conditions, the subject of this work, has not been investigated.

Inhaled PM can introduce humic-like substances (HULIS) that can chelate iron and alter Fe speciation and OH generation,[34, 88] potentially serving as a source of NTBI. HULIS are complex organics commonly identified in biomass burning and cigarette smoke particles.[34, 71] HULIS is chemically similar to humic and fulvic acids found in aquatic and terrestrial systems.[71] Both HULIS and humic substances have organic functional groups (carboxylates, phenols, ketones) that are known to chelate Fe in acidic and physiologically relevant solutions.[34, 71, 165] In general, HULIS has lower molecular weight, aromaticity and acid characteristics than humic and fulvic acids.[71] However, due to a lack of HULIS reference material, numerous studies have used humic or fulvic acid as a HULIS surrogate. In this work, we use Suwanee River Fulvic Acid (SRFA) as a substitute for HULIS due to similar molecular weight and solubility. Only a small handful of studies have investigated HULIS under physiological conditions.

In previous work we used SLF containing, 0.1-1 µM Fe(II), 0- 20 µg/mL SRFA and physiological amounts of Asc, glutathione, uric acid and citrate (100-300 µM) to investigate Fe-

mediated OH generation.[34] SRFA was found to chelate Fe(II) and enhance rates of Fe(II) mediated O_2 reduction and H_2O_2 decomposition by factors of 58 to 78, thereby enhancing OH generation over two hours (R4.8-R4.10).

$$SRFA + Fe(II) \leftrightarrow SRFA\text{-}Fe(II) \quad \text{R4.8}$$

$$SRFA\text{-}Fe(II) + O_2 \rightarrow SRFA\text{-}Fe(III) + O_2^- \quad \text{R4.9}$$

$$SRFA\text{-}Fe(II) + H_2O_2 \rightarrow SRFA\text{-}Fe(III) + OH^- + OH \quad \text{R4.10}$$

Using the same SLF formulation, Wei et al. (2018)[204] used the terephthalate probe to investigate OH generation from 1 µM Fe(II) and 10µg/mL SRFA over 1.3 hours. In agreement with our previous work, Wei et al. (2018)[204] suggests that SRFA enhances R1 and R3 but provides no kinetic rate constants. Yu et al. (2018)[108] simultaneously measured DTT consumption and OH generation from interactions of isolated ambient HULIS and SRFA with 1 µM Fe(II) in a phosphate buffer over 1.3 hours. They found that both isolated ambient HULIS and 5 µg/mL SRFA enhance OH generation from Fe(II), although they did not report the mass of isolated HULIS or the PM from extracted filters. These results indicate both HULIS and SRFA enhance OH generation by interacting with Fe(II).

Only a small handful of studies have investigated the biological effects of combinations of HULIS or SRFA with Fe. Two early studies investigated the role of coal dust and tobacco smoke derived HULIS and Fe on OH generation in human lung cell cultures and tissues in vitro.[87, 88] Measuring the oxidation products of 2-deoxy-D-ribose as a probe for OH generation, Ghio et al. (1994)[87, 88] found that the strong iron chelator deferoxamine inhibited formation of the oxidation products in both lung cell cultures

exposed to coal dust HULIS and human lung tissue exposed to tobacco smoke HULIS, implicating HULIS-Fe catalyzed OH generation. Both studies observed increasing Fe accumulation, collagen deposition and 2-deoxy-D-ribose oxidation products with increasing HULIS concentrations in the biological samples.[87, 88] However, the 2-deoxyribose assay does not directly quantify OH concentrations, and thus is limited in elucidating fundamental ROS reactions.

More recently, atmospheric particles containing HULIS and soil-derived humic substances have been proposed to induce lung injury and diseases by disrupting cellular Fe homeostasis.[195, 205] In this model, inhaled HULIS and fulvic acid deposits in the alveoli, which is followed by endocytosis by epithelial lung cells, then proceed to complex cellular Fe. This results in a HULIS/fulvic acid-induced functional Fe deficiency that if not resolved leads to oxidative stress, activation of kinases and transcription factors that release proinflammatory mediators.[87, 88] Complicating the role of HULIS/Fulvic Acid-Fe mediated ROS generation, Ghio et al. (2016),[195] used the Amplex Red assay to measure H_2O_2 generation in human bronchial epithelial cells exposed to HULIS containing wood smoke particles with and without ferric ammonium citrate. The investigators observed that H_2O_2 generation was decreased in cells that were exposed to the combination containing Fe. They suggest the extra Fe loading resolves the functional iron deficiency and thus decreases H_2O_2 generation and inflammatory response. One reason for lower H_2O_2 generation could be due to the ability of HULIS-Fe to degrade H_2O_2 more efficiently than other forms of Fe in the cell. However, this may not account for the decrease in inflammatory mediators released with extra Fe loading. Thus, it is not clear what the role

HULIS complexation of cellular Fe has on ROS generation, meriting further investigation of HULIS-Fe mediated ROS formation in the presence of biological Fe chelators and reductants. In any case, these studies suggest that Fe binding by external ligands and subsequent ROS generation plays an important, if not well-defined role.

In this work, we investigate OH generation from a series of systems to elucidate the interactions of iron-binding proteins present in lung fluid, SRFA and Fe in producing OH radicals. We use either the BALF supernatant or the saline used to obtain the BALF, with known amounts of added Alb and Tf. This saline has a pH of 5.5. Because ascorbate (Asc) is a critical reductant in lung lining fluids and in cells, but it has been depleted in BALF, physiological levels of Asc are added to both saline and BALF. We investigate the kinetics of Fe(II)-mediated OH generation from Alb/Tf mixtures, Fe and SRFA, all individually and in combination for a range of ratios of Alb:Tf:SRFA at constant Fe. Finally, we compare these results to OH generation from Fe(II)/SRFA-Fe(II) in BALF to investigate the role of metal binding proteins and SRFA in human lung lining fluids.

4.2 Materials & Methods

4.2.1 Materials

$FeSO_4 \cdot 5H_2O$ (Arcos, 99%), NaCl (Sigma, 99%), human albumin (Sigma, 98%), human apo-transferrin (Sigma, 98%), SRFA Standard II (International Humic Substances Society), L-ascorbate sodium salt (Sigma, 99%), terephthalate sodium salt (TCI, 99%), 2-hydroxyterephthalate (TCI, %). Saline Solution (0.9%), Microcentrifuge tubes, Water Bath (Isotemp 2025, Fischer Scientific), pH probe (HANNA Instruments, HI 3220).

Table 4.1 Summary of protein content and pH of BALF used for experiments.

BALF #	Date Collected	pH	Total Protein (µg/mL)	Estimated Albumin (µg/mL)	Estimated Transferrin (µg/mL)
3	10/3/2016	6	132	66	9.24
4	10/31/2016	6	140	70	9.8
5	12/2/2016	6	192	96	13.44
6	9/19/2016	6.3	124	62	8.68
7	9/2/2016	5.8	157	78.5	10.99
8	11/7/2016	6.1	130	65	9.1
10	9/26/2016	4.7	136	68	9.52
11	12/5/2015	6.2	128	64	8.96

BALF from 8 healthy patients and their corresponding total protein concentrations (41 – 192 µg/mL) were obtained by Andrew J. Ghio (EPA/UNC Chapel Hill). Alb and Tf concentrations in BALF were estimated to range from (20 – 100) µg/mL and (3 – 13.5) µg/mL respectively. These ranges were estimated by assuming that total BALF protein concentrations are composed of 50% and 7% Alb and Tf respectively.[41] Data for total protein content, estimated Alb/TF concentrations and pH of BALF used are shown in Table 4.1.

4.2.2 Cleaning Protocol and Stock Solutions

In order to avoid contamination a rigorous cleaning protocol was adapted from Kuang et al. (2017).[206] 2 mM stock solutions of $FeSO_4$ are prepared a pH 3.5 solution and diluted to 20 µM daily. 1 mg/mL stock solutions of SRFA are prepared in saline solution and refrigerated for up to a month between uses. 100 mM terephthalate solutions are prepared in saline solution and are refrigerated for up to a month. 1 mM stock solutions of hTA were prepared in DI water and refrigerated in the dark. pH 6.5 saline solutions (0.9%) are prepared by combining 9 g NaCl in 1

L of milli-Q water (18 MΩ). The pH is adjusted by adding drops of 0.1 M NaOH and measured using a pH probe (HANNA Instruments, HI 3220).

4.2.3 OH Generation from Fe(II) and SRFA-Fe(II) in BALF

To probe SRFA-Fe(II) mediated-OH formation in BALF, 10 mM terephthalate, SRFA (0, 10, 20, 30, 40, 50 µg/mL), 200 µM Asc and 1 µM $FeSO_4$ were added to BALF. Samples are prepared at a final volume of 1 mL in 1.5 mL microcentrifuge tubes. $FeSO_4$ was added immediately prior to analysis and measurements are made after 2 hours of incubation at $37^{O}C$ +/- 0.5. The Fe(II) concentration was chosen to match he lower range of clinical NTBI concentrations ([Fe] = 1 – 10 µM).[207]

4.2.4 Quantification of OH Radicals with the Terephthalate Probe

OH radicals react with terephthalate to produce the fluorescent 2-hydroxyterephthalate (hTA) molecule with a pH dependent yield.[111, 208] Fluorescence of hTA is measured at 320 nm/420 nm wavelengths using a Lumina fluorescence spectrometer (Lumina Thermo Scientific). 50-800 nM hTA calibration curves were prepared daily either in DI water (pH 5.5) or in a pH 6.5 NaCl solution (0.9% saline), depending on which solution is used for the day of the experiment. There were no significant differences in hTA calibration slopes prepared in pH 5.5 DI water, pH 5.5 saline and pH 6.5 saline. For experiments in BALF, a calibration curve in pH 5.5 DI water is used with pH specific yield of hTA to calculate OH concentrations.

The native fluorescence of SRFA interferes with measurements of hTA but this effect is negligible at [SRFA] = 5 µg/mL.[34] Samples containing SRFA were diluted to 5 µg/mL before measurements. hTA calibrations containing 5 µg/mL SRFA were used to calculate OH concentrations from samples containing SRFA.

4.2.5 Impact of Albumin and Transferrin on Fe(II) and SRFA-Fe(II) Mediated OH Formation

To investigate the interplay between Alb, Tf and SRFA with respect to their impact on Fe-mediated OH generation, SRFA (0, 10, 20, 30 µg/mL), 1 µM $FeSO_4$ and 200 µM Asc were combined in a 0.9% saline solution with or without Alb and Tf. Three sets of experiments were performed: (1) SRFA, $FeSO_4$ and Asc in saline solutions. Blanks consisted of (Asc) or (SRFA + Asc) absent of Fe(II) (2) SRFA, $FeSO_4$ and Asc combined in saline solutions containing only Alb. Blanks consisted of (Asc + Alb) or (Asc + Alb + SRFA) absent of Fe(II). (3) SRFA, $FeSO_4$ and Asc in solutions containing Alb and Tf at a fixed [Alb]/[Tf] ratio of 7.14.[41] Blanks consisted of (Asc + Alb + Tf) or (Asc + Alb + Tf + SRFA) absent of Fe(II) . A full summary of blanks, samples and concentrations of reagents are shown in Table 4.2.

Table 4.2. Summary of reagents used for different experiments.

Experiment	**Samples**	**Blanks**	**[Asc] µM**	**[Fe(II)] µM**	**[SRFA] µg/mL**	**[Alb] µg/mL**	**[Tf] µg/mL**
1	Asc, $FeSO_4$, SRFA	Asc, SRFA	200	1	0 ,10, 20, 30		
2	Asc, $FeSO_4$, Alb, SRFA	Asc, Alb, SRFA	200	1	0 ,10, 20, 30	20-500	
3	Asc, $FeSO_4$, Alb, Tf, SRFA	Asc, Alb, Tf, SRFA	200	1	0 ,10, 20, 30	20-500	2.8-70

In all experiments, components were added in sequential order as saline solution, terephthalate, Alb, Tf, and SRFA. $FeSO_4$ immediately prior to incubation. Triplicate blanks and

samples were prepared in 1.5 mL microcentrifuge tubes with a final volume of 1 mL followed by incubation at 37°C for 2 hours before measurement. Experiments were carried out in pH 5.5 and pH 6.5 saline in order to capture the pH range observed in BALF (pH = 4.7 – 6.4, Table 4.1).

4.2.6 Kinetic Analysis of OH Generation from Fe(II), Alb-Fe(II) and SRFA-Fe(II) in pH 5.5

We performed time dependent measurements of OH generation from individual and combinations of Fe(II), SRFA, and Alb in pH 5.5 saline to estimate rate constants of O_2^- formation (k_1, k_6 and k_9). First, individual systems of Fe(II), Alb-Fe(II) and SRFA-Fe(II) with 200 µM Asc were probed for OH generation kinetics over two hours. From this data we estimated k_1, k_6 and k_9 individually. We then performed experiments measuring of two hour [OH] from the combination of Fe(II), SRFA, Alb and 200 µM Asc in pH 5.5 saline at 37°C and developed a kinetic equation to predict OH generation.

4.3 Results and Discussion

4.3.1 Individual Impact of Alb and Tf on Fe(II) Mediated OH Generation

Figure 4.1 shows $[OH]_{2hr}$ as a function of [Alb] for 1 µM Fe(II) and 200 µM Asc in pH 5.5 saline solution. Intercepts indicate $[OH]_{2hr}$ from Fe(II) absent of proteins. The addition of Alb alone enhances $[OH]_{2hr}$ by Fe(II) from 160 nM to a maximum of 590 nM ([Alb] = 500 µg/mL) in a nearly linear manner (Figure 4.1 blue circles).

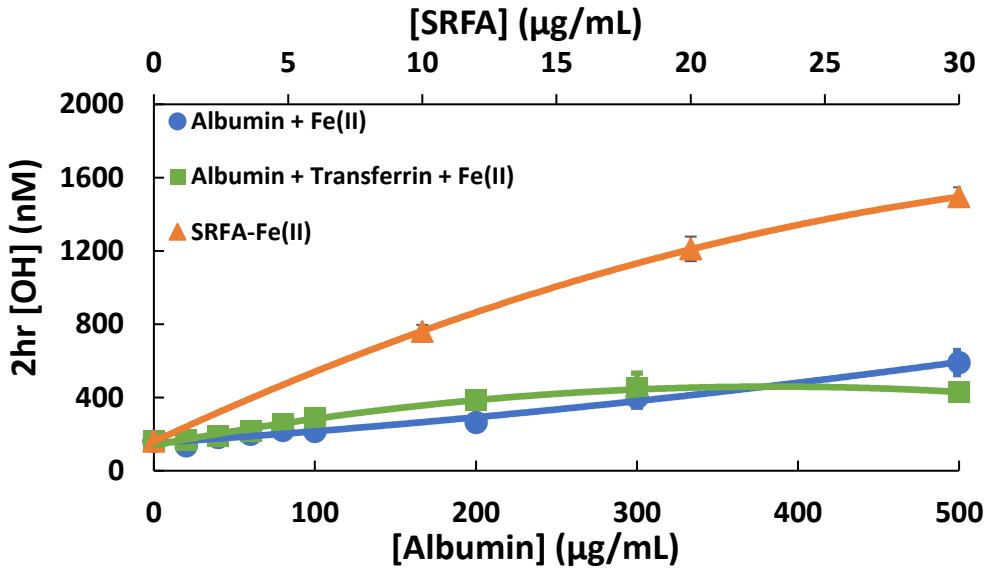

Figure 4.1. $[OH]_{2hr}$ as a function of [Alb] from pH 5.5 solutions containing Fe(II) and Alb (blue circles) and Fe(II), Alb and Tf (orange) Samples containing Tf had a fixed [Alb]:[Tf] of 7.1. The orange triangles indicate $[OH]_{2hr}$ from Fe(II) as a function of [SRFA] in pH 5.5 (secondary axis).

Relative to inorganic Fe(II) alone, Alb and Tf together, in their physiological ratio of 7.14 ([Alb]:[Tf]), enhanced $[OH]_{2hr}$ from 160 nM up to 432 nM when [Alb] = 500 µg/mL and [Tf] = 70 µg/mL (Figure 4.1, green squares). However, this enhancement plateaus when [Alb] = 300 µg/mL and [Tf] = 42 µg/mL. Similar behavior is observed at pH 6.5, as Alb and Tf linearly increased $[OH]_{2hr}$ by Fe(II) from 191 nM to by maximum of 653 nM when [Alb] = 500 µg/mL and [Tf] = 70 µg/mL (Figure 4.2, blue circles). Tf on its own did not show any ability to enhance OH generation in the1 µM Fe(II) in pH 5.5 solution suggesting that Alb is responsible for OH enhancement from Fe(II). This enhancement in OH generation is likely due to the ability of Alb to chelate Fe and enhance Fe(II) oxidation as suggested by Xu et al. (2008).[58] Tf potentially attenuates the enhancement OH generation by Alb-Fe(II) (Figure 4.1 green curve). This could be due to the ability of Tf to bind Fe(III) species and form complexes that cannot be reduced by Asc, effectively removing Fe species from being redox cycled by R4.1-R4.4.[39, 59, 61, 62]

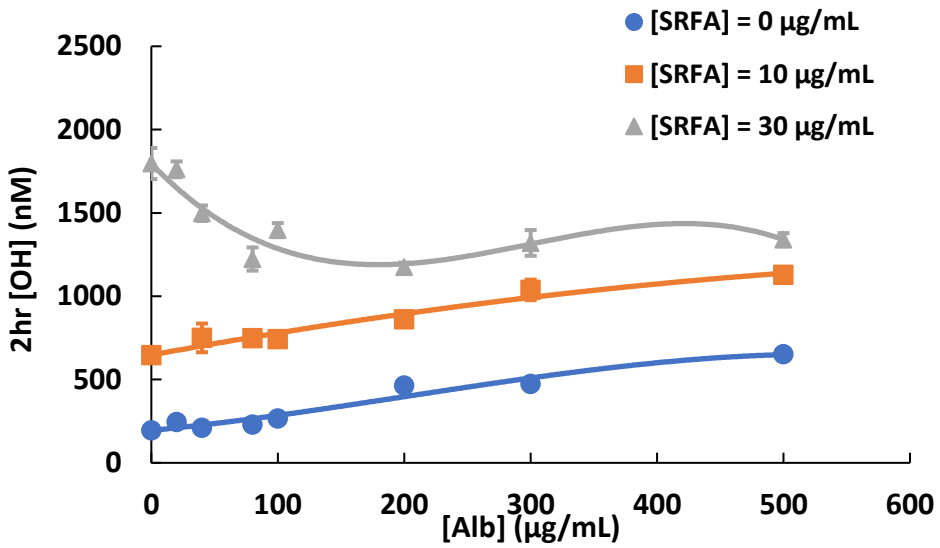

Figure 4.2. 2 hour [OH] generation from 1 µM Fe(II) in solutions containing Alb and Tf (blue circles) and solutions containing Alb, Tf and SRFA (Orange circles and grey squares) in pH 6.5 saline. Data points indicate average of three measurement and error bars indicate range of measured values. Solid lines indicate best fit curves through experimental data.

4.3.2 SRFA-Fe(II) Mediated OH Generation

For pH 5.5 solutions containing SRFA-Fe(II), SRFA enhanced $[OH]_{2hr}$ from 160 nM when [SRFA] = 0 µg/mL up to 1494 nM OH when [SRFA] = 30 µg/mL (Figure 4.1, orange triangles). Time dependent measurements in Figure 4.3 show that Fe(II) and SRFA-Fe(II) systems in pH 5.5 linearly produce OH over two hours. SRFA enhanced the rate OH generation from 1 µM Fe(II) from 1.37 nM/min to a maximum of 12.6 nM/min at [SRFA] = 30 µg/mL (Figure 4.3, slopes). Similarly in pH 6.5, 10 µg/mL SRFA enhanced the initial rate of OH generation by 1 µM Fe(II) from 3.90 nM/min to 8.42 nM/min (Figure 4.4), although OH generation in pH 6.5 is not completely linear over the entire two hours of measurement.

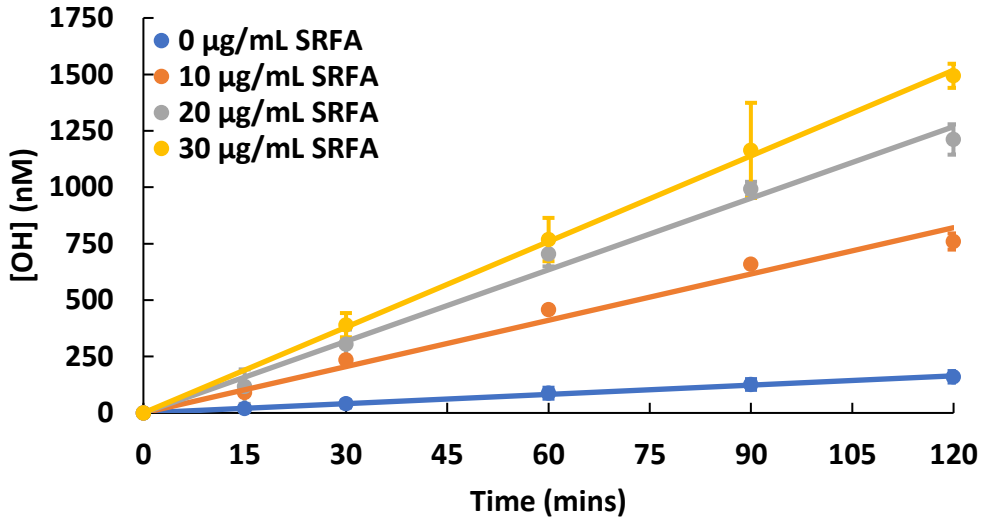

Figure 4.3. Kinetics of OH generation from 1 µM Fe(II) (blue) and Fe(II) + SRFA (Orange squares, grey diamonds and yellow triangles) with 200 µM Asc in pH 5.5 Saline. T = 37^{O}C. Data points indicate average of three measurements and error bars are range of measured values. Curves indicate best fit curve through experimental data.

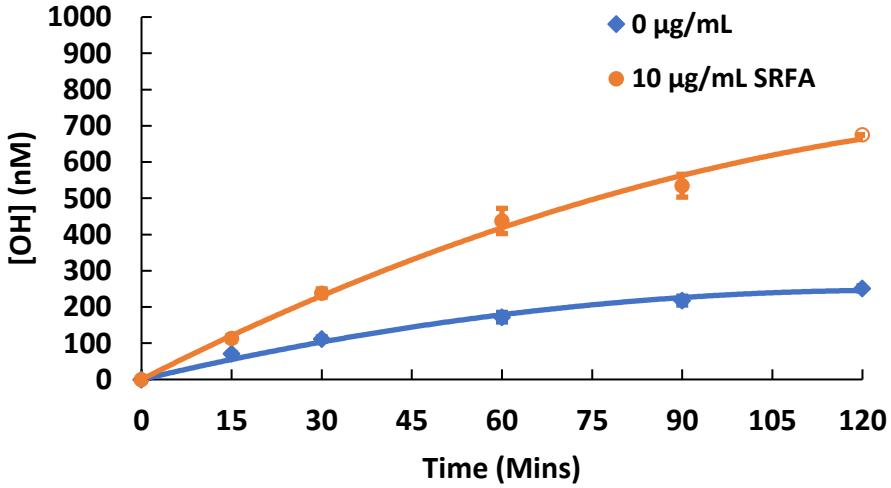

Figure 4.4. Kinetics of OH generation from 1 µM Fe(II) (blue diamonds) and 10 µg/mL SRFA (orange circles) in pH 5.5 Saline. T = 37^{O}C. Data points indicate average of three measurement and error bars indicate range of measured values. Solid lines indicate best fit curves through experimental data. The open circle indicated a single measurement.

Initial rates for OH generation from Fe(II) and are 2.8X higher in pH 6.5 (3.90 nM/min) than in pH 5.5 (1.37 nM/min). OH generation rates for Fe(II) and [SRFA] = 10 µg/mL are moderately higher in pH 6.5 (8.42 nM/min) than in pH 5.5 (6.84 nM/min). SRFA enhanced $[OH]_{2hr}$ by Fe(II) from 191 nM up to 1796 nM when [SRFA] = 30 µg/mL in pH 6.5 (Fig 4.2, intercepts). We did not measure kinetic data for 1µM Fe(II) and 30 µg/mL SRFA in pH 6.5. These results suggest that SRFA significantly enhances OH generation from Fe(II) in both pH 5.5 and 6.5, with a moderately higher enhancement in pH 6.5.

4.3.3 Impact of Albumin and Transferrin on SRFA-Fe(II) Mediated OH Generation

Figures 4.5 and 4.2 show $[OH]_{2hr}$ as a function of [Alb] concentration from 1 µM Fe(II) and varying [SRFA] with and without Alb and Tf in their physiological ratios ([Alb]:[Tf] = 7.14) in pH 5.5 and pH 6.5 respectively.

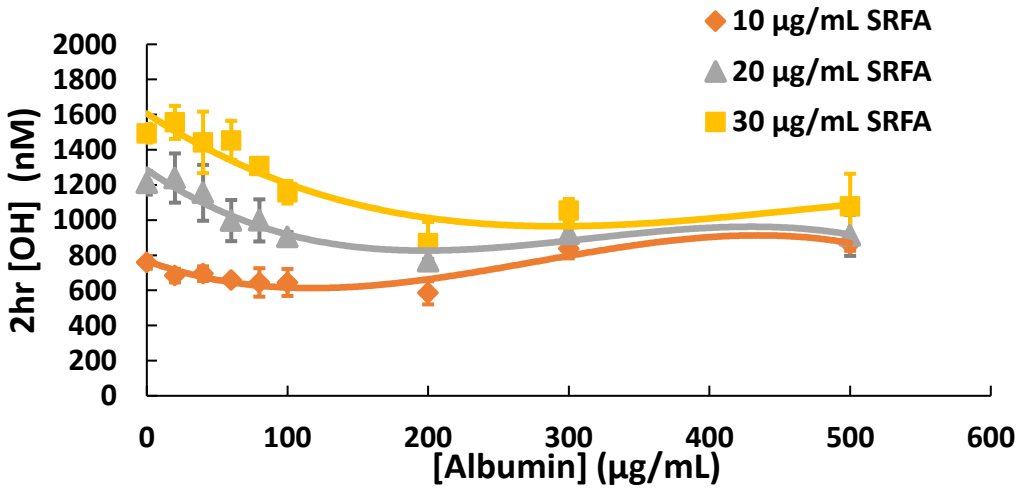

Figure 4.5. 2 hour [OH] generation as a function of albumin concentrations from 1 µM Fe(II) and varying amounts Alb, Tf and SRFA (Orange diamonds, grey triangles and yellow squares) in pH 5.5 saline. Samples containing Alb and Tf had a fixed [Alb]:[Tf] of 7.14. Data points indicate average of three measurements and error bars are range of measured values. Curves indicate best fit curve through experimental data.

In pH 5.5, Alb and Tf moderately decreases $[OH]_{2hr}$ from 10 µg/mL SRFA and 1 µM Fe(II) with increasing protein concentrations, from $[OH]_{2hr}$ = 795 nM absent of proteins to a minimum of 586 nM OH around [Alb] = 200 µg/mL. When [SRFA] = 20 µg/mL, Alb and Tf decreased $[OH]_{2hr}$ by Fe(II) from 1212 nM to a minimum of 765 nM when [Alb] = 200 µg/mL and [Tf] = 28 µg/mL. When [SRFA] = 30 µg/mL, Alb and Tf decreases $[OH]_{2hr}$ by Fe(II) from 1494 nM to a minimum of 868 nM when [Alb] = 200 µg/mL and [Tf] = 28 µg/mL. Curiously in all cases, increasing protein concentrations beyond [Alb] = 200 µg/mL slightly increases $[OH]_{2hr}$ for samples in pH 5.5. In contrast to the decreases in $[OH]_{2hr}$ observed for pH 5.5, in pH 6.5 Alb and Tf increased $[OH]_{2hr}$ by 10 µg/mL SRFA + 1 µM Fe(II) from 647 nM to a maximum of 1128 when [Alb] = 500 µg/mL and [Alb] = 70 µg/mL (Figure 4.2, Orange Squares), in a linear fashion. When [SRFA] = 30 µg/mL, Alb and Tf decreases $[OH]_{2hr}$ generation from 1796 nM to a minimum of 1175 nM OH at [Alb] = 200 µg/mL. Increasing protein concentrations beyond this slightly increases $[OH]_{2hr}$, as was observed for pH 5.5.

To analyze data from these various systems, we define a quantity called the "SRFA Enhancement Factor" (EF_{SRFA}) which is the ratio of two hour OH generation from the SRFA-Fe(II) system to the Fe(II) system in the particular solution being investigated (Eqn. 4.1). EF_{SRFA} is used to understand OH generation trends arising from interactions of SRFA, Alb, and Tf with Fe(II).

$$\boldsymbol{EF_{SRFA} = \frac{[OH]_{2hr,Fe(II)+SRFA}}{[OH]_{2hr,Fe(II)}}} \qquad \textbf{(Eqn. 4.1)}$$

Using a rate limiting approximation we derived an expression for EF_{SRFA} using appropriate binding constants $k_{4.1}$, $k_{4.6}$ and $k_{4.9}$ (Eqn. 4.2). Predictions from Eqn. 4.2 are compared to

experimental data to test the validity of the rate limiting approximation and estimated rate constants. SRFA-Fe(II) binding is defined by a single carboxylate binding site with a $\beta_{SRFA\text{-}Fe(II)}$ = 9.5 x 10^3 M^{-1} (Visual MINTEQ 3.1). Alb-Fe(II) binding is described by a single Fe(II) binding site with a $\beta_{Alb\text{-}Fe(II)}$ = 2.0 x 10^4 M^{-1} as determined by Duff et al. (2009)[198] (pH 6.4, 25^{O}C). [SRFA] and [Alb] are calculated by using molar masses of 750 g/mol and 66.5x10^3 g/mol respectively.

$$\frac{[OH]_{2hr,Fe(II)+Alb+SRFA}}{[OH]_{2hr,Fe(II)+Alb}} = 1 + \frac{\left(\frac{k_9\beta_{(SRFA-Fe)}}{k_1}\right)[SRFA]}{1+\left(\frac{k_6}{k_1}-1\right)\beta_{(Alb-Fe)}[Alb]} \qquad \textbf{(Eqn. 4.2)}$$

Figure 4.6 and 4.7 shows EF_{SRFA} as a function of total protein mass for solutions containing Fe(II), SRFA, Alb and Tf in pH 5.5 and pH 6.5 respectively.

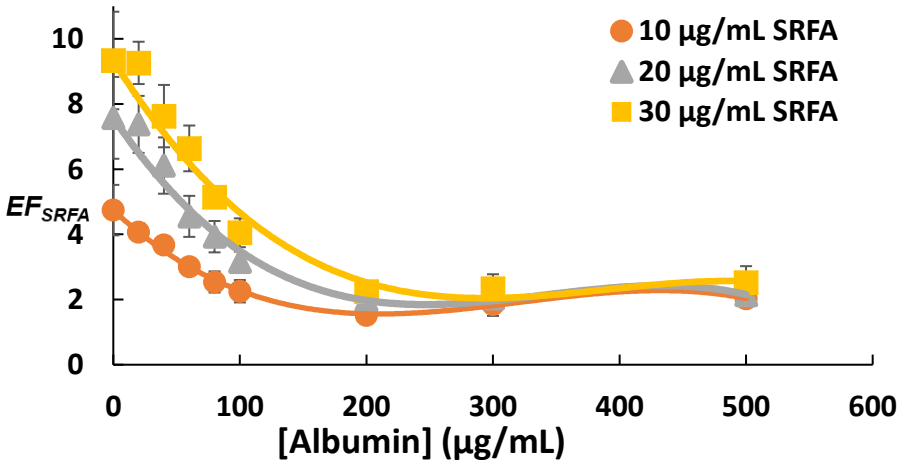

Figure 4.6 Enhancement factor (EF_{SRFA}) of the solution containing SRFA, Fe(II), Alb and Tf relative to the solution with Fe(II), Alb and Tf as function of [Alb] in pH 5.5 ([Alb]:[Tf] = 7.14 in all samples). Intercepts indicate enhancement of OH from Fe(II) by SRFA absent of proteins. Data points indicate average of three measurement and error bars indicate error propagation values. Solid lines indicate best fit curves through experimental data.

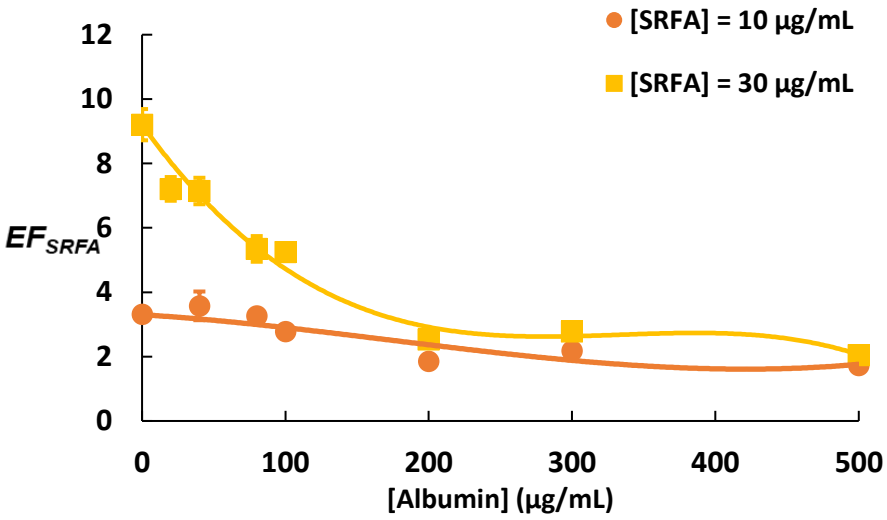

Figure 4.7 Enhancement factor (EF_{SRFA}) of the solution containing SRFA, Fe(II), Alb and Tf relative to the solution with Fe(II), Alb and Tf as function of [Alb] in pH 6.5 ([Alb]:[Tf] = 7.14 in all samples). Intercepts indicate enhancement of OH from Fe(II) by SRFA absent of proteins. Data points indicate average of three measurement and error bars indicate error propagation values. Solid lines indicate best fit curves through experimental data.

Intercepts indicate EF_{SRFA} due to SRFA-Fe(II) interactions absent of proteins. In pH 5.5 saline, the presence of 10, 20 and 30 µg/mL SRFA absent proteins enhances increases $[OH]_{2hr}$ from 1 µM Fe(II) by an EF_{SRFA} of 4.7, 7.6 and 9.3 respectively (Figure 4.6 intercepts). Increasing the concentration of Alb and Tf reduces EF_{SRFA} to a minimum of 2, 2.1 and 2.5 for 10, 20 and 30 µg/mL SRFA respectively. In pH 6.5, 10, and 30 µg/mL SRFA enhances $[OH]_{2hr}$ from 1 µM Fe(II) by 3.3, and 9.2 respectively (Figure 4.7 intercepts). Increasing the concentration of Alb and Tf reduces EF_{SRFA} to a minimum of 1.7 and 2.0 for 10 and 30 µg/mL SRFA respectively (Figure S5). For [SRFA] = 10 µg/mL, EF_{SRFA} is 42% higher in pH 5.5 (EF_{SRFA} = 4.7) than in pH 6.5 (EF_{SRFA} = 3.3), whereas EF_{SRFA} are nearly identical at both pH 5.5 and 6.5 at [SRFA] = 30 µg/mL.

Figure 4.8 show the EF_{SRFA} as a function of the SRFA:Protein mass ratio for all OH measurements from Fe(II), Alb, Tf and SRFA in pH 5.5 and pH 6.5. For both curves, intercepts are forced through 1 as shown by Equation 2 when [SRFA] = 0 µg/mL. In pH 5.5 saline, increasing SRFA enhances $[OH]_{2hr}$ from 1 µM Fe(II) by up to an EF_{SRFA} of 9.3 when the SRFA:Protein mass ratio is 1.3 (Figure 4.8 blue curve). In pH 6.5 saline, the SRFA enhancement ratio plateaus at an EF_{SRFA} of 7.2 when the SRFA:Protein mass ratio is 0.66 (Figure 4.8 red curve). The increase in EF_{SRFA} with increasing SRFA:Protein indicates that SRFA is capable of enhancing OH generation. This is likely due to the ability of SRFA to competitively chelate Fe species from Alb and Tf and form complexes that are more ROS active than Fe bound to Alb or Tf. The Fe binding capacity of Tf increases with increasing pH, reaching full binding capacity at pH > 7.4. [59, 60] This is likely due to deprotonation of tyrosine residues that induce conformational changes favoring Fe(III) binding.[199, 201]

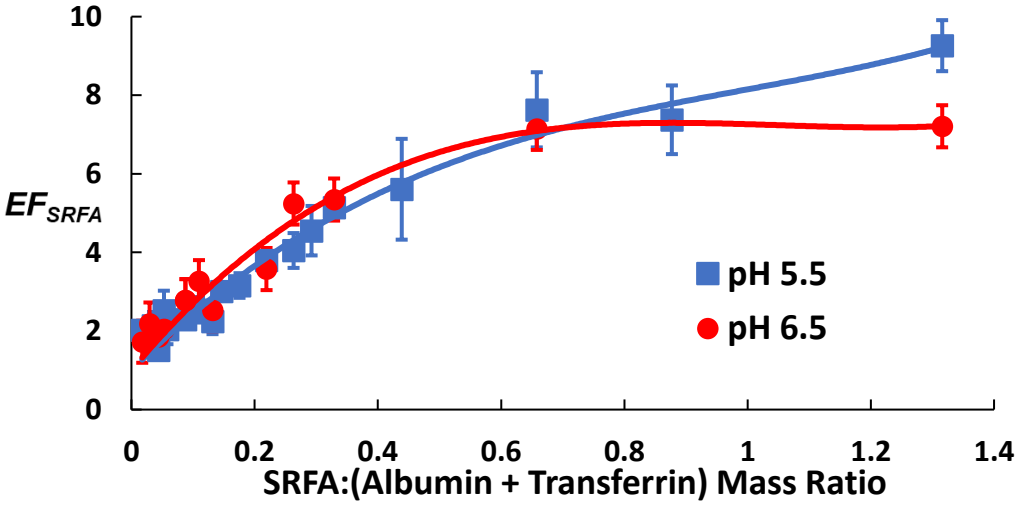

Figure 4.8 Enhancement factor (EF_{SRFA}) of the solution containing SRFA, Fe(II), Alb and Tf relative to the solution with Fe(II), Alb and Tf as function of SRFA:(Alb + Tf) ratio in pH 5.5 and pH 6.5 saline. Data points indicate average of three measurements and error bars error propagation values. Curves indicate best fit curve through experimental data.

Thus, Tf would is a more efficient Fe chelator at pH 6.5 than in pH 5.5. The EF_{SRFA} plateau observed in pH 6.5 is likely due to the enhanced ability of Tf to chelate Fe(III) with increasing pH.[59] Thus at pH 6.5, Tf likely removes Fe species from being redox cycled by Asc to a greater degree than in pH 5.5, potentially accounting for the higher EF_{SRFA} in pH 5.5 solutions. To probe this behavior further, we investigate the OH generation kinetics of Fe(II), Alb-Fe(II) and SRFA-Fe(II).

4.3.4 Kinetics of OH Generation from Fe(II), Albumin-Fe(II) and SRFA-Fe(II)

We investigated the individual impact of SRFA, Alb and Tf on Fe(II) mediated OH generation and estimated rate constants for k_1, k_6 and k_9 from kinetic and $[OH]_{2hr}$ data. Briefly, we assume that Asc quickly reduces any Fe(III) species, so that [Fe(II)] is essentially constant. In all cases we assume that reduction of O_2 by Fe(II) and the following reactions of O_2^- and H_2O_2 are the dominant source of OH (R4.1, R4.6, R4.9). From these assumptions we derive rate equations that can be used to calculate rate constants from time dependent [OH] data and binding constants. Rate constants estimated using this analysis and binding constants used are shown in Table 4.3.

Table 4.3. Summary of estimated rate constants from different experimental systems with 200μM Asc in pH 5.5 saline, T = 37^{O}C. Binding constants used were $\beta_{Alb\text{-}Fe(II)} = 2.0\times10^4\ M^{-1}$ from Duff et al. (2009) and $\beta_{SRFA\text{-}Fe(II)} = 9.5\times10^3\ M^{-1}$ from Visual MINTEQ 3.1.

Reaction	Binding Constant (M^{-1})	Rate Constant ($M^{-1}s^{-1}$)
$k_{4.1}$ Fe(II) + O_2		$(10.0 \pm 0.1)\times10^{-2}$
$k_{4.6}$ Alb-Fe(II) + O_2	2.0×10^4	(1.8 ± 0.1)
$k_{4.9}$ SRFA-Fe(II) + O_2	9.5×10^3	(2.7 ± 0.3)

The blue curve in Figure 4.3 shows the kinetics of OH generation from 1 µM Fe(II) in pH 5.5 saline absent of any chelators. Over two hours, OH is generated linearly at a rate of 1.37 nM/min. Absent of external H_2O_2, Fe(II) mediated OH formation is rate limited by on the reaction of Fe(II) with O_2 (R4.1) since O_2^- must be converted to H_2O_2 (R4.2) before OH formation occurs (R4.3).[34] Thus we assume that the rate limiting step for this system is R1 and from data in figure 2 we determined that $k_{4.1} = (10.0 \pm 0.1) \times 10^{-2}$ $M^{-1}s^{-1}$. This is in good agreement with Jones et al. (2014)[209] who reports a $k_{4.1}$ of 9×10^{-2} $M^{-1}s^{-1}$ at pH 5.5 (T = 25°C) and comparable to a $k_{4.1}$ = .111 $M^{-1}s^{-1}$ reported by Pham et al. (2008)[156] at pH 6.0 (T = 25°C and 0.1 M ionic strength).

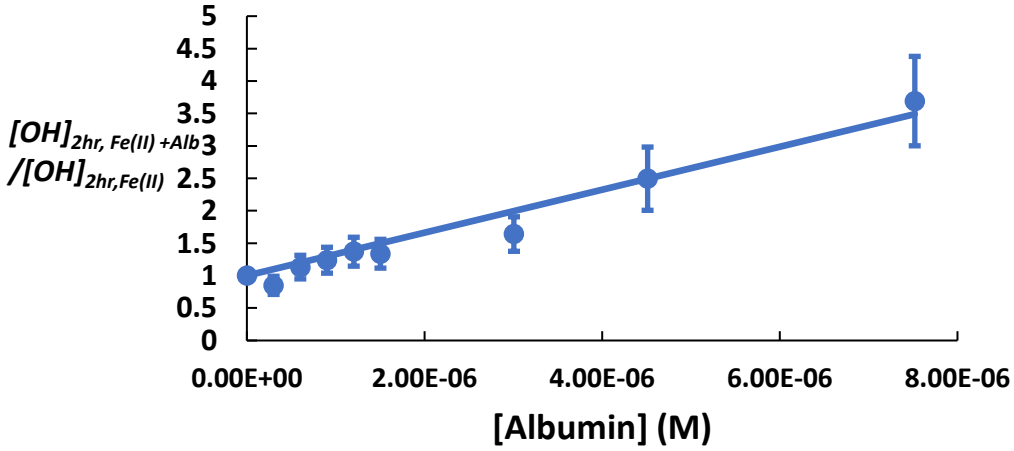

Figure 4.9. Ratio of $[OH]_{2hr}$ from the solution containing 1 µM Fe(II) + Alb to $[OH]_{2hr}$ to the solution containing from 1 µM Fe(II) system. in pH 5.5 Saline, T = 37°C, 200 µM Asc. Data points indicate average of three measurement and error bars error propagation values. Solid lines indicate best fit curves through experimental data

Figure 4.9 shows the ratio of $[OH]_{2hr}$ generated from the Alb-Fe(II) system to the Fe(II) system as a function of [Alb]. Assuming that R4.6 (Alb-Fe(II) + O_2) is the rate limiting for this system we determined $k_{4.6} = (1.8 \pm 0.1)\ M^{-1}s^{-1}$ from data in Figure 4.9. These results suggest that Alb chelates inorganic Fe(II) and enhances the rate constant of R4.1 by a factor of 18. To our knowledge, this is the first estimation for the rate constant of Alb-Fe(II) mediated O_2^- formation ($k_{4.6}$). This characterization of Alb-Fe(II) binding supports a non-specific carboxylate-Fe(II) binding site on Alb proposed by Duff et al. (2009).[198] The ROS generation from Alb-Fe(II) is consistent with carboxylate binding interactions. Carboxylate groups are known to chelate Fe species, resulting in a lower reduction potential that enhances Fe mediated ROS generation (R4.1-R4.4).[45, 210]

In a similar manner, we determined the rate constant of SRFA-Fe(II) mediated O_2^- generation $k_{4.9} = (2.7 \pm 0.3)\ M^{-1}s^{-1}$ from data in Figure 4.3, indicating that SRFA enhanced the rate of O_2^- formation (R4.1) by a factor of 25. This is comparable to our previous work where we reported that $k_{4.9} = 5.1\ M^{-1}\ s^{-1}$ for SLF containing Asc, GSH, UA and citrate at pH 7.2-7.4 (T = 25^{o}C). [34] The lower k_9 determined in this work is likely due to the protonation of carboxylate groups on SRFA at lower pH, reducing the ability of SRFA to chelate Fe(II) consistent with a general decrease in k_9 with decreasing pH observed in other studies.[91, 211] However, we could only find one study that determined k_9 at pH 5.5. Jones et al. (2015)[211] determined that $k_{4.9} = 0.02\ M^{-1}s^{-1}$ based off of the disappearance of Fe(II) species over 28 hours using a phenanthroline ligand method. However, the system investigated by Jones et al. (2015)[211] had no reducing agents and used significantly higher concentrations of SRFA (10^3 µg/mL) and Fe(II) (1 mM) than our system of 10 µg/mL SRFA and 1 µM Fe(II). Such a dramatic difference in [SRFA] and

[Fe(II)] significantly influences SRFA-Fe(II) speciation. Jones et al. (2015)[211] used MINTEQ speciation modeling and determined that Fe(II) occupied the carboxylate and phenolate SRFA binding sites in a roughly 5:4 ratio. In contrast, MINTEQ speciation modeling determined that all Fe(II) was bound to the carboxylate binding sites on SRFA for our system of 1µM Fe(II) and 10 µg/mL SRFA (data not shown). Furthermore, out measurements are based on OH generation of two hours whereas Jones et al. (2015)[211] based their calculations on Fe(II) disappearance over a significantly longer time scale (28 hrs.). Thus, the factor of 135 difference between our $k_{4.9}$ and that of Jones et al. (2015)[211] may be due to dramatic differences in reagent concentrations and a significantly different time scale use to model this chemistry.

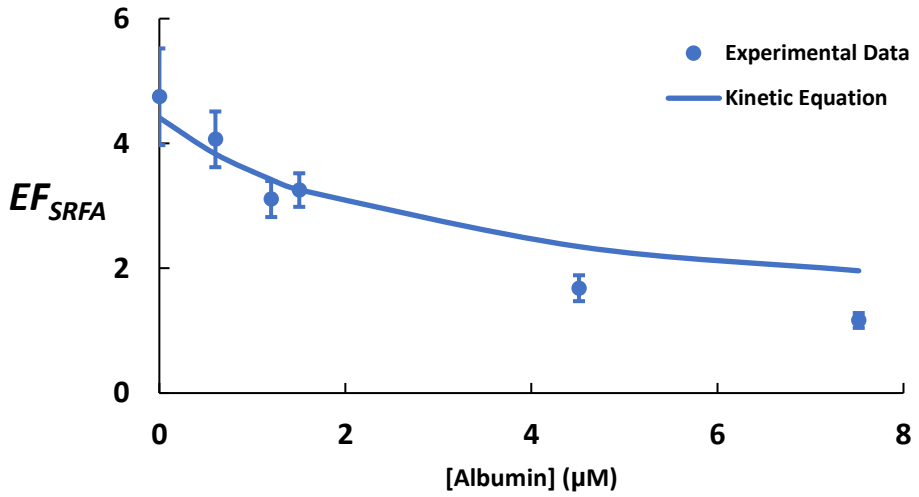

Figure 4.10. Enhancement factor (*EF_{SRFA}*) as a function of [Alb] from a system combining 1µM Fe(II), 10 µg/mL SRFA, Alb and 200 µM Asc pH 5.5 (T = 37^{O}C). Blue data points indicate average of three measurements and error bars indicate error propagation values. Solid blue line indicates predicted *EF_{SRFA}* using Equation 2.

To test the validity of the rate limiting approximation and estimated rate constants, we measured two hour OH from a system combing Fe(II), SRFA and Alb in pH 5.5 saline (Figure

4.10, data points). Using Eqn. 4.2 and rate constants in Table 1 we predict EF_{SRFA} and compare to experimental results (Figure 4.10, solid line). Both experimental data and Eqn. 4.2 predictions show that the presence of Alb decreases EF_{SRFA} with increasing [Alb]. The prediction of EF_{SRFA} for the combination of Fe(II), Alb, SRFA and Asc agrees well with experimental data for [Alb] = 0 – 1.5 µM but beyond this overpredicts SRFA enhancement ratio by a factor of 1.4 and 1.7 when [Alb] is 4.5 µM and 7.5 µM respectively. Experimental data shows that SRFA enhances two hour [OH] from Fe(II) by a factor of (4.7 ± 0.8) (Figure 4.10 intercept) which is in excellent agreement with the predicted EF_{SRFA} of 4.4 predicted by Eqn. 4.2 These results indicate that the rate limiting approximation is reasonably valid under our experimental conditions.

We propose that, Alb is capable of mobilizing Fe(II) away from SRFA and thereby decreasing the rate O_2^- and ultimately OH generation. However, in order to form OH, the formation of O_2^- by Fe(II) must be followed by the formation and destruction of H_2O_2.[34, 204, 210] It is likely that Alb enhances the ability of Fe(II) to form and oxidize H_2O_2 but this is not explicitly investigated in this work. To determine the relevance of these results in physiological lung lining fluid, we compare results to measurements of $[OH]_{2hr}$ from Fe(II) and SRFA-Fe(II) in BALF.

4.3.5 OH Formation from SRFA-Fe(II) in BALF + Ascorbate

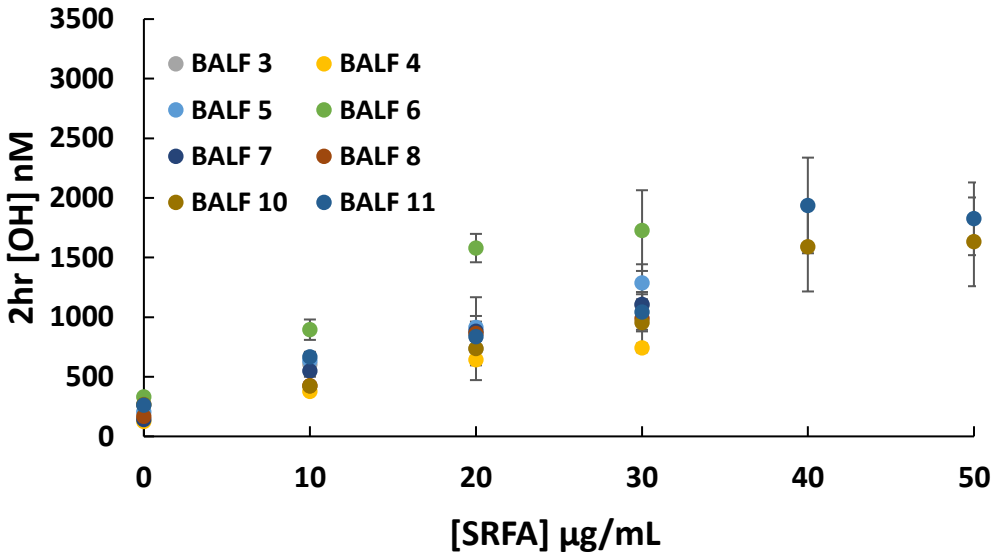

Figure 4.11. $[OH]_{2hr}$ from 1 µM Fe(II) + 200 µM Asc dissolved in different BALF (n = 8, T = 37^{O}C, pH = 4.7-6.3) as a function of [SRFA]. Data points indicate average of three measurements and error bars indicate range of values.

Figure 4.11 shows two hour [OH] as a function of [SRFA] for combinations of Fe(II), SRFA and 200 µM Asc in BALF (n = 8). Asc is added to all BALF in order to account for dilution of antioxidants during the lavage procedure as done by Sun et al. (2001).[24] Absent of SRFA, all BALF with 1 µM added Fe(II) $[OH]_{2hr}$ from 124 nM (BALF 4) to 330 nM (BALF 6) with an average of 220 nM. To our knowledge, these are the first measurements of OH from Fe(II) in BALF, but we have investigated similar systems in SLF. The range of $[OH]_{2hr}$ = 124 nM to 330 nM from 1 µM Fe(II) is significantly lower $[OH]_{2hr}$ = 1094 nM observed for the same system in SLF.[34] This dramatic differences in OH produced is likely due to the presence of citrate that forms complexes with Fe(II) that enhance ROS reactions forming OH. [34] BALF contains Alb and Tf which alter Fe(II) mediated ROS chemistry in a different manner than

citrate, indicating that citrate is not a good mimic for metal binding proteins found in lung lining fluid.

The addition of SRFA enhanced two hour [OH] from 1 μM Fe(II) approximately linearly with [SRFA] for all BALF (Figure 4.11). To our knowledge, these are the first measurements of SRFA-Fe(II) mediated OH generation in BALF but we have investigated similar systems in SLF.[34] For [SRFA] = 10 μg/mL and 1 μM Fe(II) in BALF, $[OH]_{2hr}$ ranged from 421 nM to 895 which is lower than $[OH]_{2hr}$ = 1683 nM we reported for the same system in SLF.[34] When [SRFA] = 20 μg/mL, $[OH]_{2hr}$ ranged from 642 nM to 1479 in BALF which is lower than $[OH]_{2hr}$ = 1793 nM we reported for the same system in SLF. OH measurements in BALF varied by roughly a factor of 2, possibly reflecting the differences in proteins, phospholipids and antioxidants concentrations we were unable to quantify amongst the different BALF. Aside from the of metal binding proteins that alter ROS chemistry, phospholipids and proteins can scavenge OH and potentially impact our measurements. However, since we were unable to quantify the absolute concentrations of proteins and phospholipids in BALF, we cannot quantify this effect. The higher values previously observed for the 1 μM Fe(II) and SRFA-Fe(II) systems in SLF is likely due to the high pH of 7.2-7.4 which is generally associated with faster ROS generation from SRFA-Fe(II) than in pH 5.5.[34, 91, 211]

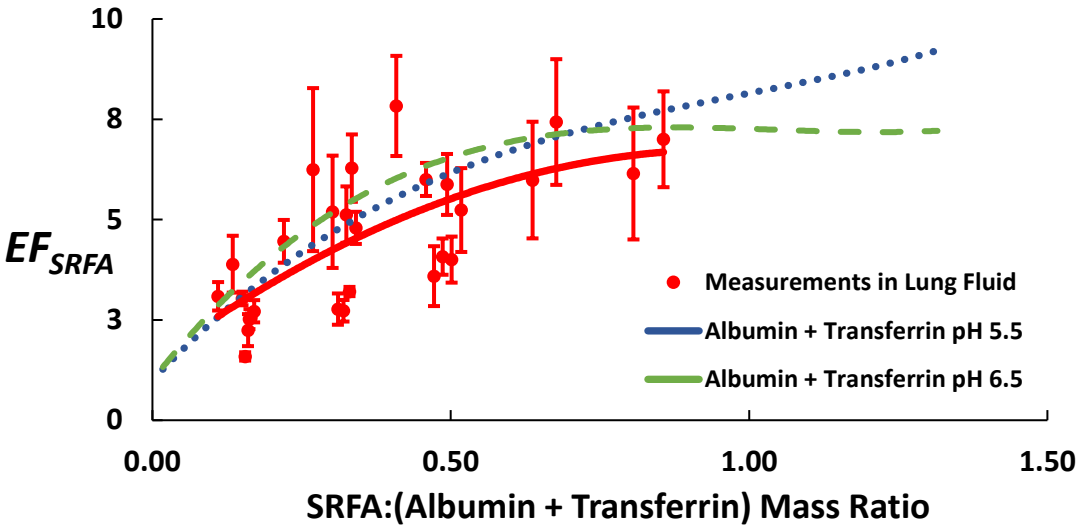

Figure 4.12. Enhancement factor (EF_{SRFA}) as a function of SRFA:Protein mass ratio from solutions containing 1 µM Fe(II) relative to solutions containing 1 µM Fe(II) and varying SRFA in BALF (red circles and solid line) pH 5.5 saline (blue dashed circles), pH 6.5 saline (green dashed line). Red data points indicate average of three measurements in BALF and error bars indicate propagated error values. Solid lines are best fit curves through experimental data. Data for best fit lines from pH 5.5 and pH 6.5 systems are shown in Figure 4.8.

Figure 4.12 shows the EF_{SRFA} as a function of SRFA:Protein mass ratio for all measurements of Fe(II) and SRFA-Fe(II) in BALF, pH 5.5 and pH 6.5 saline. Alb and Tf concentrations in BALF were estimated by assuming that Alb + Tf composed 57% of the total protein mass. The best fit line from EF_{SRFA} from 1 µM Fe(II), SRFA, Alb and Tf in pH 5.5 and 6.5 are shown in the blue and green curves respectively. The red curve indicates best fit line through all measurements of OH generation from Fe(II) and SRFA-Fe(II) in BALF and indicate a decent correlation ($R^2 = 0.5$). EF_{SRFA} data from measurements on BALF correlate reasonably well with solutions of Fe(II), SRFA, Alb and Tf in pH 5.5 and 6.5. This suggests that Alb and Tf play an important role in reducing OH generation that arises from SRFA-Fe(II).

This work suggests both Alb and Tf can mobilize Fe species from SRFA-Fe(II) binding. We propose that Alb can chelate Fe(II) away from SRFA and forms a complex that is less ROS active, yet interestingly possess an ability to enhance OH generation relative to inorganic Fe(II) alone. Tf likely chelates transient Fe(III) species produce during Fe(II) oxidation and results in Fe(III) complexes that are resistant to reduction by Asc, thus inhibiting R4.1-R4.4. To our knowledge this is the first characterization of ROS generation kinetics arising from interactions of Alb and Tf with Fe(II) in the presence of Asc. Furthermore, we report the first measurements OH generation from Fe(II) and SRFA-Fe(II) in BALF which more realistically represent human lung lining conditions.

5. Spectroscopic Characterization of HULIS from Woodsmoke and Cigarette Smoke Condensate

5.1 Introduction

Humic-like substances (HULIS) are a mixture of water soluble complex, organic, macromolecular compounds that have been identified in fog, cloud water, biomass burning aerosol and cigarette smoke.[71, 88, 212-215] HULIS are thought to play a role in the inhalation toxicity of cigarette smoke and wood smoke particles, but this role is not well defined.[88, 216, 217] The toxic properties of HULIS may result from their high content of oxygenated functional groups (ketones, carboxylates and phenolates) that form stable complexes with transition metals, in particular with Fe.[88, 217-221] The ability of HULIS to chelate Fe has been associated with reactive oxygen species (ROS) generation under physiological conditions [34, 87, 88] and functional deficiency of cellular Fe that leads to transcription factor activation and release of proinflammatory mediators and tissue injury.[205, 216] HULIS derived from biomass burning has been associated with significantly higher optical absorption and ROS activity in simulated lung fluids relative to HULIS formed from atmospheric processing,[109] although this has not been explicitly distinguished in the literature.

Two studies used FTIR spectroscopy to identify HULIS in cigarette smoke condensate and lung tissues of smokers and coal miners.[87, 88] HULIS in the lung tissues of smokers has shown to produce ROS, accumulate Fe and induce collagen deposition, suggesting that HULIS-Fe binding plays a significant role in lung injury from PM inhalation. Ghio et al. (1994)[88] showed that cigarette smoke-derived HULIS introduced into the lungs of an animal model is phagocytosed and leads to intracellular accumulation of Fe. Ghio et al. (2015)[216] exposed the water soluble fraction of wood smoke particles to BEAS-2B epithelial lung cells and observed

increased cellular ROS generation, sequestration of mitochondrial Fe, mitogen-activated protein kinase activation, NrF2 transcription activation and release of interleukin-6 and interleukin-8 proinflammatory mediators.[216] The authors hypothesized that these effects were due to endocytosis of HULIS found in woodsmoke particles; suggesting the introduction of HULIS chelates cellular Fe, causing a functional Fe deficiency and inducing a cascade of proinflammatory events that may manifest as lung injury.[216] Ghio et al. (2017)[205] suggests that HULIS mediated disruption of cellular Fe homeostasis is a common step for pulmonary and systemic health effects arising from exposure to cigarette smoke, biomass burning aerosols and ambient urban PM. These studies highlight the importance of the ability of HULIS to bind Fe and induce determinantal health effects, suggesting characterization of HULIS is important for PM health studies.

HULIS derives its name from its physical and chemical similarities to terrestrial and aquatic humic acids (HA) and fulvic acids (FA).[71] Traditionally, soil humic substances have been extracted at alkaline pH (pH 13-14), to separate it from an insoluble material, referred to as humin. Acidification of the alkaline extract to pH 1 produces a precipitant that is defined as the humic acid (HA) fraction and the remaining supernatant is the fulvic acid (FA) fraction.[71] Thus the fractions of soil humic substances are operationally defined as humin (insoluble), HA (alkaline soluble) and FA (soluble at all pH). A variety of gel permeation chromatography methods have been developed to remove inorganic impurities and concentrate fractions of humic substances.[71] Early studies on atmospheric HULIS have used alkaline extraction and gel permeation chromatography methods to study both the soluble and insoluble components.[73-75] Recent studies have focused on the water soluble fraction of ambient HULIS that by definition is more similar to FA.[71]

Spectroscopic characterization has revealed that HULIS shares numerous functional groups with HA and FA, including carboxylic and phenolic groups but HULIS generally has weaker acid characteristics, lower molecular weight and aromaticity and higher aliphatic character.[71, 72] Fluorescence characterization of HULIS has been used to identify fluorophores that bear similarities to those in HA and FA.[71, 72] Two distinct excitation/emission peaks (ex/em) have been identified in HULIS, a FA-like ex/em pair at 330-350 nm/420-480 nm and a HA-like ex/em pair at 250-260 nm/380-480 nm.[222] HULIS from PM and fog water have shorter wavelength fluorescence peaks when compared to soil humic substances.[77, 79] This has been attributed to a lower aromatic content and higher condensed conjugated bonds and aliphatic character in HULIS.[77, 79]

FTIR spectroscopy is a useful tool for characterizing HULIS as it reveals information on organic functional groups. HA, FA and HULIS all share some similar FTIR peaks, yet some differences in HULIS have been identified.[71, 72] Generally, these FTIR spectra reveal a broad absorption peak centered around 3300 cm^{-1}, (O-H stretch from alcohols, phenols and carboxylic acids), 2960-2860 cm^{-1} (C-H stretch from aliphatic), 1720 cm^{-1} (C=O stretch mostly from carboxylic acids), 1600-1660 cm^{-1} (C=C stretch from aromatics and C=O stretches from conjugated carbonyls), a broad peak around 1400 cm^{-1} (C-H stretch aliphatics), 1220 cm^{-1} (C=O stretch and O-H bending from carboxylates) and a pair of peaks ranging from 2970-2840 cm^{-1} and 3030 cm^{-1} (C-H stretch from aliphatics).[75, 77, 78, 223] These peaks have also been identified in humic substances, and SRFA in particular has shown strikingly similar FTIR spectra to ambient HULIS extracts.[78] No standard HULIS material exists, but due to the similarity functional groups, solubility and molecular weight[71] several studies have used FA (usually Suwannee River Fulvic Acid) as a HULIS surrogate.[34, 108, 204] However, HULIS samples have shown a relatively

strong discrete peaks at 1589 cm^{-1}, 1280 cm^{-1} and 863 cm^{-1}, indicating organic nitrate groups (R-ONO_2) that are not found in soil humic substances.[78]

In this work we use fluorescence and FTIR spectroscopy to characterize HULIS from cigarette smoke condensate and wood smoke particles. Spectroscopic characterization is performed on the water-soluble fraction of cigarette smoke condensate (Cig-WS), the water-soluble fraction of wood smoke particles (Wood-WS) and Suwannee River Fulvic Acid (SRFA). Using a traditional alkaline extraction method, we isolate the FA fraction of HULIS from cigarette smoke condensate (Cig-FA) and wood smoke particle (Wood-FA). We then use fluorescence and FTIR spectroscopy to characterize Cig-FA and Wood-FA and compare it to their water-soluble counterparts and SRFA. Fluorescence excitation-emission matrix (EEM) and FTIR spectroscopy are used to compare fluorophores and organic functional groups present among the different samples.

5.2 Materials Methods

5.2.1 Isolation of Fulvic Acid Like Fraction of Cigarette Smoke and Wood Smoke

Cigarette smoke condensate (Tobacco Health Research Institute, University of Kentucky) was employed in this study. Preparation from the mainstream smoke of burning Kentucky Reference 1R1 cigarettes was automated and has been previously described.[224] Cig-WS was prepared by agitating 10 mg condensate in 1.0 mL Hank's buffered saline solution for 2 hr, centrifugation of the suspension at 10000 G x 10 minutes, and separating the supernatant.

Wood smoke was generated by heating white oak wood on an electric heating element (Brinkmann Corporation, Dallas, TX) in a Quadrafire 3100 woodstove (Colville, WA). Wood smoke particles were collected by bubbling it into 100% ethanol and this suspension was treated

in both a SpeedVac Concentrator (Savant, Life Technologies Corporation, Grand Island, NY) and a lyophilizer (Labconco, Fort Scott, KS). The elemental/organic carbon in the wood smoke particles was 0.004 ± 0.002 (Sunset Labs, Hillsborough, NC).[225] Wood-WS was prepared by agitating 10 mg wood smoke particle/1.0 mL HBSS for 2 hr, centrifugation of the suspension at 10000 G x 10 minutes, and separating the supernatant.

To isolate the Cig-FA and Wood-FA, the alkaline extraction procedure commonly used to for isolate soil HA and FA is used. Briefly, Cig-WS and Wood-WS are brought to pH 13 using 1 M NaOH and centrifuged at 10000 G x 10 minutes, separating the supernatant. The resulting supernatant was acidified to pH 1 using HCl and centrifuged at 10000 G x 10 minutes, separating the supernatant. This resulting Cig-FA and Wood-FA are brought to a pH of 5.5-6 using 1 M NaOH and then stored in a freezer (0^{o}C) until analysis.

5.2.2 Fluorescence and Fourier Transform Infrared Analysis of Materials

Fluorescence excitation-emission matrix (EEM) scans are performed on all samples using a Lumina Spectrometer, (Thermo Scientific). Fluorescence excitation-emission matrix spectra covering λ_{ex} = 250-700 nm and λ_{em} = 255-705 nm in 5 nm intervals at a scan speed of 60 nm/min were obtained. Fluorometer parameters included an excitation/emission slit size of 10 nm and an integration time of 10 ms. Fluorescence analysis is performed on the aqueous solutions of Cig-WS, Wood-WS, Cig-FA, Wood-FA and SRFA.

FTIR scans are performed on Cig-FA, Wood-FA and SRFA using a UATR Two FTIR spectrometer (Perkin-Elmer). In order to minimize solvent interferences, Cig-FA and Wood-FA samples were evaporated to dryness with a gentle stream of N_2 at room temperature. SRFA was analyzed as a solid, as received from IHSS. Nordic Fulvic Acid FTIR data is provided by

International Humic Substances Society (IHSS). In all fluorescence EEM spectra, the diagonal line across spectra is an instrument artifact due to Rayleigh scattering.[226]

5.3 Results

5.3.1 Fluorescence Excitation-Emission Matrix Spectra

Figure 5.1 shows the fluorescence EEM spectra of 30 µg/mL aqueous SRFA and Nordic Fulvic Acid. SRFA shows two distinct fluorescence peaks centered at ex/em = (325-350) nm/460 nm and ex/em = (320-325) nm/420 nm. Nordic Fulvic Acid has markedly different EEM features than SRFA, with two distinct fluorescence peaks centered at ex/em = 410 nm/470 nm and ex/em 455 nm/(500-580) nm. The reasons for this are not known.

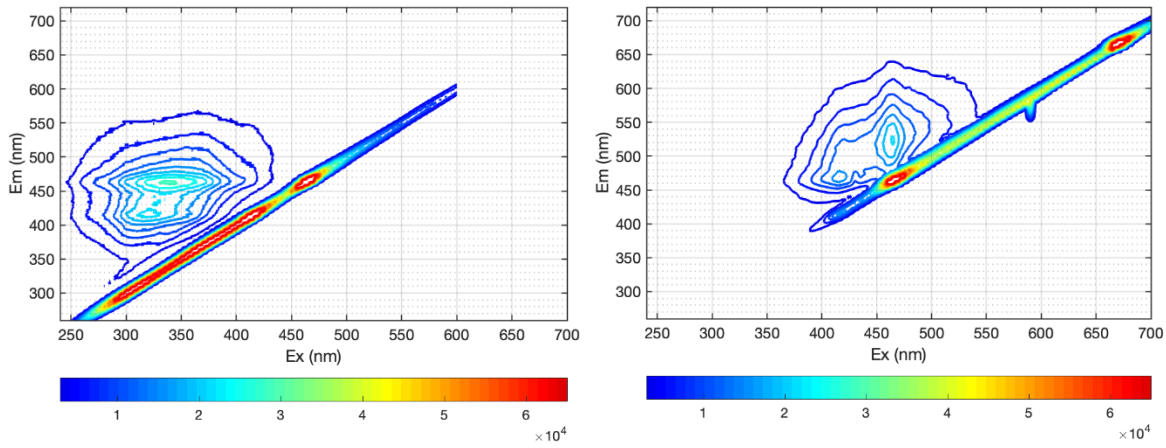

Figure 5.1 Fluorescence excitation-emission matrices of SRFA Standard II (Left) and Nordic Fulvic Acid (Right) in H_2O.

The fluorescence EEM spectrum of Cig-WS and the Cig-FA are shown in Figure 5.2. Cig-WS was diluted to a final concentration of 5.4 µg/mL to avoid signal saturation and related red shifting of fluorescence contours. Cig-FA was diluted by 100×, but the mass concentration of Cig-FA is not known. Both Cig-WS and CSC-FA have very similar fluorescence EEM, with two sets of distinct peaks at ex/em = (340-355) nm/460 nm and ex/em = (325-350) nm/420 nm.

These peaks are similar to the fluorescence peaks observed for SRFA EEM (Fig. 5.1). This indicates that the bulk if not all of Cig-WS is composed of Cig-FA with fluorophores resembling those of SRFA. However, both CSC and CSC-FA EEMs (Fig. 5.2) have contours stretching into lower wavelengths, features not observed in SRFA EEM. This could be due to the presence of lower molecular weight substances with lower aromatic systems and unsaturated bonds, consistent with observations of ambient HULIS extracts.[77, 79]

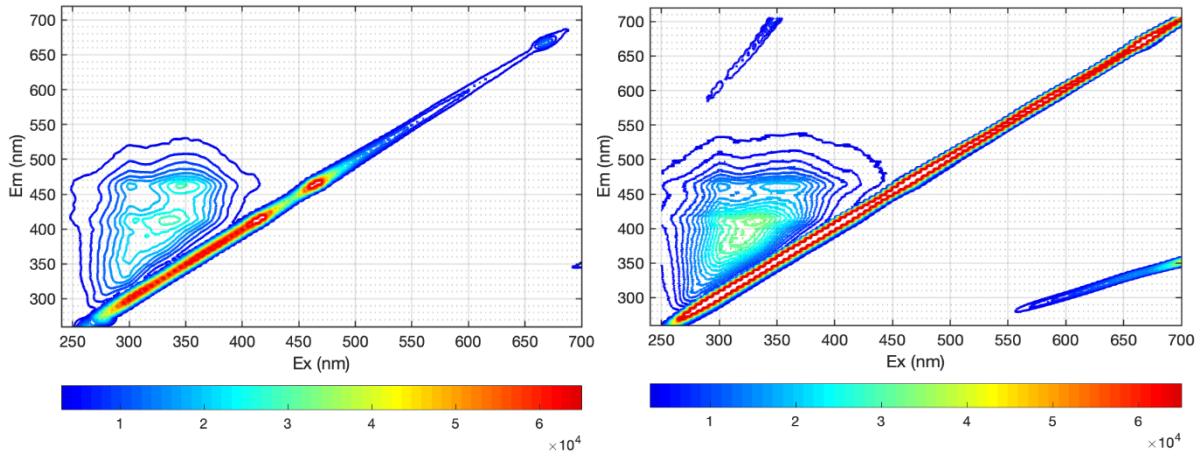

Figure 5.2. Excitation emission matrices of Cig-WS (Left) and Cig-FA (Right).

The fluorescence EEM spectra for 5.4 µg/mL Wood-WS and Wood-FA are shown in Figure 5.3. Wood-FA was diluted by 50×, but the mass concentration is not known. The fluorescence EEM of Wood-WS and Wood-FA show strikingly different features (Figure 5.3). Wood-WS exhibits two peaks at ex/em = 410 nm/465 nm and ex/em = 455 nm/(515-550) nm, nearly identical to fluorescence features of Nordic Fulvic Acid (Figure 5.1). The Wood-FA fraction shows two distinct peaks at ex/em = (320-350) nm/(405-420) nm and ex/em = (345-355) nm/460 nm that resemble those of SRFA, Cig-WS and Cig-FA but have lower overall fluorescence intensity than Wood-WS. The differences in EEM features indicate that the

dominant fluorophores in Wood-WS are markedly different than the Wood-FA fraction. Interestingly, the Wood-FA fraction shows a third distinct peak centered at ex/em = 275 nm/(300-320) nm not observed in Cig-WS, Cig-FA, SRFA or Nordic Fulvic Acid. This could be due to the presence of single oxygenated aromatic molecules, such as phenols and methoxyphenols, that are commonly associated with the water-soluble fraction of woodsmoke particles. Interestingly, none of the EEM exhibited the commonly reported HA-like ex/em pair at (250-260) nm/(380-480) nm.[222]

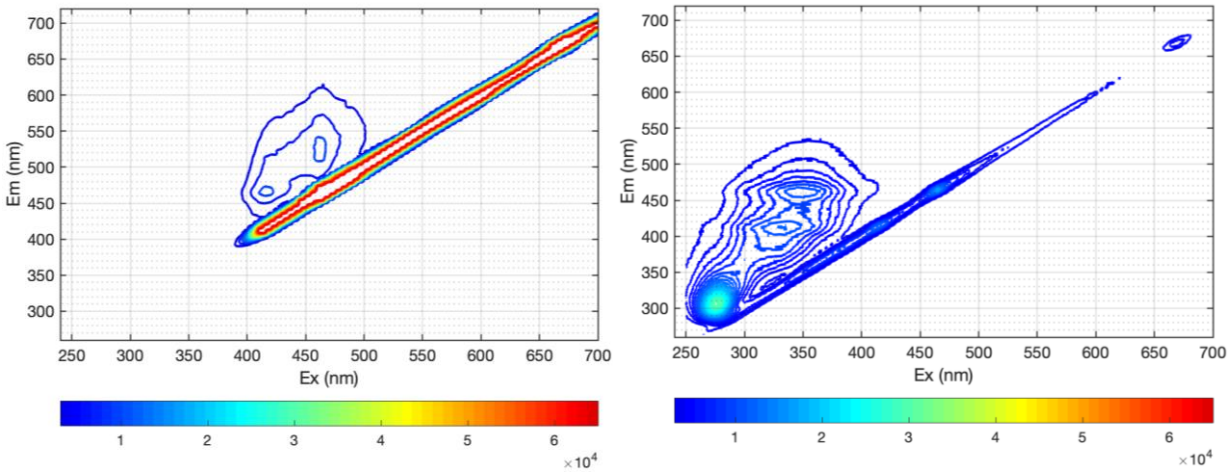

Figure 5.3. EEM of WSP (Left) FA Fraction of WSP (right).

5.3.2 FTIR spectra

FTIR spectra of solid Cig-FA, Wood-FA and SRFA are shown in Figure 5.4A and 5.4B. Common FTIR absorbances and functional groups between Cig-FA, Wood-FA, SRFA, and Nordic Fulvic Acid are summarized in Table 5.1. All FTIR spectra exhibit several striking similarities. All samples have a broad peak near 3300-3400 cm^{-1} indicating O-H stretching in alcohols, phenols or carboxylates. Peaks centered near 2938-2975 cm^{-1} indicate C-H stretching from aliphatic groups. Another infrared absorption of interest is the peak at 1707-1727 cm^{-1}

characteristic of C=O stretching from carboxylates and to a lesser degree ketones and aldehydes.[77, 78] All samples have somewhat broad peaks centered around 1615 cm^{-1} indicating C=C stretching in aromatic rings and C=O stretches in conjugated carbonyl systems. However, Cig-FA has a discrete sharp peak at 1639 cm^{-1} that is somewhat overlaps with a broader peak around 1615 cm^{-1} (Figure 5.4A). This could be due to organic nitrates ($R\text{-}ONO_2$) that absorb in the same region but typically have sharp and discrete peaks.[227] Cig-FA, SRFA and Nordic Fulvic Acid all exhibit broad peaks centered near 1388-1403 cm^{-1} indicating C-H bending from aliphatic groups (Figure 5.4B); interestingly, this feature was absent in Wood-FA spectra. All samples have broad peaks centered near 1195-1211 cm^{-1} that have be attributed to C=O stretching and OH bending from carboxylic acids (Figure 5.4B).[78] These FTIR features of Cig-FA and Wood-FA are consistent with spectra of HULIS isolated from ambient PM, [78] cigarette smoke condensate[88] and water-soluble organic fraction of PM extracts.[71, 75, 79, 81]

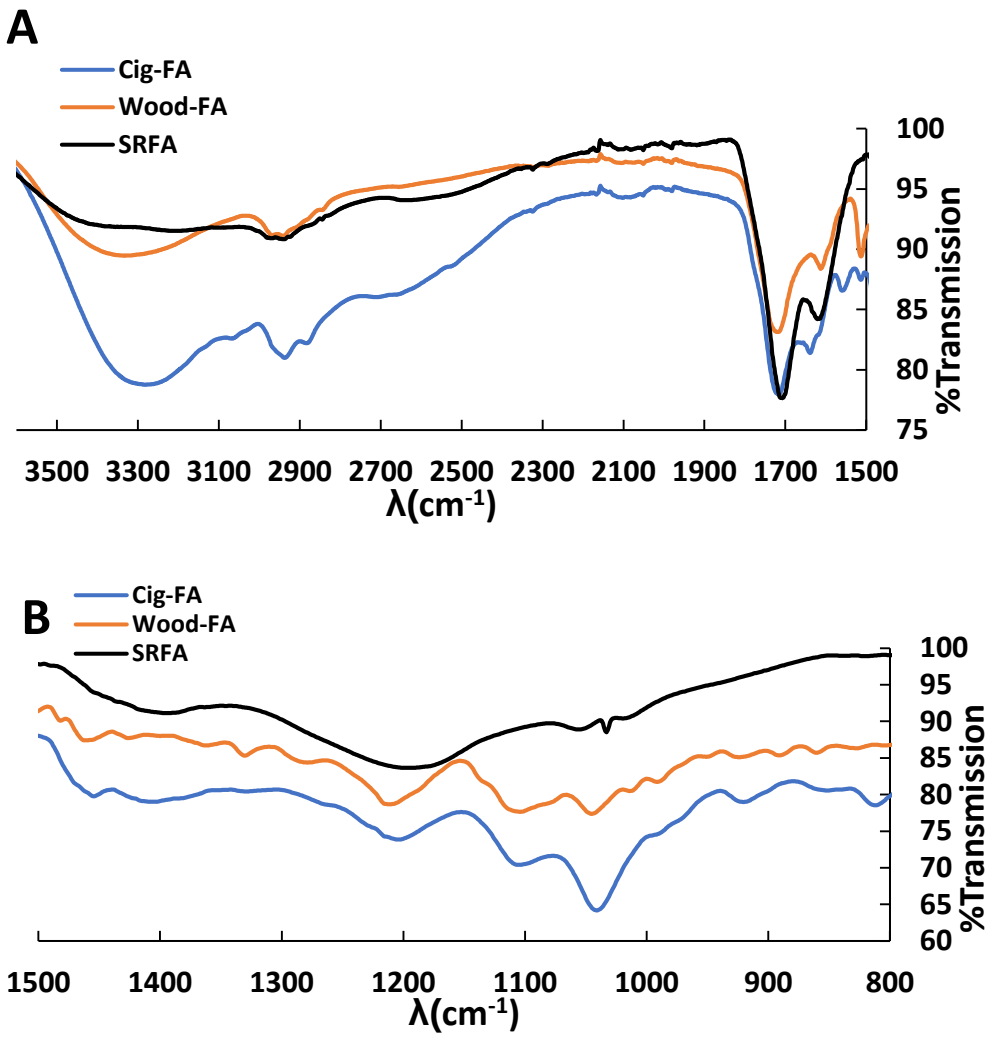

Figure 5.4. FTIR Spectra of the fulvic acid fraction of wood smoke particles (Wood-FA), fulvic acid fraction of cigarette smoke condensate (Cig-FA) and Suwannee River Fulvic Acid (SRFA).

Both Cig-FA and Wood-FA have peaks that are not seen in SRFA and Nordic Fulvic Acid. Both Cig-FA and Wood-FA have discrete peaks near 1512 cm^{-1} may indicate aromatic nitro compounds (C-NO_2).[227] Cig-FA shows a discrete peak near 1561 cm^{-1} that may indicate N-O stretching in organic nitro compounds (R-NO_2), although this peak is not seen in Wood-FA. Peaks centered near 1460 cm^{-1} are associated with C-H bonds from aliphatic groups. One peak centered near 1105 cm^{-1} indicates C-O bonds from aliphatic ethers (Figure 5.4A). The peaks centered near 1460 cm^{-1} and 1105 cm^{-1} that are not seen in SRFA are consistent with more

aliphatic character observed in HULIS.[71, 72] The peak at 1045 cm^{-1} indicates C-OH bond from primary alcohols and has been observed in urban HULIS reported by Chen et al. (2016).[228] The Cig-FA spectrum shows a discrete sharp peak around 815 cm^{-1} that might be attributed to organic nitrates and inorganic nitrates.[227] We conclude that Cig-FA and Wood-FA fractions contain significant amounts HULIS bearing similar functional groups to SRFA and Nordic Fulvic Acid, but with a more aliphatic, organic nitro and organic nitrate character.

Table 5.1. Summary of common FTIR peaks among samples.

SRFA	Nordic FA*	Cig-FA	Wood-FA	Bond	Functional Group
3308	3398	3280	3333	O-H	Alcohols, Phenols, Carboxylic acids
2938	2975	2937	2950	C-H	Aliphatic
1707	1723	1715	1720	C=O	Carboxylic Acids, Ketones, Aldehydes
1620	1620	1639	1611	C=C C=O	Aromatic and Conjugated Systems
1398	1388	1403		C-H	Alkane
1195	1208	1204	1211	C-O	Esters

5.4 Conclusion

Both fluorescence EEM spectra and FTIR demonstrate strong similarities between Cig-WS, Cig-FA, Wood-FA and SRFA. This is consistent with prior results showing HULIS, including a FA-like substance, in cigarette smoke condensate and ambient air particles.[71, 214]

These results indicate that HULIS is a significant component of cigarette smoke condensate and wood smoke particle and contains oxygenated organic functional groups capable of chelating Fe.

6.Malondialdehyde in Atmospheric Aerosols: Application of the Thiobarbituric Acid Method

6.1 Introduction

The thiobarbituric acid (TBA) assay to quantify malondialdehyde (MDA) has been widely used as an indicator of aqueous reactive oxygen species (ROS), lipid peroxidation, oxidative stress and rancidity in food products.[92-95] MDA is a product of lipid peroxidation[92, 229] and OH oxidation of 2-deoxy-D-ribose (2-DR) oxidation.[93, 101, 102] MDA has also been shown to be toxic and mutagenic to humans, suggesting a role more significant than an indicator for oxidation in biological systems[229-231] Several studies have implicated MDA in mammalian mutagenicity, carcinogenesis and atherosclerosis.[229-232] Basu et al. (1983)[230] exposed MDA salts in differing amounts to strains of *salmonella typhimurium*, a bacteria commonly found in the intestines. Using a mutagenicity assay they determined MDA induces 5 reverants per µM of MDA, providing evidence of the mutagenic nature of MDA. MDA can form adducts with guanine and adenine bases in DNA molecules which in turn causes mutagenic effects associated with carcinogenesis.[232, 233] Ma et al. (2014)[234] developed a method to measure a MDA-Deoxyguanosine adduct (M_1dG) in human leukocyte DNA. M1dG is a premutagenic lesion suspected to contribute to carcinogenesis by inducing mutations of guanine to thymine and adenine.[235] Niedernhofer et al. (2003)[231] suggested that MDA interactions with nucleic acids induces interstrand cross linking of DNA molecules which yields mutagenicity in human embryonic kidney cells *in vitro*. Voitkun et al. (1999)[236] observed that MDA initiates DNA-protein cross linking, due to reaction of MDA with proteins followed by crosslinking between DNA molecules and histones. MDA has been shown to react with primary amines and induce lysine-lysine crosslinks.[237] These lysine-lysine crosslinks products have been identified in

oxidized lipoproteins and are thought to interfere with lipoproteins interactions with macrophages—an underlying behavior of atherogenisis.[229, 238] Furthermore, MDA may harden cardiovascular tissues due to induced cross-linking of collagen.[239]

While most widely employed as a marker for oxidation, there is literature suggesting MDA forms in the atmosphere.[103-105] We found three studies that measured the formation of gas phase MDA formation in laboratory simulations.[103-105] Liu et al. (1999)[103, 104] observed MDA formation in experimental chamber photo-oxidation of 2-butenedial, 4-oxo-pentenal and 1,3-butadiene, byproducts of oxidized aromatic compounds. Zhou et al. (2014)[105] found that ozonolylsis of polyunsaturated fatty acids at the surface of an aqueous layer produces gaseous MDA. Only one study claims to have measured MDA in ambient air using a derivatization method coupled with High-Resolution Gas Chromatography/Ion Trap Mass Spectrometry in San Francisco, CA.[240] The authors claim that MDA co-elutes with an internal standard that is distinguishable by interpreting multiple electron ionization, methane chemical ionization and derivative chemical ionization spectra. However, they did not quantify MDA concentrations and their experimental design did not distinguish between gas or particle phase MDA. We could find no studies that quantified gaseous MDA concentrations.

Like other atmospheric carbonyls, MDA potentially enters the aqueous or organic phase following Henry's Law or Pankow's absorptive theory[241] but this has never been investigated experimentally and there is a lack of thermodynamic data for MDA. Only one modeling study has addressed MDA dissolution into atmospherically relevant waters. Okochi et al. (2002)[242] used a bond contribution method to estimate the Henry's Law Constant for MDA (1.4×10^4 M atm^{-1}) and modeled MDA dissolution in fog droplets. Their model predicted that 8-9% of gas

phase MDA would partition into fog droplet at pH 6 when [MDA] = 10-10^{-4} ppb but this partitioning ceased at pH 2. This pH dependence of MDA dissolution is driven by acid-base equilibria, since aqueous MDA exists mainly in its enol form with a pK_a of 4.7 (Figure 6.1). Their model further predicts that MDA complexation to Cu(II) and Ni(II) at the droplet surface enhances MDA partitioning.[242]

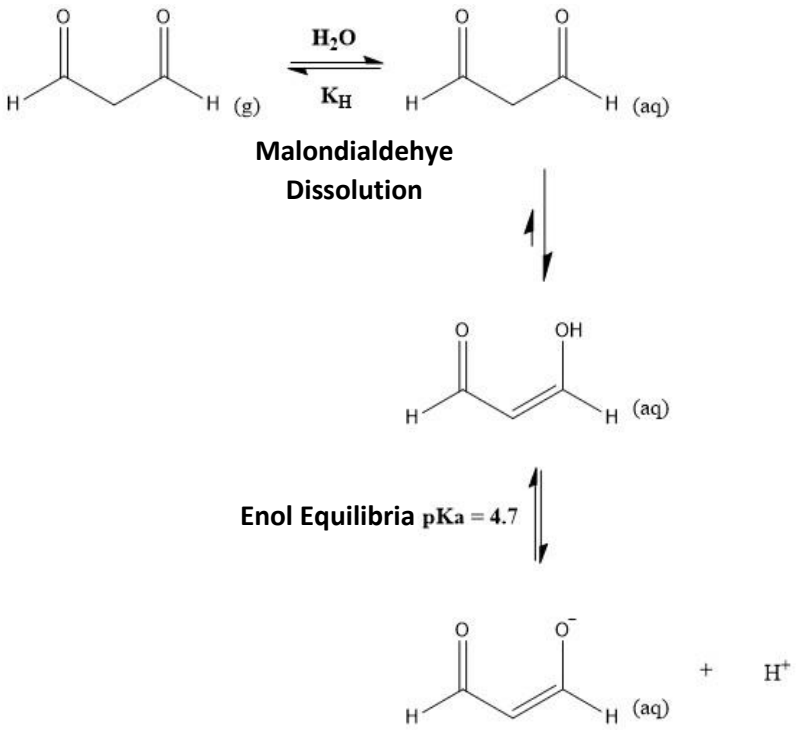

Figure 6.1. Mechanism of MDA dissolution and enol/enolate equilibria.

Furthermore, Beeby et al. (1987)[243] found that photolysis of glycoaldehyde in aqueous solutions produced MDA, suggesting formation of MDA can occur the bulk aerosol or cloud water. These studies highlight the possibility that MDA is present in ambient aerosols. Interestingly, MDA toxicity is associated with the same health effects observed from ambient $PM_{2.5}$ exposure. Thus, if MDA is present in ambient $PM_{2.5}$, it may contribute to the toxicity of inhaled $PM_{2.5.}$ Despite this, MDA has yet to be quantified in the ambient atmosphere or PM.

Derivatization of MDA by TBA is the most common and easily accessible method for measuring MDA, yet it has some setbacks. Two TBA molecules react with MDA in the presence of acid and heat to form an absorbing adduct (TBA_2-MDA) that can be measured via absorbance or fluorescence spectroscopy (Fig. 6.2). There is a large amount of literature employing the TBA assay with varying protocols on a diverse array of biological systems. Generally, optical detection methods are plagued by interferences from MDA precursors that form $(TBA)_2$-MDA upon heating and non-MDA products that absorb or fluorescence at similar wavelengths.[229] Such interferences are greatly improved by using high performance liquid chromatography (HPLC) or mass spectrometry.[98, 99] While arguably better methods to quantify lipid peroxidation and ROS have been developed, MDA has remained of interest due to its inherent toxicity.

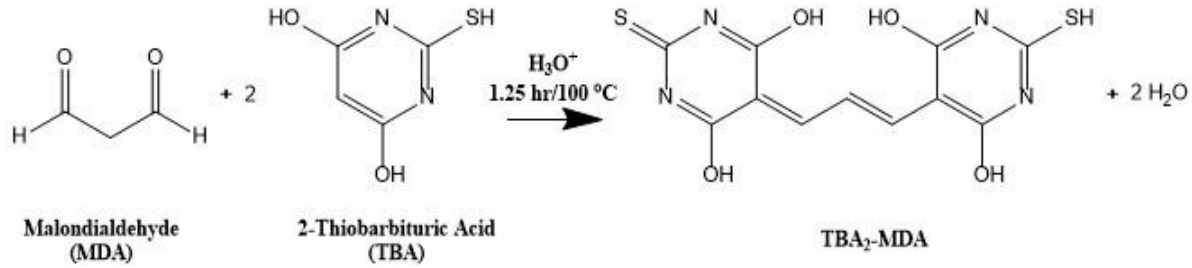

Figure 6.2. Condensation Reaction of MDA and TBA to form TBA_2-MDA.

To our knowledge, there have been no quantification of MDA in atmospheric aerosols. Here we use an altered HPLC-fluorescence method to apply the TBA assay on $PM_{2.5}$ extracts for the first time. This application of the TBA assay is used to estimate MDA concentrations in biomass burning aerosols (BBA) and urban $PM_{2.5.}$ We use fluorescence excitation-emission (EEM) scans reveal fluorescence features of extracted PM samples, characterize the TBA_2-MDA, potential interfering compounds and other fluoresce peaks of interest.

6.2 Methods

6.2.1 Materials and Chemicals

Malondialdehyde tetrabutyl ammonium salt (≥ 96%), 2-thiobarbituric acid (Sigma-Aldrich, ≥ 96%) and acrolein (analytical standard) were purchased from Sigma-Aldrich. 0.1 N sulfuric acid was purchased from Titripur. HPLC-grade acetonitrile was purchased from Omnisolve. HPLC-grade methanol was purchased from Fischer Scientific and a stir and hot plate (Cimarec Basic) and 15mL Falcon tubes (Corning Brand), was obtained from Thermo Scientific. Ultra-high purity Argon and Nitrogen was purchased from AirGas N_2 gas. formaldehyde (36.5%-37.5% in water), sodium formate (99.9%), and oxalic acid (99.9%) were obtained from Aldrich. sodium malonate dibasic monohydrate (Bioextra) was purchased through Sigma. Glyoxal (40% in water) and methylglyoxal (40% in water) were purchased from Tokyo Chemical Industry (TCI).

6.2.2 Estimation of Malondialdehyde Using 2-Thiobarbituric Acid

Quantification of TBA_2-MDA (Fig. 6.2) was performed using a High Performance Liquid Chromatography (HPLC) with a fluorescence detector (Shimadzu RF-10AXL detector) coupled to a reversed phase C-18 chromatography column (GL Sciences Inc., Intersil ODS-2, 5 µm, 4.6 x 250 mm) and guard column (Thermo Scientific, ODS Hypersil JAVELIN Filter, 5 µm, 4 x 10 mm). A wide variety of protocols exist for HPLC-fluorescence detection of TBA_2-MDA in biological samples but the TBA assay has never been applied to PM extracts. Because the TBA_2-MDA adduct is most stable under acidic conditions (pH 2-3)[244] we carry out the assay at pH 3. An eluent of 7:3 acetonitrile and milli-Q water (18MΩ) acidified to pH 3 (0.1 N sulfuric acid) suggested by Fukunaga et al. (1995),[245] worked well with our experimental system. The eluent

was continuously degassed by a gentle stream of argon and delivered at a rate of 1.0 mL/min. The TBA_2-MDA adduct elutes at 6 minutes, and fluorescence is measured at $\lambda_{ex}/\lambda_{em}$ = 530 nm/550nm. The HPLC was calibrated daily with four MDA standards ranging from 0.25 µM to 2.5 µM. A typical TBA_2-MDA calibration curve is shown in Figure 6.3.

To prepare calibration standards, stock solutions of 20 mM malondialdehyde tetrabutylammonium and 100 mM TBA are prepared in pH 3. 10 mL TBA stock solution is prepared in 50 mL Teflon tubes and stirred with a magnetic stir bar under gentle heating for approximately 15 minutes until all TBA powder is dissolved. The TBA is used immediately after preparation because a precipitate forms after approximately 20 minutes at room temperature. In all standards, 4 mM TBA and 0.25 µM to 2.5 µM MDA are combined with pH 3 water in 15 mL Falcon tubes and sealed tightly. Blanks consisted of 4 mM TBA in pH 3 for calibrations and PM extracts. Standards are incubated in a boiling water bath for 1.25 hours upon which the solution turns a pink-purple color. Solutions are cooled in a refrigerator at 4^{o}C for 15 minutes before immediate analysis. Chromatography peaks from the HPLC are analyzed using Chromperfect software (Shimadzu).

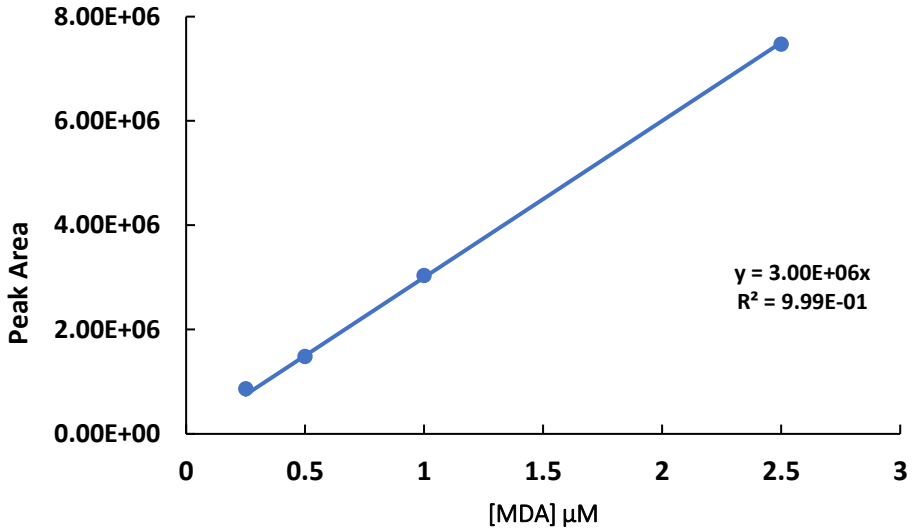

Figure 6.3. Calibration curve for TBA_2-MDA adduct measured on HPLC-Fluorescence detector. Peaks eluted at a retention time of 6 minutes and peak areas were determined by Chromperfect software.

6.2.3 Excitation-Emission Matrix and Interfering Compounds (3D Fluorescence)

The Excitation-Emission Matrix (EEM) scan mode was used to determine fluorescence features (Lumina Fluorometer, Thermo Scientific) of MDA calibrations, BBA extracts, PM samples and potential interfering compounds. Scans were performed with 10 nm excitation and emission slit widths, scanning intervals of 5 nm at 60 nm per second with a 20 ms integration time. To characterize potential interfering compounds, we performed the TBA assay on several compounds that may be present in atmospheric aerosols. We tested solutions of 10 mM formaldehyde, formate, oxalic acid, malonate, glyoxal, methylglyoxal and acrolein with 4 mM of TBA heated in pH 3 (100^{o}C, 1.25 hrs.). Samples are scanned with EEM mode to determine fluorescence features of the TBA_2-MDA adduct and any other fluorescent products, if any.

6.2.4 Application of 2-Thiobarbituric Acid Method to Measure MDA in Ambient $PM_{2.5}$

A sample containing substantial BBA mixed with urban emissions was collected in Fresno, CA as described in previous work.[34] The sample was collected from September 10-16, 2015 and corresponds to an average of 3.0 $\mu g/m^3$ $PM_{2.5}$. During the winter, the site is influenced by residential wood burning especially at night and during the morning hours.[109, 206] BBA content was characterized using an aethalometer with optical absorption.[109] Urban $PM_{2.5}$ from Los Angeles, CA (Urban LA) were collected on the roof of the Math Sciences Building at UCLA. Urban LA samples were collected on acid washed and pre-weighed PTFE filters (PALL, 47 mm 2 µm pore size) using a URG cyclone connected to a high-volume air pump. Flowrates were monitored using rotameters (Kings Instruments 7530) set at 92.5 liters per minute, corresponding to a cut size of 2.5 microns. Three samples were collected for approximately 24 hours during March 27^{th}-30^{th} 2019. The mass of collected particles were determined immediately after collection using a microbalance (1 µg precision, ME 5, Sartorius). To remove charge on the PTFE filters a charge neutralizer was passed over filters for 30 seconds before weighing. The three urban LA samples contained 201 µg, 551 µg and 835 µg corresponding to average PM concentrations of 1.6 $\mu g/m^3$, 4.3 $\mu g/m^3$ and 6.3 $\mu g/m^3$ respectively.

$PM_{2.5}$ samples were extracted in methanol by placing them into 15mL Falcon tubes with 7.5 mL HPLC-grade methanol and incubating for 1 hour at room temperature covered from light. The filters were then removed, and the methanol extracts evaporated to dryness using a gentle stream of N_2 at room temperature. To concentrate the extracts, the extracts were reconstituted in 750 µL of water at pH 3. This was followed by the addition of TBA to reach a concentration of 4 mM and incubated at 100^oC for 1.25 hours. Prior to TBA addition and incubation, a gentle

stream of argon was bubbled through for approximately 30 seconds to remove any oxygen and reduce ROS generation during the assay. To investigate the potential impact of ROS on the assay, we analyzed calibration standards in oxic and anoxic conditions. No difference was observed indicating that oxygen does not impact the condensation reaction between TBA and MDA (data not shown) and ROS do not affect the calibration. After incubation, samples are cooled in a fridge (4^{o}C) and are immediately analyzed for MDA on the HPLC and with EEM scans. For samples analyzed on HPLC, 3 aliquots are injected in order to confirm reproducibility of a single sample.

6.3 Results and Discussion

6.3.1 Malondialdehyde in Fresno BBA and Los Angeles $PM_{2.5}$

Figure 6.4 shows an EEM for a 1 µM MDA standard reacted with 4 mM TBA. Fluorescence contours indicate a fluorophore with peak fluorescence centered at $\lambda_{ex}/\lambda_{em}$ = 530 nm/550nm, corresponding to the TBA_2-MDA adduct.[98, 99, 229]

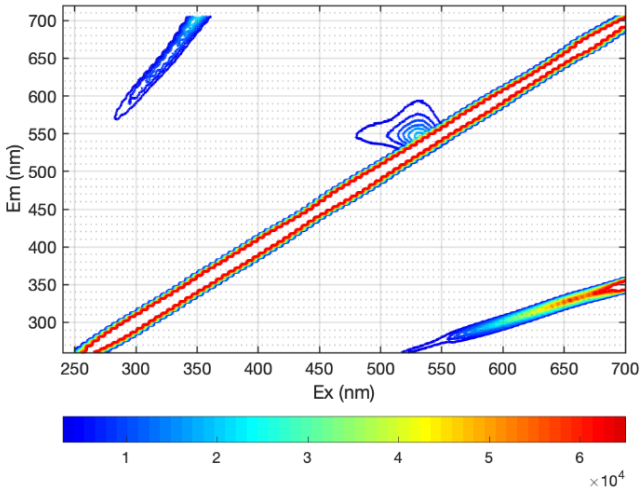

Figure 6.4. Excitation-emission matrix scan of 1 µM MDA assayed with 4 mM TBA in pH 3.

All PM extracts showed signal at $\lambda_{ex}/\lambda_{em}$ = 530 nm/550nm on the HPLC with a retention time of 6 minutes, indicating the presence of TBA_2-MDA in all PM extracts. Figure 6.5 shows the estimated MDA mass as a function of PM mass from Fresno BBA and Urban LA samples, assuming the measured TBA_2-MDA fluorescence corresponds to the presence of MDA only. Increasing amounts of Fresno BBA extract produced a linear response indicating 51.4 ng, 67.8 ng and 92.0 ng MDA (Fig. 6.5, orange squares), corresponding to an average of 30.0 ng/m^3 MDA. All Urban LA samples assayed with TBA exhibited signal for the TBA_2-MDA adduct (Fig. 6.5 and Fig. 6.7) Extracted and concentrated solutions Urban LA samples appear to contain 51.1 ng, 96.5 ng and 72.4 ng MDA corresponding to 40.7 ng/m^3, 75.3 ng/m^3, and 54.6 ng/m^3 MDA respectively. To our knowledge, this is the first quantification of MDA in ambient $PM_{2.5}$ and thus we cannot compare this range of MDA concentrations. However, two similar C_3 organic compounds, methylglyoxal and malonic acid have been quantified in ambient urban $PM_{2.5}$.[240, 241, 246-249] Methylglyoxal, the α-carbonyl isomer of MDA, have reported concentrations ranging 0.8 – 242 ng/m^3 in urban $PM_{2.5}$.[240, 241, 246-249] Malonic acid is a potential acid catalyzed oxidation product of MDA and measurements indicate a range 17.6-233 ng/m^3 malonic acid in urban $PM_{2.5}$.[246, 247, 249] Thus, our reported range of 30.0 – 75.3 ng/m^3 MDA are comparable to reported particle phase concentrations of MDA related C_3 compounds methylglyoxal and malonic acid.

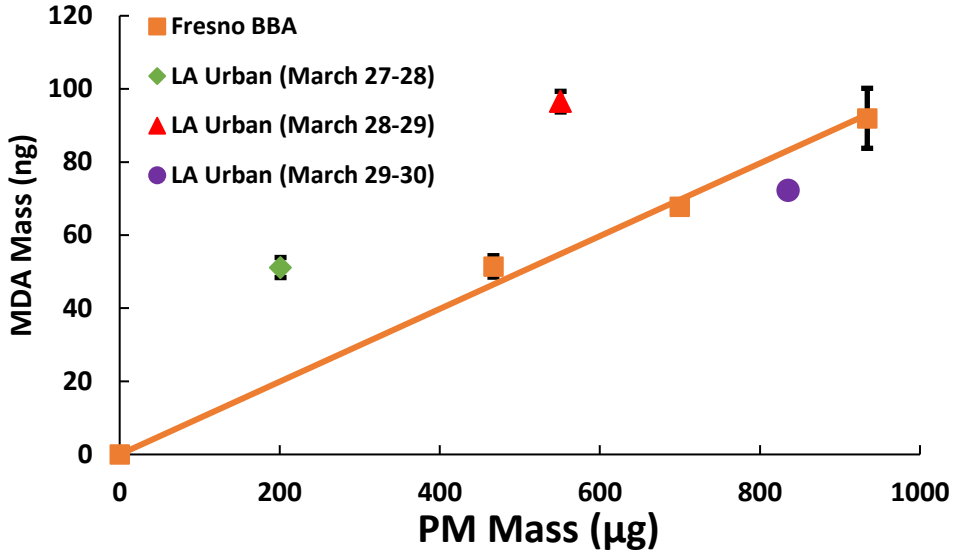

Figure 6.5. Mass of MDA measured from TBA assay on Fresno biomass burning aerosol (BBA, orange squares) and urban Los Angeles $PM_{2.5}$ (Urban LA) extracts (green diamond, red triangle, purple circle). MDA mass was calculated attributing all fluorescence at 550 to the TBA_2-MDA. Error bars indicate range of three values measured on the HPLC from the same sample extract.

6.3.2 EEM Scans of Fresno BBA and Los Angeles $PM_{2.5}$

Figure 6.6A shows the EEM of the concentrated 467 µg Fresno BBA extracts without addition of TBA. The fluorescence spectrum has two fluorescence peaks centered at $\lambda_{ex}/\lambda_{em}$ = 350 nm/460 nm and $\lambda_{ex}/\lambda_{em}$ = 330 nm/410 nm; these are characteristic of atmospheric humic-like substances (HULIS) and similar to Fulvic Acids.[71, 206] Figure 6.6B shows EEM scans for the same 467 µg Fresno BBA concentrate assayed with 4 mM TBA. The scan shows that after reaction with TBA, the sample retains some of the fluorescence features of HULIS, and adds a fluorescent feature matching the TBA_2-MDA fluorophore centered at $\lambda_{ex}/\lambda_{em}$ = 530 nm/550 nm. Interestingly, there is another fluorophore centered at $\lambda_{ex}/\lambda_{em}$ = 455 nm/470 nm with a similar trapezoidal shape of the TBA_2-MDA fluorophore. This fluorophore could be due to formation of a TBA-aldehyde adduct caused by the condensation of a different aldehyde or other species.

However, we were unable to recreate this fluorophore using a range of compounds other than MDA, as discussed below.

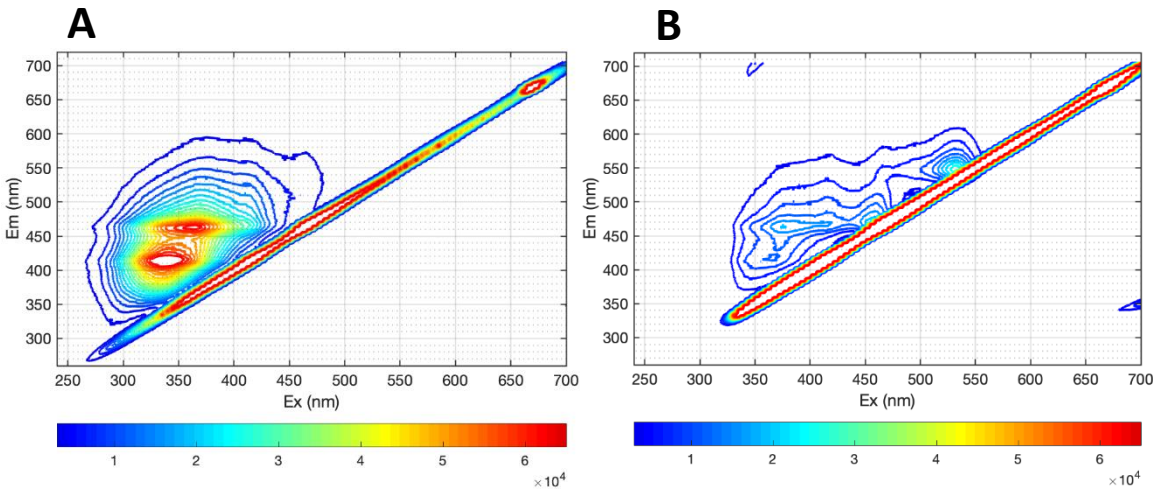

Figure 6.6. Excitation-emission matrix of 467 µg Fresno BBA extracted in methanol and reconstituted in pH 3 (A) and (B) 467 µg Fresno BBA extract assayed with 4 mM TBA in pH 3.

Figures 6.7A-C show EEM scans of the concentrated Urban LA $PM_{2.5}$ extracts collected on three different days reacted with 4 mM TBA. Concentrated extracts of Urban LA $PM_{2.5}$ without addition of TBA have no observable fluorescence. EEMs for all three samples show the characteristic fluorescence of the TBA_2-MDA adduct centered at $\lambda_{ex}/\lambda_{em}$ = 530 nm/550 nm. Two additional trapezoidal-shaped peaks are also observed on either side of the MDA peak, at $\lambda_{ex}/\lambda_{em}$ = 455 nm/470 nm and $\lambda_{ex}/\lambda_{em}$ = 640 nm/665 nm. Like the Fresno BBA EEM, these fluorescence features could be due to the reaction of TBA with other aldehyde or similar molecules, potentially with one carbon bridging the two aromatic rings rather than three. The peak at $\lambda_{ex}/\lambda_{em}$ = 640 nm/665 nm may also be due to an analog of MDA or a related compound. However, we have been unable to recreate the two satellite fluorescent peaks in laboratory experiments.

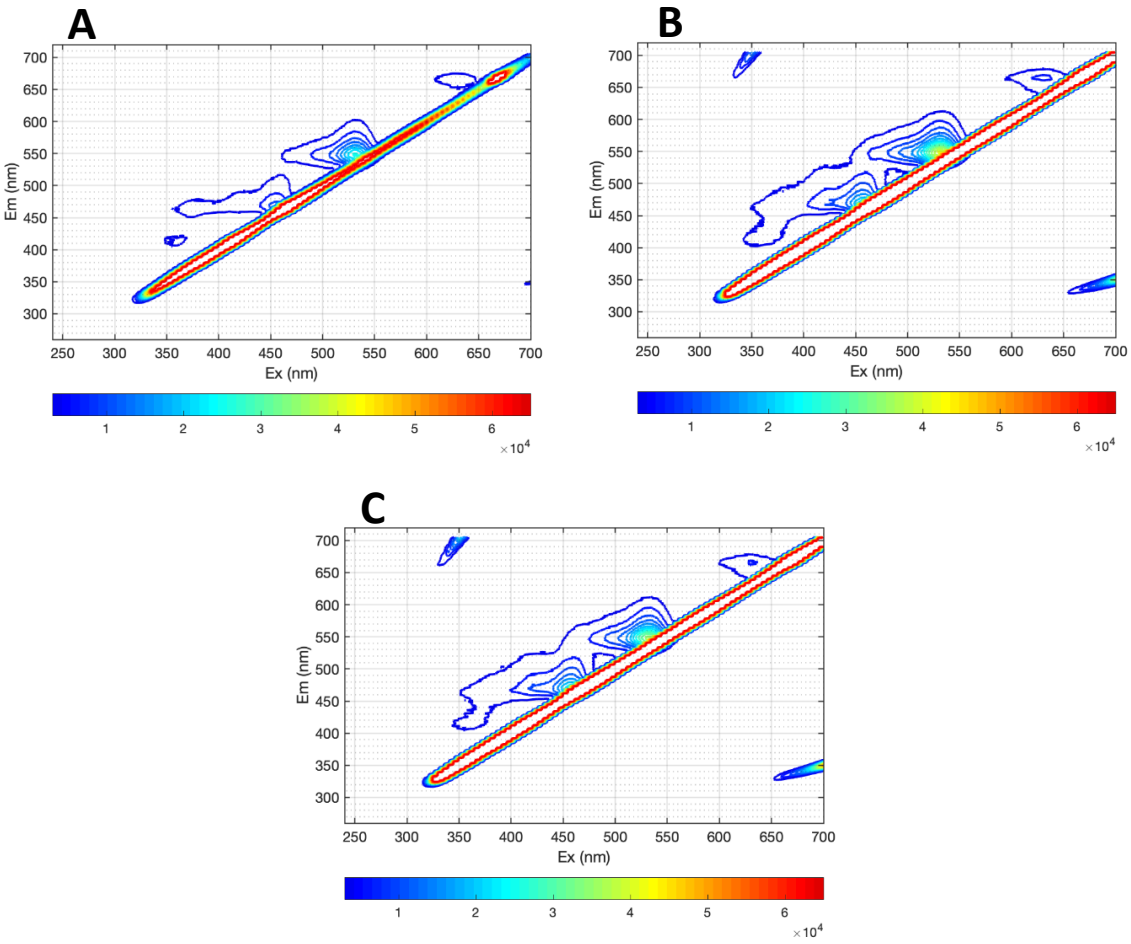

Figure 6.7. Excitation-emission matrix of urban Los Angeles $PM_{2.5}$ (Urban LA) assayed with TBA in pH 3 (A) 201 µg (B) 551 µg (C) 835 µg. Urban Los Angeles $PM_{2.5}$ extracts without addition of TBA show no fluorescence features.

6.3.3 Interfering Compounds

To determine whether any components of PM may interfere with the measurement of MDA, we reacted a variety of different compounds with 4 mM TBA. Of all compounds tested, only acrolein produced any measurable TBA_2-MDA. Triplicate samples of 1 mM and 10 mM acrolein were reacted with 4 mM TBA under oxygenated conditions produced (0.450 ± 0.070) µM and (0.868 ± 0.181) µM of MDA respectively (Table 6.1). This corresponds to 0.004% -

0.008% conversion of acrolein to MDA suggesting minimal interferences since ~1mM of acrolein is likely much higher than would be found in any of our extracts.

Table 6.1. MDA measured from reaction of 1mM and 10 mM acrolein with 4 mM TBA at 100^{o}C in pH 3 under oxygenated conditions.

[Acrolein](mM)	[MDA] Produced (µM)	%Converted to MDA
1 mM	**(0.450 ± .070)**	**.008%**
10 mM	**(0.868 ± .181)**	**.004%**

Acrolein may produce MDA through acid hydration of the alkene followed by oxidation as proposed in Figure 6.8 and the MDA may have been present in the bottle from the manufacturer. Under this mechanism, protonation of the alkene group produces a primary and secondary carbocation, followed hydration that produces 2-hydroxypropanal and 3-hydroxypropanal. Two possible oxidation products of these hydration products are glyoxal and MDA. The hydration of acrolein to 3-hydroxypropanal has been identified under acidic conditions,[250-252] but we could find no studies identifying MDA as a product of acrolein hydration and oxidation. Furthermore, primary carbocations are known to be less stable than secondary carbocations. Thus, one would expect that the formation of MDA from acrolein is a minor pathway, consistent with the observation of a very small part of MDA associated with the acrolein.

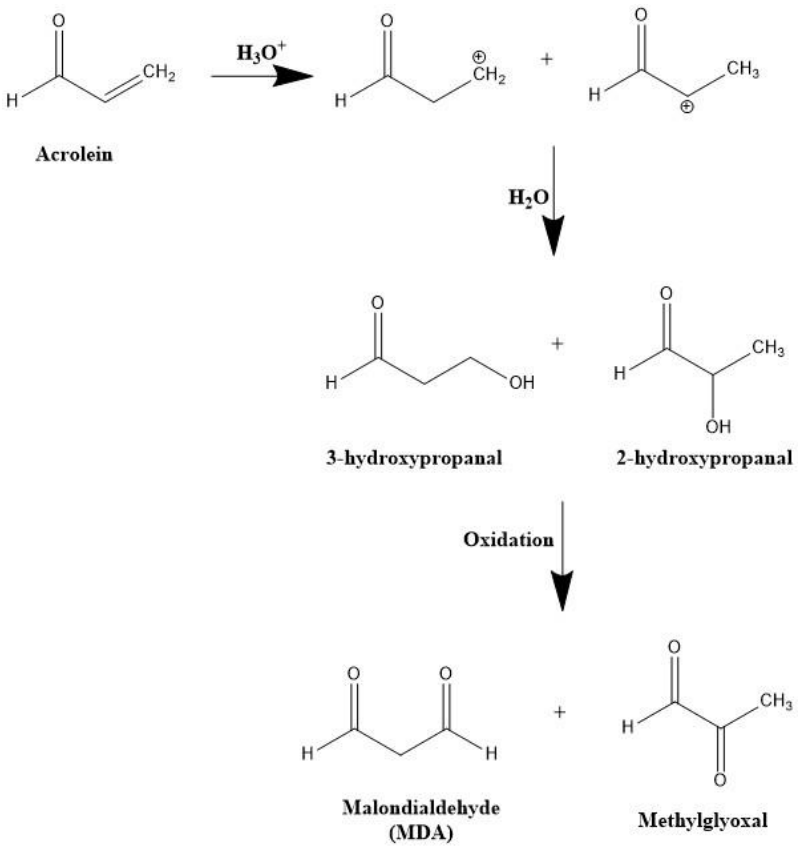

Figure 6.8. Proposed mechanism for conversion of acrolein to MDA under acidic, oxygenated conditions.

6.4 Potential Sources of Atmospheric MDA

Elucidating the source of MDA from these atmospheric aerosols is difficult due to the small amount of literature on this topic. A possible explanation for MDA in Fresno BBA and Urban LA $PM_{2.5}$ is secondary MDA formation due to photo-oxidation, ozonolysis or OH oxidation of organic precursors as described be Liu et al. (1999).[103, 104] However, these studies did not consider particle phase MDA and there is limited information on gas-particle partitioning of MDA. Although ambient MDA has not been previously quantified, the α-carbonyl isomer of MDA, methylglyoxal has been studied extensively and may provide insight on the physicochemical properties of atmospheric MDA. Gaseous methylglyoxal ranges between .03 –

0.9 ppb in urban air[241, 248] and is recognized as a potentially important contributor to secondary organic aerosol (SOA) formation.[70, 241, 253] Recent field measurements indicate that the Henry's Law constants and partitioning coefficients for methylglyoxal are up to five orders of magnitude higher than predicted theoretical values.[241] Since MDA and methylglyoxal have similar theoretical Henry's Law constants ($\sim 10^4$ M atm^{-1})[241, 242] and similar molecular structures, it is possible that they share similar gas-particle partitioning behavior. An important difference is that MDA forms an enol upon dissolution whereas glyoxal does not, potentially enhancing MDA partitioning into the aqueous phase. Since MDA has a pK_a of 4.7, dissolution is potentially inhibited under dilute acidic conditions relevant to cloud and fog droplets (pH 1-3). MDA complexation to Cu(II) and Ni(II) at the droplet surface may enhance MDA uptake,[242] but more experimental investigation with other abundant transition metals (Fe) is needed to confirm the atmospheric relevance of this process. Interestingly, MDA has a higher boiling point (108 ^{o}C) than methylglyoxal (72 ^{o}C), and thus may partition more readily than methylglyoxal due to a lower vapor pressure. We hypothesize that MDA undergoes gas-particle partitioning into the aqueous and organic phase of ambient aerosols. Particle phase MDA may be capable of undergoing hydration and oligomerization reactions similar to other small carbonyls,[241] potentially revealing a previously unrecognized contributor to SOA.

It is also possible that photochemical reactions within aerosol waters produce MDA as suggested by Beeby et al. (1987).[243] One can speculate that ROS generation from redox active transition metals and organic peroxides could also oxidize organics into MDA under dark conditions, but no literature on this chemistry specific to MDA exists. Polyunsaturated fatty acids are MDA precursors in biological systems, but they also have been identified in marine

aerosols.[254] Therefore, it may be possible to form MDA from oxidation of unsaturated fatty acids components in $PM_{2.5}$

While Fresno BBA are mixed with urban emissions, the biomass burning component may introduce an alternative mechanism for MDA formation. Biomass material is composed of a variety of polysaccharides such as cellulose, hemicellulose, lignin, and free sugars. It is well documented that the aqueous oxidation of 2-DR sugar produces MDA.[93, 102] Since oxidation of an individual sugar can lead to MDA formation, it may be possible that combustion of polysaccharides and free carbohydrates in biomass produces MDA. Such mechanisms of MDA formation are beyond the scope of this work, but merit further investigation.

7. Conclusions

Inhaled PM is associated with a wide array of adverse health effects in humans, but the biological mechanisms and PM components contributing to health effects are poorly defined.[7, 8] Inflammation initiated by an overproduction of ROS is thought to be a common step in the pathogenesis of PM induced diseases.[7, 8] OH radicals are thought to be most damaging ROS as they are capable of oxidizing lipids, proteins and DNA. It is hypothesized that PM components that produce ROS in the body contribute to the inhalation toxicity of PM. However, it is important to note that ROS generation from inhaled PM is not the only pathway for PM induced diseases. Many studies have highlighted the ability of inhaled PM components (HULIS) to alter iron homeostasis, suggesting that water soluble organic compound that chelate cellular iron contributes to PM toxicity.[195, 205, 216, 255] Furthermore, ambient PM is known to contain a variety of aldehyde compounds. The toxicity of aldehydes has been well documented and is thought to involve reactions with amino and nucleic acids.[256] Malondialdehyde is a toxic aldehyde that has mostly been studied in biological systems because it is a byproduct of lipid peroxidation.[98, 229-231, 235] There is some evidence that malondialdehyde exists in ambient particles, and given its toxicity, could contribute to overall particle toxicity. In this work we have elucidated mechanisms of HULIS-Fe mediated OH formation in representative lung lining fluids, spectroscopically characterized ambient HULIS and measured malondialdehyde in ambient PM for the first time.

Quantifying OH radicals from ambient PM and their components requires accurate measurement methods. OH radicals in aqueous solutions are difficult to measure directly due to low concentrations, short lifetimes and spectroscopic similarities to water. Terephthalate is a particularly sensitive probe for OH, with a detection limit as low as 2 nM.[111, 112] Terephthalate

reacts with OH to form a fluorescent product, 2-hydroxyterephthalic acid (hTA), with a moderate dependence on pH and temperature.[111, 112] However, there is disagreement in the literature on the yield of the fluorescent product (Y_{hTA}), which introduces a large uncertainty in the quantification of OH. Using a pH 3.5 dark ferrous Fenton system to generate OH radicals, we find that Y_{hTA} =31.5 ± 7%. This is about double the recent literature value measured by Charbouillot et al. (2011),[112] but in excellent agreement with earlier measurements by Matthews et al. (1980).[111] In chapter 3 and 4, we measured OH radicals in representative lung lining fluids with a pH ranging from 5.5 to 7.4. For these analyses, we used the data set from Matthews et al. (1980)[111] to calculate OH concentrations at varying pH.

Fe(II) is a key player in ROS formation in surrogate lung fluids (SLF) containing the antioxidants, Asc, GSH, UA and citrate. HULIS in particulate matter such as biomass burning aerosol chelate Fe(II), but the effect on ROS formation in the presence of lung antioxidants is not known. We used SRFA as a surrogate for HULIS and investigate its effect on OH formation from Fe(II) in SLF. For the first time, a chemical kinetics model was developed to explain behavior of Fe(II) and SRFA in SLF. Model and experimental results were used to find best-fit rate coefficients for key reactions. Modeling results indicate SRFA enhances Fe-mediated reduction of O_2 to O_2^- and destruction of H_2O_2 to OH to 5.1 ± 1.5 and (4.3 ± 1.4) × 10^3 M^{-1} s^{-1} respectively. Best-fit rates for Citrate–Fe(II) mediated O_2 to O_2^- and H_2O_2 to OH were 3.0 ± 0.7 and (4.2 ± 1.7) × 10^3 M^{-1} s^{-1} respectively. The kinetics model agrees with both the experimental results and thermodynamic model calculations of chemical speciation for 0 and 5 μg/mL SRFA, but both models were less successful at predicting further enhancements to OH formation at higher SRFA concentrations. These results suggest that SRFA, and thereby HULIS, are capable

of strongly chelating Fe species and produce a substantial amount of OH radicals under conditions relevant to the lung. This is consistent with previous studies that suggested HULIS generates OH in human lung tissues, contributing to iron accumulation, collagen deposition and inflammation.[87, 88]

SLF lacks the Fe binding lung proteins, Albumin (Alb) and Transferrin (Tf), which limits their physiological relevance. To approach more physiologically relevant conditions, we investigated OH generation from SRFA-Fe(II) in human BALF. Consistent with our results in SLF, we find that SRFA enhances OH generation from Fe(II) in BALF collected from 8 healthy patients. We found that Alb and Tf suppresses OH generation from SRFA-Fe(II) mixtures, suggesting an important role that is poorly characterized. Furthermore, it is well accepted that Alb chelates Fe(II) and suppresses ROS activity, yet there have been no measurements of Alb-Fe mediated OH generation. Interestingly, we found that albumin enhances OH generation from inorganic Fe(II) by a factor of 20 yet suppresses OH generation from SRFA-Fe(II) in pH 5.5 saline solutions containing physiological amounts of Asc. Using an approximation that assumes O_2 to O_2^- reduction is the rate limiting step for OH generation, we derived a kinetic equation and estimated the rate constant for Alb-Fe(II) and SRFA-Fe(II) mediated O_2 to O_2^- reduction. We find that Alb and SRFA enhanced the rate constant to Fe(II) mediated O_2 reduction to (1.8 ± 0.1) M^{-1} $s^{-1}$and (2.7 ± 0.3) M^{-1} s^{-1} respectively. The OH generation predicted by the kinetic approximation and estimated rate constants agree well with OH measurements from a combined system of Fe(II), Alb and SRFA.

We have spectroscopically characterized the fulvic acid fraction of HULIS from the water-soluble component of cigarette smoke condensate (Cig-WS) and wood smoke particles

(Wood-WS). Fluorescence spectra indicate that the fulvic acid fraction of HULIS from cigarette smoke condensate (Cig-FA) and wood smoke (Wood-FA) contain fluorophores bearing striking similarities to SRFA. However, Cig-FA and Wood-FA also contain lower wavelength fluorescence features than SRFA, indicating the presence of smaller molecules with less aromatic and conjugated character than SRFA.[72] FTIR spectra of HULIS derived from Cig-FA and Wood-FA show striking similarities to FTIR spectra of SRFA as observed by previous studies.[88] Consistent with previous characterization of HULIS, Cig-FA and Wood-FA FTIR spectra revealed organic nitro and organic nitrate compounds not observed in SRFA and exhibited higher aliphatic character.[71, 72] This indicates that isolated HULIS derived from cigarette smoke and wood smoke share chemical similarities and functionalities with SRFA. Like SRFA, Cig-FA and Wood-FA may be capable of strongly chelating Fe species, potentially contributing to physiological ROS generation and disruption of cellular Fe homeostasis.

We have applied the 2-thiobarbituric acid assay on $PM_{2.5}$ extracts to quantify malondialdehyde in atmospheric aerosols for the first time. We estimated of biomass burning and urban $PM_{2.5}$ contains 30.0 ng/m^3 – 75.3 ng/m^3 of malondialdehyde accounting for (1.37 ± 0.12) $\times 10^{-2}$ % of total PM mass. These concentrations of ambient malondialdehyde are comparable to reported concentrations of the related C_3 compounds methylglyoxal and malonic acid.[241, 248] Malondialdehyde in ambient PM may result from oxidation of aromatic VOCs,[103, 104] oxidation of lipids at the ocean surface[105] and combustion of polysaccharide structures in biomass. Since malondialdehyde is a highly toxic and mutagenic compound, it may contribute to the toxicity of ambient PM. Interestingly, malondialdehyde has been implicated in the development of some

PM related health effects such as atherosclerosis and cancer. The scant literature on the formation, prevalence and toxicity of atmospheric malondialdehyde merits further investigations.

8. Bibliography

1. Dockery, D. W.; Pope, C. A.; Xu, X.; Spengler, J. D.; Ware, J. H.; Fay, M. E.; Ferris Jr, B. G.; Speizer, F. E., An association between air pollution and mortality in six US cities. *New England journal of medicine* **1993,** *329*, (24), 1753-1759.

2. Laden, F.; Neas, L. M.; Dockery, D. W.; Schwartz, J., Association of fine particulate matter from different sources with daily mortality in six US cities. *Environmental health perspectives* **2000,** *108*, (10), 941.

3. Beelen, R.; Raaschou-Nielsen, O.; Stafoggia, M.; Andersen, Z. J.; Weinmayr, G.; Hoffmann, B.; Wolf, K.; Samoli, E.; Fischer, P.; Nieuwenhuijsen, M., Effects of long-term exposure to air pollution on natural-cause mortality: an analysis of 22 European cohorts within the multicentre ESCAPE project. *The Lancet* **2014,** *383*, (9919), 785-795.

4. Brook, R. D.; Rajagopalan, S.; Pope III, C. A.; Brook, J. R.; Bhatnagar, A.; Diez-Roux, A. V.; Holguin, F.; Hong, Y.; Luepker, R. V.; Mittleman, M. A., Particulate matter air pollution and cardiovascular disease: an update to the scientific statement from the American Heart Association. *Circulation* **2010,** *121*, (21), 2331-2378.

5. McConnell, R.; Islam, T.; Shankardass, K.; Jerrett, M.; Lurmann, F.; Gilliland, F.; Gauderman, J.; Avol, E.; Künzli, N.; Yao, L., Childhood incident asthma and traffic-related air pollution at home and school. *Environmental health perspectives* **2010,** *118*, (7), 1021-1026.

6. Thorne, P. S., Inhalation toxicology models of endotoxin-and bioaerosol-induced inflammation. *Toxicology* **2000,** *152*, (1-3), 13-23.

7. Imlay, J. A., Pathways of oxidative damage. *Annual Reviews in Microbiology* **2003,** *57*, (1), 395-418.

8. Dellinger, B.; Pryor, W. A.; Cueto, R.; Squadrito, G. L.; Hegde, V.; Deutsch, W. A., Role of free radicals in the toxicity of airborne fine particulate matter. *Chemical research in toxicology* **2001,** *14*, (10), 1371-1377.

9. Ghio, A. J.; Soukup, J. M.; Case, M.; Dailey, L. A.; Richards, J.; Berntsen, J.; Devlin, R. B.; Stone, S.; Rappold, A., Exposure to wood smoke particles produces inflammation in healthy volunteers. *Occup Environ Med* **2012,** *69*, (3), 170-175.

10. Danielsen, P. H.; Loft, S.; Jacobsen, N. R.; Jensen, K. A.; Autrup, H.; Ravanat, J.-L.; Wallin, H.; Møller, P., Oxidative stress, inflammation, and DNA damage in rats after intratracheal instillation or oral exposure to ambient air and wood smoke particulate matter. *Toxicological Sciences* **2010,** *118*, (2), 574-585.

11. Dockery, D. W., Health effects of particulate air pollution. *Annals of epidemiology* **2009,** *19*, (4), 257-263.

12. Krewski, D.; Burnett, R. T.; Goldberg, M. S.; Hoover, K.; Siemiatycki, J.; Abrahamowicz, M.; White, W. H., Validation of the Harvard Six Cities Study of particulate air pollution and mortality. *New England Journal of Medicine* **2004,** *350*, (2), 198-199.

13. EPA, U., National ambient air quality standards for particulate matter: Final rule. *Federal Register* **1997,** *62*, 38651-38760.

14. Thannickal, V. J.; Fanburg, B. L., Reactive oxygen species in cell signaling. *American Journal of Physiology-Lung Cellular and Molecular Physiology* **2000,** *279*, (6), L1005-L1028.

15. Ray, P. D.; Huang, B.-W.; Tsuji, Y., Reactive oxygen species (ROS) homeostasis and redox regulation in cellular signaling. *Cellular signalling* **2012,** *24*, (5), 981-990.

16. Jiang, F.; Zhang, Y.; Dusting, G. J., NADPH oxidase-mediated redox signaling: roles in cellular stress response, stress tolerance, and tissue repair. *Pharmacological reviews* **2011,** *63*, (1), 218-242.

17. Kennedy, T.; Ghio, A. J.; Reed, W.; Samet, J.; Zagorski, J.; Quay, J.; Carter, J.; Dailey, L.; Hoidal, J. R.; Devlin, R. B., Copper-dependent inflammation and nuclear factor-κ B activation by particulate air pollution. *American journal of respiratory cell and molecular biology* **1998,** *19*, (3), 366-378.

18. Li, N.; Xia, T.; Nel, A. E., The role of oxidative stress in ambient particulate matter-induced lung diseases and its implications in the toxicity of engineered nanoparticles. *Free radical biology and medicine* **2008,** *44*, (9), 1689-1699.

19. Halliwell, B.; Cross, C. E., Oxygen-derived species: their relation to human disease and environmental stress. *Environmental health perspectives* **1994,** *102*, (Suppl 10), 5.

20. Guo, Y.; Zhang, W.; Yan, Y.; Ma, C.; Wang, X.; Wang, C.; Zhao, J., Triterpenoid pristimerin induced HepG2 cells apoptosis through ROS-mediated mitochondrial dysfunction. *J BUON* **2013,** *18*, (2), 477-85.

21. Winterbourn, C. C., Hydroxyl radical production in body fluids Roles of metal ions, ascorbate and superoxide. *Biochemical Journal* **1981,** *198*, (1), 125-131.

22. Ayres, J. G.; Borm, P.; Cassee, F. R.; Castranova, V.; Donaldson, K.; Ghio, A.; Harrison, R. M.; Hider, R.; Kelly, F.; Kooter, I. M., Evaluating the toxicity of airborne particulate matter and nanoparticles by measuring oxidative stress potential—a workshop report and consensus statement. *Inhalation toxicology* **2008,** *20*, (1), 75-99.

23. Kuang, X. M.; Scott, J. A.; da Rocha, G. O.; Betha, R.; Price, D. J.; Russell, L. M.; Cocker, D. R.; Paulson, S. E., Hydroxyl radical formation and soluble trace metal content in

particulate matter from renewable diesel and ultra-low sulfur diesel in at-sea operations of a research vessel. *Aerosol Science and Technology* **2017**, 1-12.

24. Sun, G.; Crissman, K.; Norwood, J.; Richards, J.; Slade, R.; Hatch, G. E., Oxidative interactions of synthetic lung epithelial lining fluid with metal-containing particulate matter. *American Journal of Physiology-Lung Cellular and Molecular Physiology* **2001,** *281*, (4), L807-L815.

25. Charrier, J. G.; McFall, A. S.; Richards-Henderson, N. K.; Anastasio, C., Hydrogen peroxide formation in a surrogate lung fluid by transition metals and quinones present in particulate matter. *Environmental science & technology* **2014,** *48*, (12), 7010-7017.

26. Charrier, J. G.; Anastasio, C., Rates of Hydroxyl Radical Production from Transition Metals and Quinones in a Surrogate Lung Fluid. *Environmental science & technology* **2015,** *49*, (15), 9317-9325.

27. Gonzalez, D. H.; Cala, C. K.; Peng, Q. Y.; Paulson, S. E., HULIS Enhancement of Hydroxyl Radical Formation from Fe(II): Kinetics of Fulvic Acid-Fe(II) Complexes in the Presence of Lung Antioxidants. *Env. Sci. Tech.* **2017,** *51*, (13), 7676-7685.

28. Chen, R.; Pignatello, J. J., Role of quinone intermediates as electron shuttles in Fenton and photoassisted Fenton oxidations of aromatic compounds. *Environmental science & technology* **1997,** *31*, (8), 2399-2406.

29. Chung, M. Y.; Lazaro, R. A.; Lim, D.; Jackson, J.; Lyon, J.; Rendulic, D.; Hasson, A. S., Aerosol-borne quinones and reactive oxygen species generation by particulate matter extracts. *Environmental science & technology* **2006,** *40*, (16), 4880-4886.

30. Duesterberg, C. K.; Waite, T. D., Kinetic modeling of the oxidation of p-hydroxybenzoic acid by Fenton's reagent: implications of the role of quinones in the redox cycling of iron. *Environmental science & technology* **2007,** *41*, (11), 4103-4110.

31. Shang, Y.; Chen, C.; Li, Y.; Zhao, J.; Zhu, T., Hydroxyl radical generation mechanism during the redox cycling process of 1, 4-naphthoquinone. *Environmental science & technology* **2012,** *46*, (5), 2935-2942.

32. Charrier, J. G.; Anastasio, C., Impacts of antioxidants on hydroxyl radical production from individual and mixed transition metals in a surrogate lung fluid. *Atmospheric Environment* **2011,** *45*, (40), 7555-7562.

33. Godri, K. J.; Harrison, R. M.; Evans, T.; Baker, T.; Dunster, C.; Mudway, I. S.; Kelly, F. J., Increased oxidative burden associated with traffic component of ambient particulate matter at roadside and urban background schools sites in London. *PLoS One* **2011,** *6*, (7), e21961.

34. Gonzalez, D. H.; Cala, C. K.; Peng, Q.; Paulson, S. E., HULIS Enhancement of Hydroxyl Radical formation from Fe (II): Kinetics of Fulvic Acid-Fe (II) Complexes in the Presence of Lung Anti-Oxidants. *Environmental Science & Technology* **2017**.

35. Boisa, N.; Elom, N.; Dean, J. R.; Deary, M. E.; Bird, G.; Entwistle, J. A., Development and application of an inhalation bioaccessibility method (IBM) for lead in the PM 10 size fraction of soil. *Environment international* **2014,** *70*, 132-142.

36. Pelfrêne, A.; Cave, M. R.; Wragg, J.; Douay, F., In Vitro Investigations of Human Bioaccessibility from Reference Materials Using Simulated Lung Fluids. *International journal of environmental research and public health* **2017,** *14*, (2), 112.

37. Cross, C. E.; van der Vliet, A.; O'Neill, C. A.; Louie, S.; Halliwell, B., Oxidants, antioxidants, and respiratory tract lining fluids. *Environmental Health Perspectives* **1994,** *102,* (Suppl 10), 185.

38. Roche, M.; Rondeau, P.; Singh, N. R.; Tarnus, E.; Bourdon, E., The antioxidant properties of serum albumin. *FEBS letters* **2008,** *582*, (13), 1783-1787.

39. Pacht, E. R.; Davis, W. B., Role of transferrin and ceruloplasmin in antioxidant activity of lung epithelial lining fluid. *Journal of Applied Physiology* **1988,** *64*, (5), 2092-2099.

40. Zhou, Q.; Wang, L.; Cao, Z.; Zhou, X.; Yang, F.; Fu, P.; Wang, Z.; Hu, J.; Ding, L.; Jiang, W., Dispersion of atmospheric fine particulate matters in simulated lung fluid and their effects on model cell membranes. *Science of the Total Environment* **2016,** *542,* 36-43.

41. Bicer, E. M. Compositional characterisation of human respiratory tract lining fluids for the design of disease specific simulants. Doctoral Thesis 2014.

42. Fischer, H., Function of proton channels in lung epithelia. *Wiley Interdisciplinary Reviews: Membrane Transport and Signaling* **2012,** *1*, (3), 247-258.

43. Bodem, C. R.; Lampton, L. M.; Miller, D. P.; Tarka, E. F.; Everett, E. D., Endobronchial pH: Relevance to Aminoglycoside Activity in Gram-Negative Bacillary Pneumonia 1, 2. *American Review of Respiratory Disease* **1983,** *127*, (1), 39-41.

44. Vidrio, E.; Jung, H.; Anastasio, C., Generation of hydroxyl radicals from dissolved transition metals in surrogate lung fluid solutions. *Atmospheric Environment* **2008,** *42,* (18), 4369-4379.

45. Merkofer, M.; Kissner, R.; Hider, R. C.; Brunk, U. T.; Koppenol, W. H., Fenton chemistry and iron chelation under physiologically relevant conditions: electrochemistry and kinetics. *Chemical research in toxicology* **2006,** *19,* (10), 1263-1269.

46. Pham, A. N.; Waite, T. D., Modeling the kinetics of Fe (II) oxidation in the presence of citrate and salicylate in aqueous solutions at pH 6.0− 8.0 and 25 C. *The Journal of Physical Chemistry A* **2008,** *112*, (24), 5395-5405.

47. Strathmann, T., Redox reactivity of organically complexed iron (II) species with aquatic contaminants. *Aquatic redox chemistry* **2011,** *1071*, 283-313.

48. Santana-Casiano, J. M.; González-Dávila, M.; Millero, F. J., Oxidation of nanomolar levels of Fe (II) with oxygen in natural waters. *Environmental science & technology* **2005,** *39*, (7), 2073-2079.

49. Rizvi, M. A., Complexation modulated redox behavior of transition metal systems. *Russian Journal of General Chemistry* **2015,** *85*, (4), 959-973.

50. Engelmann, M. D.; Bobier, R. T.; Hiatt, T.; Cheng, I. F., Variability of the Fenton reaction characteristics of the EDTA, DTPA, and citrate complexes of iron. *Biometals* **2003,** *16*, (4), 519-527.

51. Vukosav, P.; Mlakar, M.; Tomišić, V., Revision of iron (III)–citrate speciation in aqueous solution. Voltammetric and spectrophotometric studies. *Anal. Chim. Acta* **2012,** *745*, 85-91.

52. Taverna, M.; Marie, A.-L.; Mira, J.-P.; Guidet, B., Specific antioxidant properties of human serum albumin. *Annals of intensive care* **2013,** *3*, (1), 4.

53. Quinlan, G. J.; Martin, G. S.; Evans, T. W., Albumin: biochemical properties and therapeutic potential. *Hepatology* **2005,** *41*, (6), 1211-1219.

54. Gutteridge, J. M.; Wilkins, S., Copper salt-dependent hydroxyl radical formation: damage to proteins acting as antioxidants. *Biochimica et Biophysica Acta (BBA)-General Subjects* **1983,** *759*, (1-2), 38-41.

55. Loban, A.; Kime, R.; Powers, H., Iron-binding antioxidant potential of plasma albumin. *Clinical science (London, England: 1979)* **1997,** *93*, (5), 445-451.

56. Aruoma, O. I.; Halliwell, B., Superoxide-dependent and ascorbate-dependent formation of hydroxyl radicals from hydrogen peroxide in the presence of iron. Are lactoferrin and transferrin promoters of hydroxyl-radical generation? *Biochemical Journal* **1987,** *241*, (1), 273-278.

57. Marx, G.; Chevion, M., Site-specific modification of albumin by free radicals. Reaction with copper (II) and ascorbate. *Biochemical Journal* **1986,** *236*, (2), 397-400.

58. Xu, X.; Zhang, L.; Shen, D.; Wu, H.; Liu, Q., Oxygen-dependent oxidation of Fe (II) to Fe (III) and interaction of Fe (III) with bovine serum albumin, leading to a hysteretic effect on the fluorescence of bovine serum albumin. *Journal of fluorescence* **2008,** *18*, (1), 193-201.

59. Princiotto, J. V.; Zapolski, E. J., Functional heterogeneity and pH-dependent dissociation properties of human transferrin. *Biochimica et Biophysica Acta (BBA)-General Subjects* **1976,** *428*, (3), 766-771.

60. Chung, M. C. M., Structure and function of transferrin. *Biochemical Education* **1984,** *12*, (4), 146-154.

61. Harris, D. C.; Rinehart, A. L.; Hereld, D.; Schwartz, R. W.; Burke, F. P.; Salvador, A. P., Reduction potential of iron in transferrin. *Biochimica et Biophysica Acta (BBA)-General Subjects* **1985,** *838*, (3), 295-301.

62. Dhungana, S.; Taboy, C. H.; Zak, O.; Larvie, M.; Crumbliss, A. L.; Aisen, P., Redox properties of human transferrin bound to its receptor. *Biochemistry* **2004,** *43*, (1), 205-209.

63. Brissot, P.; Ropert, M.; Le Lan, C.; Loréal, O., Non-transferrin bound iron: a key role in iron overload and iron toxicity. *Biochimica et Biophysica Acta (BBA)-General Subjects* **2012,** *1820*, (3), 403-410.

64. Aljwaid, H.; White, D. L.; Collard, K. J.; Moody, A. J.; Pinkney, J. H., Non-transferrin-bound iron is associated with biomarkers of oxidative stress, inflammation and endothelial dysfunction in type 2 diabetes. *Journal of Diabetes and its Complications* **2015,** *29*, (7), 943-949.

65. Patel, M.; Ramavataram, D., Non transferrin bound iron: nature, manifestations and analytical approaches for estimation. *Indian journal of clinical biochemistry* **2012,** *27*, (4), 322-332.

66. Mayol-Bracero, O.; Guyon, P.; Graham, B.; Roberts, G.; Andreae, M.; Decesari, S.; Facchini, M.; Fuzzi, S.; Artaxo, P., Water-soluble organic compounds in biomass burning aerosols over Amazonia 2. Apportionment of the chemical composition and importance of the polyacidic fraction. *Journal of Geophysical Research: Atmospheres (1984–2012)* **2002,** *107*, (D20), LBA 59-1-LBA 59-15.

67. Baduel, C.; Voisin, D.; Jaffrezo, J.-L., Comparison of analytical methods for Humic Like Substances (HULIS) measurements in atmospheric particles. *Atmospheric Chemistry and Physics* **2009,** *9*, (16), 5949-5962.

68. Lin, P.; Huang, X.-F.; He, L.-Y.; Yu, J. Z., Abundance and size distribution of HULIS in ambient aerosols at a rural site in South China. *Journal of Aerosol Science* **2010,** *41*, (1), 74-87.

69. Lin, P.; Engling, G.; Yu, J., Humic-like substances in fresh emissions of rice straw burning and in ambient aerosols in the Pearl River Delta Region, China. *Atmospheric Chemistry and Physics* **2010,** *10*, (14), 6487-6500.

70. Altieri, K.; Seitzinger, S.; Carlton, A.; Turpin, B.; Klein, G.; Marshall, A., Oligomers formed through in-cloud methylglyoxal reactions: Chemical composition, properties, and mechanisms investigated by ultra-high resolution FT-ICR mass spectrometry. *Atmospheric Environment* **2008,** *42*, (7), 1476-1490.

71. Graber, E.; Rudich, Y., Atmospheric HULIS: How humic-like are they? A comprehensive and critical review. *Atmospheric Chemistry and Physics* **2006,** *6*, (3), 729-753.

72. Win, M. S.; Tian, Z.; Zhao, H.; Xiao, K.; Peng, J.; Shang, Y.; Wu, M.; Xiu, G.; Lu, S.; Yonemochi, S., Atmospheric HULIS and its ability to mediate the reactive oxygen species (ROS): A review. *Journal of Environmental Sciences* **2018,** *71*, 13-31.

73. Simoneit, B. R., Eolian particulates from oceanic and rural areas—their lipids fulvic and humic acids and residual carbon. *Physics and Chemistry of the Earth* **1980,** *12*, 343-352.

74. Mukai, H.; Ambe, Y., Characterization of a humic acid-like brown substance in airborne particulate matter and tentative identification of its origin. *Atmospheric Environment (1967)* **1986,** *20*, (5), 813-819.

75. Havers, N.; Burba, P.; Lambert, J.; Klockow, D., Spectroscopic characterization of humic-like substances in airborne particulate matter. *Journal of Atmospheric Chemistry* **1998,** *29*, (1), 45-54.

76. Subbalakshmi, Y.; Patti, A.; Lee, G.; Hooper, M., Structural characterisation of macromolecularorganic material in air particulate matter using Py-GC-MS and solid state 13C-NMR. *Journal of Environmental Monitoring* **2000,** *2*, (6), 561-565.

77. Duarte, R. M.; Pio, C. A.; Duarte, A. C., Spectroscopic study of the water-soluble organic matter isolated from atmospheric aerosols collected under different atmospheric conditions. *Analytica Chimica Acta* **2005,** *530*, (1), 7-14.

78. Kristensen, T. B.; Du, L.; Nguyen, Q. T.; Nøjgaard, J.; Koch, C. B.; Nielsen, O. F.; Hallar, A.; Lowenthal, D.; Nekat, B.; Van Pinxteren, D., Chemical properties of HULIS from three different environments. *Journal of Atmospheric Chemistry* **2015,** *72*, (1), 65-80.

79. Krivacsy, Z.; Kiss, G.; Varga, B.; Galambos, I.; Sárvári, Z.; Gelencser, A.; Molnar, A.; Fuzzi, S.; Facchini, M.; Zappoli, S., Study of humic-like substances in fog and interstitial aerosol by size-exclusion chromatography and capillary electrophoresis. *Atmospheric Environment* **2000,** *34*, (25), 4273-4281.

80. Varga, B.; Kiss, G.; Ganszky, I.; Gelencsér, A.; Krivácsy, Z., Isolation of water-soluble organic matter from atmospheric aerosol. *Talanta* **2001,** *55*, (3), 561-572.

81. Kiss, G.; Varga, B.; Galambos, I.; Ganszky, I., Characterization of water-soluble organic matter isolated from atmospheric fine aerosol. *Journal of Geophysical Research: Atmospheres* **2002,** *107*, (D21), ICC 1-1-ICC 1-8.

82. Peuravuori, J.; Pihlaja, K.; Trubetskaya, O.; Trubetskoj, O., The effects of a strong disaggregating agent on SEC-PAGE of aquatic and soil humic matter. *International Journal of Environmental Analytical Chemistry* **2001,** *79*, (3), 217-228.

83. Decesari, S.; Facchini, M.; Matta, E.; Mircea, M.; Fuzzi, S.; Chughtai, A.; Smith, D., Water soluble organic compounds formed by oxidation of soot. *Atmospheric Environment* **2002,** *36*, (11), 1827-1832.

84. Kostić, I.; Anđelković, T.; Nikolić, R.; Bojić, A.; Purenović, M.; Blagojević, S.; Anđelković, D., Copper (II) and lead (II) complexation by humic acid and humic-like ligands. *J Serb Chem Soc* **2011,** *76*, (9), 1325-1336.

85. Lin, P.; Yu, J. Z., Generation of reactive oxygen species mediated by humic-like substances in atmospheric aerosols. *Environmental science & technology* **2011,** *45*, (24), 10362-10368.

86. Verma, V.; Rico-Martinez, R.; Kotra, N.; King, L.; Liu, J.; Snell, T. W.; Weber, R. J., Contribution of water-soluble and insoluble components and their hydrophobic/hydrophilic subfractions to the reactive oxygen species-generating potential of fine ambient aerosols. *Environmental science & technology* **2012,** *46*, (20), 11384-11392.

87. Ghio, A. J.; Quigley, D. R., Complexation of iron by humic-like substances in lung tissue: role in coal workers' pneumoconiosis. *American Journal of Physiology-Lung Cellular and Molecular Physiology* **1994,** *267*, (2), L173-L179.

88. Ghio, A. J.; Stonehuerner, J.; Quigley, D. R., Humic-like substances in cigarette smoke condensate and lung tissue of smokers. *American Journal of Physiology-Lung Cellular and Molecular Physiology* **1994,** *266*, (4), L382-L388.

89. Miller, C. J.; Rose, A. L.; Waite, T. D., Hydroxyl radical production by H2O2-mediated oxidation of Fe (II) complexed by Suwannee River fulvic acid under circumneutral freshwater conditions. *Environmental science & technology* **2012,** *47*, (2), 829-835.

90. Fujii, M.; Rose, A. L.; Waite, T. D.; Omura, T., Oxygen and superoxide-mediated redox kinetics of iron complexed by humic substances in coastal seawater. *Environmental science & technology* **2010,** *44*, (24), 9337-9342.

91. Lee, Y. P.; Fujii, M.; Kikuchi, T.; Terao, K.; Yoshimura, C., Variation of iron redox kinetics and its relation with molecular composition of standard humic substances at circumneutral pH. *PloS one* **2017,** *12*, (4), e0176484.

92. Buege, J. A.; Aust, S. D., [30] Microsomal lipid peroxidation. In *Methods Enzymol.*, Elsevier: 1978; Vol. 52, pp 302-310.

93. Halliwell, B.; Gutteridge, J., Formation of a thiobarbituric-acid-reactive substance from deoxyribose in the presence of iron salts. *FEBS Lett.* **1981,** *128*, (2), 347-352.

94. Zeb, A.; Ullah, F., A simple spectrophotometric method for the determination of thiobarbituric acid reactive substances in fried fast foods. *Journal of analytical methods in chemistry* **2016,** *2016*.

95. Agarwal, A.; Majzoub, A., Laboratory tests for oxidative stress. *Indian journal of urology: IJU: journal of the Urological Society of India* **2017,** *33*, (3), 199.

96. Hodges, D. M.; DeLong, J. M.; Forney, C. F.; Prange, R. K., Improving the thiobarbituric acid-reactive-substances assay for estimating lipid peroxidation in plant tissues containing anthocyanin and other interfering compounds. *Planta* **1999,** *207*, (4), 604-611.

97. Lovell, M. A.; Ehmann, W. D.; Butler, S. M.; Markesbery, W. R., Elevated thiobarbituric acid-reactive substances and antioxidant enzyme activity in the brain in Alzheimer's disease. *Neurology* **1995,** *45*, (8), 1594-1601.

98. Moselhy, H. F.; Reid, R. G.; Yousef, S.; Boyle, S. P., A specific, accurate, and sensitive measure of total plasma malondialdehyde by HPLC. *Journal of lipid research* **2013,** *54*, (3), 852-858.

99. Domijan, A. M.; Ralić, J.; Radić Brkanac, S.; Rumora, L.; Žanić-Grubišić, T., Quantification of malondialdehyde by HPLC-FL–application to various biological samples. *Biomedical Chromatography* **2015,** *29*, (1), 41-46.

100. Lapenna, D.; Ciofani, G.; Pierdomenico, S. D.; Giamberardino, M. A.; Cuccurullo, F., Reaction conditions affecting the relationship between thiobarbituric acid reactivity and lipid peroxidesin human plasma. *Free Radical Biology and Medicine* **2001,** *31*, (3), 331-335.

101. Genaro-Mattos, T. C.; Dalvi, L. T.; Oliveira, R. G.; Ginani, J. S.; Hermes-Lima, M., Reevaluation of the 2-deoxyribose assay for determination of free radical formation. *Biochimica et Biophysica Acta (BBA)-General Subjects* **2009,** *1790*, (12), 1636-1642.

102. Gutteridge, J.; Halliwell, B., The deoxyribose assay: an assay both for'free'hydroxyl radical and for site-specific hydroxyl radical production. *Biochemical Journal* **1988,** *253*, (3), 932.

103. Liu, X.; Jeffries, H. E.; Sexton, K. G., Atmospheric photochemical degradation of 1, 4-unsaturated dicarbonyls. *Environmental science & technology* **1999,** *33*, (23), 4212-4220.

104. Liu, X.; Jeffries, H. E.; Sexton, K. G., Hydroxyl radical and ozone initiated photochemical reactions of 1, 3-butadiene. *Atmospheric Environment* **1999,** *33*, (18), 3005-3022.

105. Zhou, S.; Gonzalez, L.; Leithead, A.; Finewax, Z.; Thalman, R.; Vlasenko, A.; Vagle, S.; Miller, L.; Li, S.-M.; Bureekul, S., Formation of gas-phase carbonyls from heterogeneous oxidation of polyunsaturated fatty acids at the air–water interface and of the sea surface microlayer. *Atmospheric Chemistry and Physics* **2014,** *14*, (3), 1371-1384.

106. Charrier, J.; Anastasio, C., On dithiothreitol (DTT) as a measure of oxidative potential for ambient particles: evidence for the importance of soluble transition metals. *Atmospheric chemistry and physics (Print)* **2012,** *12*, (5), 11317.

107. Cho, A. K.; Sioutas, C.; Miguel, A. H.; Kumagai, Y.; Schmitz, D. A.; Singh, M.; Eiguren-Fernandez, A.; Froines, J. R., Redox activity of airborne particulate matter at different sites in the Los Angeles Basin. *Environmental Research* **2005,** *99*, (1), 40-47.

108. Yu, H.; Wei, J.; Cheng, Y.; Subedi, K.; Verma, V., Synergistic and antagonistic interactions among the particulate matter components in generating reactive oxygen species based on the dithiothreitol assay. *Environmental science & technology* **2018,** *52*, (4), 2261-2270.

109. Paulson, S. E.; Anastasio, C.; Hasson, A., Probing the Intrinsic Ability of Particles to Generate Reactive Oxygen Species and the Effect of Physiologically Relevant Solutes. *https://www.arb.ca.gov/research/apr/past/10-314-1.pdf. California ARB.* **2016**.

110. Rota, C.; Chignell, C. F.; Mason, R. P., Evidence for free radical formation during the oxidation of 2′-7′-dichlorofluorescin to the fluorescent dye 2′-7′-dichlorofluorescein by horseradish peroxidase:: Possible implications for oxidative stress measurements. *Free Radical Biology and Medicine* **1999,** *27*, (7-8), 873-881.

111. Matthews, R. W., The Radiation Chemistry of the Terephthalate Dosimeter. *Radiation Research* **1980,** *83*, (1), 27-41.

112. Charbouillot, T.; Brigante, M.; Mailhot, G.; Maddigapu, P. R.; Minero, C.; Vione, D., Performance and selectivity of the terephthalic acid probe for (OH)-O-center dot as a function of temperature, pH and composition of atmospherically relevant aqueous media. *J. Photochem. Photobiol. a-Chem.* **2011,** *222*, (1), 70-76.

113. Shrivastava, M. K.; Lane, T. E.; Donahue, N. M.; Pandis, S. N.; Robinson, A. L., Effects of gas particle partitioning and aging of primary emissions on urban and regional organic aerosol concentrations. *J. Geophys. Res.-Atmos.* **2008,** *113*, (D18), 16.

114. Shilling, J. E.; King, S. M.; Mochida, M.; Martin, S. T., Mass spectral evidence that small changes in composition caused by oxidative aging processes alter aerosol CCN properties. *J. Phys. Chem. A* **2007,** *111*, (17), 3358-3368.

115. Suda, S. R.; Petters, M. D.; Yeh, G. K.; Strollo, C.; Matsunaga, A.; Faulhaber, A.; Ziemann, P. J.; Prenni, A. J.; Carrico, C. M.; Sullivan, R. C.; Kreidenweis, S. M., Influence of Functional Groups on Organic Aerosol Cloud Condensation Nucleus Activity. *Env. Sci. Tech.* **2014,** *48*, (17), 10182-10190.

116. Kim, H.; Paulson, S. E., Real refractive indices and volatility of secondary organic aerosol generated from photooxidation and ozonolysis of limonene, alpha-pinene and toluene. *Atmos. Chem. Phys.,* **2013,** *13*, (15), 7711-7723.

117. Goldstone, J. V.; Pullin, M. J.; Bertilsson, S.; Voelker, B. M., Reactions of hydroxyl radical with humic substances: Bleaching, mineralization, and production of bioavailable carbon substrates. *Env. Sci. Tech.* **2002,** *36*, (3), 364-372.

118. Lindsey, M. E.; Tarr, M. A., Inhibition of hydroxyl radical reaction with aromatics by dissolved natural organic matter. *Env. Sci. Tech.* **2000,** *34*, (3), 444-449.

119. Rosenfeldt, E. J.; Linden, K. G., Degradation of endocrine disrupting chemicals bisphenol A, ethinyl estradiol, and estradiol during UV photolysis and advanced oxidation processes. *Env. Sci. Tech.* **2004,** *38*, (20), 5476-5483.

120. Lesser, M. P., Oxidative stress in marine environments: Biochemistry and physiological ecology. In *Annu. Rev. Physiol.*, Annual Reviews: Palo Alto, 2006; Vol. 68, pp 253-278.

121. Fernandez-Castro, P.; Vallejo, M.; San Roman, M. F.; Ortiz, I., Insight on the fundamentals of advanced oxidation processes. Role and review of the determination methods of reactive oxygen species. *J. Chem. Tech. Biotech.* **2015,** *90*, (5), 796-820.

122. Brook, R. D.; Rajagopalan, S.; Pope, C. A.; Brook, J. R.; Bhatnagar, A.; Diez-Roux, A. V.; Holguin, F.; Hong, Y.; Luepker, R. V.; Mittleman, M. A.; Peters, A.; Siscovick, D.; Smith, S. C.; Whitsel, L.; Kaufman, J. D., Particulate Matter Air Pollution and Cardiovascular Disease. *An*

Update to the Scientific Statement From the American Heart Association **2010,** *121*, (21), 2331-2378.

123. Beelen, R.; Raaschou-Nielsen, O.; Stafoggia, M.; Andersen, Z. J.; Weinmayr, G.; Hoffmann, B.; Wolf, K.; Samoli, E.; Fischer, P.; Nieuwenhuijsen, M.; Vineis, P.; Xun, W. W.; Katsouyanni, K.; Dimakopoulou, K.; Oudin, A.; Forsberg, B.; Modig, L.; Havulinna, A. S.; Lanki, T.; Turunen, A.; Oftedal, B.; Nystad, W.; Nafstad, P.; De Faire, U.; Pedersen, N. L.; Östenson, C.-G.; Fratiglioni, L.; Penell, J.; Korek, M.; Pershagen, G.; Eriksen, K. T.; Overvad, K.; Ellermann, T.; Eeftens, M.; Peeters, P. H.; Meliefste, K.; Wang, M.; Bueno-de-Mesquita, B.; Sugiri, D.; Krämer, U.; Heinrich, J.; de Hoogh, K.; Key, T.; Peters, A.; Hampel, R.; Concin, H.; Nagel, G.; Ineichen, A.; Schaffner, E.; Probst-Hensch, N.; Künzli, N.; Schindler, C.; Schikowski, T.; Adam, M.; Phuleria, H.; Vilier, A.; Clavel-Chapelon, F.; Declercq, C.; Grioni, S.; Krogh, V.; Tsai, M.-Y.; Ricceri, F.; Sacerdote, C.; Galassi, C.; Migliore, E.; Ranzi, A.; Cesaroni, G.; Badaloni, C.; Forastiere, F.; Tamayo, I.; Amiano, P.; Dorronsoro, M.; Katsoulis, M.; Trichopoulou, A.; Brunekreef, B.; Hoek, G., Effects of long-term exposure to air pollution on natural-cause mortality: an analysis of 22 European cohorts within the multicentre ESCAPE project. *Lancet* **2014,** *383*, (9919), 785-795.

124. Bates, J. T.; Weber, R. J.; Abrams, J.; Verma, V.; Fang, T.; Klein, M.; Strickland, M. J.; Sarnat, S. E.; Chang, H. H.; Mulholland, J. A.; Tolbert, P. E.; Russell, A. G., Reactive Oxygen Species Generation Linked to Sources of Atmospheric Particulate Matter and Cardiorespiratory Effects. *Env. Sci. Tech.* **2015,** *49*, (22), 13605-13612.

125. Faust, B. C.; Allen, J. M., Aqueous-phase photochemical formation of hydroxyl radical in authentic cloudwaters and fogwaters. *Env. Sci. Tech.* **1993,** *27*, (6), 1221-1224.

126. Zepp, R. G.; Faust, B. C.; Hoigne, J., Hydroxyl radical formation in aqueous reactions (pH 3-8) of iron (II) with hydrogen peroxide: the photo-Fenton reaction. *Env. Sci. Tech.* **1992,** *26*, (2), 313-319.

127. Jung, H.; Guo, B.; Anastasio, C.; Kennedy, I. M., Quantitative measurements of the generation of hydroxyl radicals by soot particles in a surrogate lung fluid. *Atmos. Environ.* **2006,** *40*, (6), 1043-1052.

128. Matthews, R. W., The radiation-chemistry of the terephthalate dosimeter. *Radiation Res.* **1980,** *83*, (1), 27-41.

129. Page, S. E.; Arnold, W. A.; McNeill, K., Terephthalate as a probe for photochemically generated hydroxyl radical. *J. Environ. Monitor.* **2010,** *12*, (9), 1658-1665.

130. Saran, M.; Summer, K. H., Assaying for hydroxyl radicals: Hydroxylated terephthalate is a superior fluorescence marker than hydroxylated benzoate. *Free Radical Res.* **1999,** *31*, (5), 429-436.

131. Snyrychova, I.; Kos, P.; Hideg, E., First application of terephthalate as a fluorescent probe for hydroxyl radicals in thylakoid membranes. *Photosynthesis Res.* **2007,** *91*, (2-3), 307-307.

132. Fang, X. W.; Mark, G.; vonSonntag, C., OH radical formation by ultrasound in aqueous solutions .1. The chemistry underlying the terephthalate dosimeter. *Ultrasonics Sonochem.* **1996,** *3*, (1), 57-63.

133. Shi, T. M.; Schins, R. P. F.; Knaapen, A. M.; Kuhlbusch, T.; Pitz, M.; Heinrich, J.; Borm, P. J. A., Hydroxyl radical generation by electron paramagnetic resonance as a new method to monitor ambient particulate matter composition. *J. Env. Monitor.* **2003,** *5*, (4), 550-556.

134. Armstrong, W. A.; Facey, R. A.; Grant, D. W.; Humphreys, W. G., A tissue-equivalent chemical dosimeter sensitive to 1 rad. *Can. J. Chem.* **1963,** *41*, (6), 1575-1577.

135. Shen, H.; Anastasio, C., A comparison of hydroxyl radical and hydrogen peroxide generation in ambient particle extracts and laboratory metal solutions. *Atmos. Environ.* **2012,** *46*, 665-668.

136. Son, Y.; Mishin, V.; Welsh, W.; Lu, S.-E.; Laskin, J.; Kipen, H.; Meng, Q., A Novel High-Throughput Approach to Measure Hydroxyl Radicals Induced by Airborne Particulate Matter. *Int. J. Env. Res. Public Health* **2015,** *12*, (11), 13678.

137. Freinbichler, W.; Colivicchi, M. A.; Fattori, M.; Ballini, C.; Tipton, K. F.; Linert, W.; Della Corte, L., Validation of a robust and sensitive method for detecting hydroxyl radical formation together with evoked neurotransmitter release in brain microdialysis. *J. Neurochem.* **2008,** *105*, (3), 738-749.

138. Linxiang, L.; Abe, Y.; Nagasawa, Y.; Kudo, R.; Usui, N.; Imai, K.; Mashino, T.; Mochizuki, M.; Miyata, N., An HPLC assay of hydroxyl radicals by the hydroxylation reaction of terephthalic acid. *Biomed. Chromatogr.* **2004,** *18*, (7), 470-474.

139. Charbouillot, T.; Brigante, M.; Mailhot, G.; Maddigapu, P. R.; Minero, C.; Vione, D., Performance and selectivity of the terephthalic acid probe for (OH)-O-center dot as a function of temperature, pH and composition of atmospherically relevant aqueous media. *J. Photochem. Photobio* **2011,** *222*, (1), 70-76.

140. Saran, M.; Summer, K. H., Assaying for hydroxyl radicals: Hydroxylated terephthalate is a superior fluorescence marker than hydroxylated benzoate. *Free Radical Res.* **1999,** *31*, (5), 429-436.

141. Page, S. E.; Arnold, W. A.; McNeill, K., Terephthalate as a probe for photochemically generated hydroxyl radical. *J. Environ. Monit.* **2010,** *12*, (9), 1658-1665.

142. Mark, G.; Tauber, A.; Laupert, R.; Schuchmann, H.-P.; Schulz, D.; Mues, A.; von Sonntag, C., OH-radical formation by ultrasound in aqueous solution – Part II: Terephthalate and Fricke dosimetry and the influence of various conditions on the sonolytic yield. *Ultrason. Sonochem.* **1998,** *5*, (2), 41-52.

143. Batista, A. P. S.; Teixeira, A. C. S. C.; Cooper, W. J.; Cottrell, B. A., Correlating the chemical and spectroscopic characteristics of natural organic matter with the photodegradation of sulfamerazine. *Water Res.* **2016,** *93*, (Supplement C), 20-29.

144. An, J.; Li, G.; An, T.; Nie, X., Indirect photochemical transformations of acyclovir and penciclovir in aquatic environments increase ecological risk. *Env. Tox. Chem.* **2016,** *35*, (3), 584-592.

145. Tafer, R.; Sleiman, M.; Boulkamh, A.; Richard, C., Photomineralization of aqueous salicylic acids. Photoproducts characterization and formation of light induced secondary OH precursors (LIS-OH). *Water Res.* **2016,** *106*, 496-506.

146. Huang, W.; Brigante, M.; Wu, F.; Hanna, K.; Mailhot, G., Effect of ethylenediamine-N,N′-disuccinic acid on Fenton and photo-Fenton processes using goethite as an iron source: optimization of parameters for bisphenol A degradation. *Envir. Sci. Poll. Res.* **2013,** *20*, (1), 39-50.

147. Paušová, Š.; Krýsa, J.; Jirkovský, J.; Forano, C.; Mailhot, G.; Prevot, V., Insight into the photocatalytic activity of ZnCr–CO3 LDH and derived mixed oxides. *Applied Catalysis B: Environmental* **2015,** *170-171*, (Supplement C), 25-33.

148. Li, R.; Zhao, C.; Yao, B.; Li, D.; Yan, S.; O'Shea, K. E.; Song, W., Photochemical Transformation of Aminoglycoside Antibiotics in Simulated Natural Waters. *Env. Sci. Tech.* **2016,** *50*, (6), 2921-2930.

149. Page, S. E.; Sander, M.; Arnold, W. A.; McNeill, K., Hydroxyl Radical Formation upon Oxidation of Reduced Humic Acids by Oxygen in the Dark. *Env. Sci. Tech.* **2012,** *46*, (3), 1590-1597.

150. Falconer, R.; Falconer, P., Determination of cloud water acidity at a mountain observatory in the Adirondack Mountains of New York State. *Journal of Geophysical Research: Oceans* **1980,** *85*, (C12), 7465-7470.

151. Stookey, L. L., Ferrozine---a new spectrophotometric reagent for iron. *Anal. Chem.* **1970,** *42*, (7), 779-781.

152. Arellanes, C.; Paulson, S. E.; Fine, P. M.; Sioutas, C., Exceeding of Henry's Law by Hydrogen Peroxide Associated with Urban Aerosols. . *Envir. Sci. Tech.* **2006,** *40* (16), 4859-4866.

153. De Laat, J.; Le, T. G., Kinetics and modeling of the Fe (III)/H2O2 system in the presence of sulfate in acidic aqueous solutions. *Environmental science & technology* **2005,** *39*, (6), 1811-1818.

154. Walling, C.; Goosen, A., Mechanism of the ferric ion catalyzed decomposition of hydrogen peroxide. Effect of organic substrates. *J. Am. Chem. Soc.* **1973,** *95*, (9), 2987-2991.

155. Klöpffer, W.; Kohl, E.-G., Bimolecular OH rate constants of organic compounds in solution: 1. Measurements in water using hydrogen peroxide as an OH source. *Ecotoxicology and environmental safety* **1991,** *22*, (1), 67-78.

156. Pham, A. N.; Waite, T. D., Oxygenation of Fe (II) in natural waters revisited: Kinetic modeling approaches, rate constant estimation and the importance of various reaction pathways. *Geochimica et Cosmochimica Acta* **2008,** *72*, (15), 3616-3630.

157. Bielski, B. H.; Cabelli, D. E.; Arudi, R. L.; Ross, A. B., Reactivity of HO2/O− 2 radicals in aqueous solution. *Journal of Physical and Chemical Reference Data* **1985,** *14*, (4), 1041-1100.

158. De Laat, J.; Le, T. G., Kinetics and modeling of the Fe (III)/H2O2 system in the presence of sulfate in acidic aqueous solutions. *Env. Sci. Tech.* **2005,** *39*, (6), 1811-1818.

159. Zuo, Y.; Hoigne, J., Formation of hydrogen peroxide and depletion of oxalic acid in atmospheric water by photolysis of iron (III)-oxalato complexes. *Env. Sci. Tech.* **1992,** *26*, (5), 1014-1022.

160. Halliwell, B.; Whiteman, M., Measuring reactive species and oxidative damage in vivo and in cell culture: how should you do it and what do the results mean? *British journal of pharmacology* **2004,** *142*, (2), 231-255.

161. Lund, L. G.; Aust, A. E., Iron mobilization from crocidolite asbestos greatly enhances crocidolite-dependent formation of DNA single-strand breaks in øX174 RFI DNA. *Carcinogenesis* **1992,** *13*, (4), 637-642.

162. Smith, K. R.; Aust, A. E., Mobilization of iron from urban particulates leads to generation of reactive oxygen species in vitro and induction of ferritin synthesis in human lung epithelial cells. *Chemical research in toxicology* **1997,** *10*, (7), 828-834.

163. Paglione, M.; Kiendler-Scharr, A.; Mensah, A.; Finessi, E.; Giulianelli, L.; Sandrini, S.; Facchini, M.; Fuzzi, S.; Schlag, P.; Piazzalunga, A., Identification of humic-like substances (HULIS) in oxygenated organic aerosols using NMR and AMS factor analyses and liquid chromatographic techniques. *Atmos. Chem. Phys* **2014,** *14*, 25-45.

164. Paciolla, M.; Kolla, S.; Jansen, S., The reduction of dissolved iron species by humic acid and subsequent production of reactive oxygen species. *Advances in environmental research* **2002,** *7*, (1), 169-178.

165. Voelker, B. M.; Sulzberger, B., Effects of fulvic acid on Fe (II) oxidation by hydrogen peroxide. *Environmental Science & Technology* **1996,** *30*, (4), 1106-1114.

166. Dou, J.; Lin, P.; Kuang, B.-y.; Yu, J. Z., Reactive Oxygen Species production mediated by Humic-like substances in Atmospheric Aerosols: Enhancement effects by pyridine, imidazole and their derivatives. *Environmental science & technology* **2015,** *49*, (11), 6457-6465.

167. Kinniburgh, D. G.; Milne, C. J.; Benedetti, M. F.; Pinheiro, J. P.; Filius, J.; Koopal, L. K.; Van Riemsdijk, W. H., Metal ion binding by humic acid: application of the NICA-Donnan model. *Environmental Science & Technology* **1996,** *30*, (5), 1687-1698.

168. Milne, C. J.; Kinniburgh, D. G.; Tipping, E., Generic NICA-Donnan model parameters for proton binding by humic substances. *Environmental Science & Technology* **2001,** *35*, (10), 2049-2059.

169. Kuang, X. M.; Gonzalez , D. H.; de la Rocha, G. O.; Scott, J. A.; Cala, C. K.; Paulson, S. E., The Terephthalate probe for Hydroxyl Radicals: Yield of 2-Hydroxy Terephthalate and Separation from Complex Organics in Environmental Samples. *Submitted* **2017**.

170. Frank, N.; Rice, J.; Tikvart, J., Optical Measurements Of CSN and FRM Teflon Filters To Estimate Elemental Carbon To Support Health Studies, PM2. 5 NAAQS Implementation And Climate. **2010**.

171. Jimenez, J.; Claiborn, C.; Larson, T.; Gould, T.; Kirchstetter, T. W.; Gundel, L., Loading effect correction for real-time aethalometer measurements of fresh diesel soot. *Journal of the Air & Waste Management Association* **2007,** *57*, (7), 868-873.

172. Majestic, B. J.; Schauer, J. J.; Shafer, M. M.; Turner, J. R.; Fine, P. M.; Singh, M.; Sioutas, C., Development of a wet-chemical method for the speciation of iron in atmospheric aerosols. *Environmental science & technology* **2006,** *40*, (7), 2346-2351.

173. Zepp, R. G.; Faust, B. C.; Hoigne, J., Hydroxyl radical formation in aqueous reactions (pH 3-8) of iron (II) with hydrogen peroxide: the photo-Fenton reaction. *Environmental Science & Technology* **1992,** *26*, (2), 313-319.

174. Li, Y.; Bachas, L. G.; Bhattacharyya, D., Selected chloro-organic detoxifications by polychelate (poly (acrylic acid)) and citrate-based Fenton reaction at neutral pH environment. *Industrial & Engineering Chemistry Research* **2007,** *46*, (24), 7984-7992.

175. Rush, J.; Maskos, Z.; Koppenol, W., Reactions of iron (II) nucleotide complexes with hydrogen peroxide. *FEBS letters* **1990,** *261*, (1), 121-123.

176. Lewis, S.; Lynch, A.; Bachas, L.; Hampson, S.; Ormsbee, L.; Bhattacharyya, D., Chelate-modified Fenton reaction for the degradation of trichloroethylene in aqueous and two-phase systems. *Environmental engineering science* **2009,** *26*, (4), 849-859.

177. Buettner, G. R.; Schafer, F. Q., Ascorbate (Vitamin C), its Antioxidant Chemistry.

178. Christensen, H.; Sehested, K.; Corfitzen, H., Reactions of hydroxyl radicals with hydrogen peroxide at ambient and elevated temperatures. *The Journal of Physical Chemistry* **1982,** *86*, (9), 1588-1590.

179. Jayson, G.; Parsons, B.; Swallow, A. J., Some simple, highly reactive, inorganic chlorine derivatives in aqueous solution. Their formation using pulses of radiation and their role in the mechanism of the Fricke dosimeter. *Journal of the Chemical Society, Faraday Transactions 1: Physical Chemistry in Condensed Phases* **1973,** *69*, 1597-1607.

180. Monod, A.; Poulain, L.; Grubert, S.; Voisin, D.; Wortham, H., Kinetics of OH-initiated oxidation of oxygenated organic compounds in the aqueous phase: new rate constants, structure–activity relationships and atmospheric implications. *Atmospheric Environment* **2005,** *39*, (40), 7667-7688.

181. Lindsey, M. E.; Tarr, M. A., Inhibition of hydroxyl radical reaction with aromatics by dissolved natural organic matter. *Environmental science & technology* **2000,** *34*, (3), 444-449.

182. Miller, C. J.; Rose, A. L.; Waite, T. D., Phthalhydrazide chemiluminescence method for determination of hydroxyl radical production: modifications and adaptations for use in natural systems. *Analytical chemistry* **2010,** *83*, (1), 261-268.

183. Mao, J.; Fan, S.; Jacob, D. J.; Travis, K. R., Radical loss in the atmosphere from Cu-Fe redox coupling in aerosols. *Atmos. Chem. Phys.* **2013,** *13*, (2), 509-519.

184. El-Ayaan, U.; Linert, W., A kinetic study of the reaction between glutathione and iron (III) in the pH range from 1 to 3. *Journal of Coordination Chemistry* **2002,** *55*, (11), 1309-1314.

185. Hamed, M. Y.; Silver, J., Studies on the reactions of ferric iron with glutathione and some related thiols. Part II. Complex formation in the pH range three to seven. *Inorganica Chimica Acta* **1983,** *80*, 115-122.

186. Rose, A. L.; Waite, T. D., Kinetic Model for Fe(II) Oxidation in Seawater in the Absence and Presence of Natural Organic Matter. *Environmental Science & Technology* **2002,** *36*, (3), 433-444.

187. Miller, C. J.; Vincent Lee, S. M.; Rose, A. L.; Waite, T. D., Impact of natural organic matter on H2O2-mediated oxidation of Fe (II) in coastal seawaters. *Environmental science & technology* **2012,** *46*, (20), 11078-11085.

188. Rose, A. L.; Waite, T. D., Effect of dissolved natural organic matter on the kinetics of ferrous iron oxygenation in seawater. *Environmental science & technology* **2003,** *37*, (21), 4877-4886.

189. Miller, C. J.; Rose, A. L.; Waite, T. D., Impact of natural organic matter on H 2 O 2-mediated oxidation of Fe (II) in a simulated freshwater system. *Geochimica et cosmochimica Acta* **2009,** *73*, (10), 2758-2768.

190. Wang, Y.; Arellanes, C.; Curtis, D.; Paulson, S. E., Probing the Source of Hydrogen Peroxide Generation by Coarse Mode Aerosols in Southern California. *Env. Sci. Tech.* **2010,** *44*, 4070-4075.

191. Pope III, C.; Muhlestein, J. B.; May, H. T.; Renlund, D. G.; Anderson, J. L.; Horne, B. D., Ischemic heart disease events triggered by short-term exposure to fine particulate air pollution. *Circulation* **2006,** *114*, (23), 2443-2448.

192. Halliwell, B.; Gutteridge, J. M., *Free radicals in biology and medicine*. Oxford University Press, USA: 2015.

193. Kumar, A.; Terakosolphan, W.; Hassoun, M.; Vandera, K.-K.; Novicky, A.; Harvey, R.; Royall, P. G.; Bicer, E. M.; Eriksson, J.; Edwards, K., A Biocompatible Synthetic Lung Fluid Based on Human Respiratory Tract Lining Fluid Composition. *Pharm. Res.* **2017,** *34*, (12), 2454-2465.

194. Vidrio, E.; Phuah, C. H.; Dillner, A. M.; Anastasio, C., Generation of hydroxyl radicals from ambient fine particles in a surrogate lung fluid solution. *Environmental science & technology* **2009,** *43*, (3), 922-927.

195. Ghio, A. J.; Soukup, J. M.; Dailey, L. A., Air pollution particles and iron homeostasis. *Biochimica et Biophysica Acta (BBA)-General Subjects* **2016,** *1860*, (12), 2816-2825.

196. Welch, K. D.; Davis, T. Z.; Van Eden, M. E.; Aust, S. D., Deleterious iron-mediated oxidation of biomolecules. *Free Radical Biol. Med.* **2002,** *32*, (7), 577-583.

197. Outten, F. W.; Theil, E. C., Iron-based redox switches in biology. *Antioxidants & redox signaling* **2009,** *11*, (5), 1029-1046.

198. Duff Jr, M. R.; Kumar, C. V., The metallomics approach: use of Fe (II) and Cu (II) footprinting to examine metal binding sites on serum albumins. *Metallomics* **2009,** *1*, (6), 518-523.

199. Abdizadeh, H.; Atilgan, A. R.; Atilgan, C., Mechanisms by which salt concentration moderates the dynamics of human serum transferrin. *The Journal of Physical Chemistry B* **2017,** *121*, (18), 4778-4789.

200. Williams, J.; Moreton, K., The distribution of iron between the metal-binding sites of transferrin human serum. *Biochemical Journal* **1980,** *185*, (2), 483-488.

201. Mujika, J.; Escribano, B.; Akhmatskaya, E.; Ugalde, J.; Lopez, X., Molecular dynamics simulations of iron-and aluminum-loaded serum transferrin: protonation of Tyr188 is necessary to prompt metal release. *Biochemistry* **2012,** *51*, (35), 7017-7027.

202. Turcot, I.; Stintzi, A.; Xu, J.; Raymond, K. N., Fast biological iron chelators: kinetics of iron removal from human diferric transferrin by multidentate hydroxypyridonates. *JBIC Journal of Biological Inorganic Chemistry* **2000,** *5*, (5), 634-641.

203. Grootveld, M.; Bell, J. D.; Halliwell, B.; Aruoma, O.; Bomford, A.; Sadler, P. J., Non-transferrin-bound iron in plasma or serum from patients with idiopathic hemochromatosis. Characterization by high performance liquid chromatography and nuclear magnetic resonance spectroscopy. *Journal of Biological Chemistry* **1989,** *264*, (8), 4417-4422.

204. Wei, J.; Yu, H.; Wang, Y.; Verma, V., Complexation of Iron and Copper in Ambient Particulate Matter and Its Effect on the Oxidative Potential Measured in a Surrogate Lung Fluid. *Environmental science & technology* **2018,** *53*, (3), 1661-1671.

205. Ghio, A. J.; Madden, M. C., Human lung injury following exposure to humic substances and humic-like substances. *Environmental Geochemistry and Health* **2017**, 1-11.

206. KUANG, X. M. Formation of Reactive Oxygen Species by Ambient Particulate Matter: Probing causative agents and the underlying mechanism. UCLA, 2017.

207. Silva, A. M.; Hider, R. C., Influence of non-enzymatic post-translation modifications on the ability of human serum albumin to bind iron: implications for non-transferrin-bound iron speciation. *Biochimica et Biophysica Acta (BBA)-Proteins and Proteomics* **2009,** *1794*, (10), 1449-1458.

208. Gonzalez, D. H.; Kuang, X. M.; Scott, J. A.; Rocha, G. O.; Paulson, S. E., Terephthalate Probe for Hydroxyl Radicals: Yield of 2-Hydroxyterephthalic Acid and Transition Metal Interference. *Anal. Lett.* **2018**, 1-10.

209. Jones, A. M.; Griffin, P. J.; Collins, R. N.; Waite, T. D., Ferrous iron oxidation under acidic conditions–The effect of ferric oxide surfaces. *Geochimica et Cosmochimica Acta* **2014,** *145*, 1-12.

210. Zhang, Y.; Zhou, M., A critical review of the application of chelating agents to enable Fenton and Fenton-like reactions at high pH values. *Journal of hazardous materials* **2019,** *362*, 436-450.

211. Jones, A. M.; Griffin, P. J.; Waite, T. D., Ferrous iron oxidation by molecular oxygen under acidic conditions: the effect of citrate, EDTA and fulvic acid. *Geochimica et Cosmochimica Acta* **2015,** *160*, 117-131.

212. Jacobson, M.; Hansson, H. C.; Noone, K.; Charlson, R., Organic atmospheric aerosols: Review and state of the science. *Reviews of Geophysics* **2000,** *38*, (2), 267-294.

213. Dinar, E.; Mentel, T.; Rudich, Y., The density of humic acids and humic like substances (HULIS) from fresh and aged wood burning and pollution aerosol particles. *Atmospheric Chemistry and Physics* **2006,** *6*, (12), 5213-5224.

214. Forrister, H.; Liu, J.; Scheuer, E.; Dibb, J.; Ziemba, L.; Thornhill, K. L.; Anderson, B.; Diskin, G.; Perring, A. E.; Schwarz, J. P., Evolution of brown carbon in wildfire plumes. *Geophysical Research Letters* **2015,** *42*, (11), 4623-4630.

215. Hoffer, A.; Gelencsér, A.; Guyon, P.; Kiss, G.; Schmid, O.; Frank, G.; Artaxo, P.; Andreae, M., Optical properties of humic-like substances (HULIS) in biomass-burning aerosols. *Atmospheric Chemistry and Physics* **2006,** *6*, (11), 3563-3570.

216. Ghio, A. J.; Soukup, J. M.; Dailey, L. A.; Tong, H.; Kesic, M. J.; Budinger, G. S.; Mutlu, G. k. M., Wood smoke particle sequesters cell iron to impact a biological effect. *Chemical research in toxicology* **2015,** *28*, (11), 2104-2111.

217. Ghio, A. J.; Stonehuerner, J.; Pritchard, R. J.; Piantadosi, C. A.; Quigley, D. R.; Dreher, K. L.; Costa, D. L., Humic-like substances in air pollution particulates correlate with concentrations of transition metals and oxidant generation. *Inhalation toxicology* **1996,** *8*, (5), 479-494.

218. Erdogan, S.; Baysal, A.; Akba, O.; Hamamci, C., Interaction of Metals with Humic Acid Isolated from Oxidized Coal. *Polish Journal of Environmental Studies* **2007,** *16*, (5).

219. Yang, R.; van den Berg, C. M., Metal complexation by humic substances in seawater. *Environmental science & technology* **2009,** *43*, (19), 7192-7197.

220. Yamamoto, M.; Nishida, A.; Otsuka, K.; Komai, T.; Fukushima, M., Evaluation of the binding of iron (II) to humic substances derived from a compost sample by a colorimetric method using ferrozine. *Bioresource technology* **2010,** *101*, (12), 4456-4460.

221. Town, R. M.; Duval, J. r. m. F.; Buffle, J.; van Leeuwen, H. P., Chemodynamics of metal complexation by natural soft colloids: Cu (II) binding by humic acid. *The Journal of Physical Chemistry A* **2012,** *116*, (25), 6489-6496.

222. Leenheer, J. A.; Croué, J.-P., Peer reviewed: characterizing aquatic dissolved organic matter. In ACS Publications: 2003.

223. Salma, I.; Ocskay, R.; Chi, X.; Maenhaut, W., Sampling artefacts, concentration and chemical composition of fine water-soluble organic carbon and humic-like substances in a continental urban atmospheric environment. *Atmospheric Environment* **2007,** *41*, (19), 4106-4118.

224. Elmenhorst, H., A completely automatic smoking machine for the preparation of a large quantity of cigarette smoke condensate. *Beier. Tabakforschung* **1966,** *3*, 545-553.

225. Birch, M.; Cary, R., Elemental carbon-based method for monitoring occupational exposures to particulate diesel exhaust. *Aerosol Science and Technology* **1996,** *25*, (3), 221-241.

226. Andersen, C. M.; Bro, R., Practical aspects of PARAFAC modeling of fluorescence excitation-emission data. *Journal of Chemometrics: A Journal of the Chemometrics Society* **2003,** *17*, (4), 200-215.

227. Garnes, L. A.; Allen, D. T., Size distributions of organonitrates in ambient aerosol collected in Houston, Texas. *Aerosol Science & Technology* **2002,** *36*, (10), 983-992.

228. Chen, Q.; Ikemori, F.; Higo, H.; Asakawa, D.; Mochida, M., Chemical structural characteristics of HULIS and other fractionated organic matter in urban aerosols: results from

mass spectral and FT-IR analysis. *Environmental science & technology* **2016,** *50*, (4), 1721-1730.

229. Del Rio, D.; Stewart, A. J.; Pellegrini, N., A review of recent studies on malondialdehyde as toxic molecule and biological marker of oxidative stress. *Nutrition, metabolism and cardiovascular diseases* **2005,** *15*, (4), 316-328.

230. Basu, A. K.; Marnett, L. J., Unequivocal demonstration that malondialdehyde is a mutagen. *Carcinogenesis* **1983,** *4*, (3), 331-333.

231. Niedernhofer, L. J.; Daniels, J. S.; Rouzer, C. A.; Greene, R. E.; Marnett, L. J., Malondialdehyde, a product of lipid peroxidation, is mutagenic in human cells. *J. Biol. Chem.* **2003,** *278*, (33), 31426-31433.

232. VanderVeen, L. A.; Hashim, M. F.; Shyr, Y.; Marnett, L. J., Induction of frameshift and base pair substitution mutations by the major DNA adduct of the endogenous carcinogen malondialdehyde. *Proceedings of the National Academy of Sciences* **2003,** *100*, (24), 14247-14252.

233. Marnett, L. J., Lipid peroxidation—DNA damage by malondialdehyde. *Mutation Research/Fundamental and Molecular Mechanisms of Mutagenesis* **1999,** *424*, (1-2), 83-95.

234. Ma, B.; Villalta, P. W.; Balbo, S.; Stepanov, I., Analysis of a malondialdehyde–deoxyguanosine adduct in human leukocyte DNA by liquid chromatography nanoelectrospray–high-resolution tandem mass spectrometry. *Chemical research in toxicology* **2014,** *27*, (10), 1829-1836.

235. Fink, S. P.; Reddy, G. R.; Marnett, L. J., Mutagenicity in Escherichia coli of the major DNA adduct derived from the endogenous mutagen malondialdehyde. *Proceedings of the National Academy of Sciences* **1997,** *94*, (16), 8652-8657.

236. Voitkun, V.; Zhitkovich, A., Analysis of DNA–protein crosslinking activity of malondialdehyde in vitro. *Mutation Research/Fundamental and Molecular Mechanisms of Mutagenesis* **1999,** *424*, (1-2), 97-106.

237. Uchida, K., Role of reactive aldehyde in cardiovascular diseases. *Free Radical Biology and Medicine* **2000,** *28*, (12), 1685-1696.

238. Palinski, W.; Ord, V. A.; Plump, A. S.; Breslow, J. L.; Steinberg, D.; Witztum, J. L., ApoE-deficient mice are a model of lipoprotein oxidation in atherogenesis. Demonstration of oxidation-specific epitopes in lesions and high titers of autoantibodies to malondialdehyde-lysine in serum. *Arteriosclerosis and thrombosis: a journal of vascular biology* **1994,** *14*, (4), 605-616.

239. Slatter, D.; Bolton, C.; Bailey, A., The importance of lipid-derived malondialdehyde in diabetes mellitus. *Diabetologia* **2000,** *43*, (5), 550-557.

240. Destaillats, H.; Spaulding, R. S.; Charles, M. J., Ambient air measurement of acrolein and other carbonyls at the Oakland-San Francisco Bay Bridge toll plaza. *Environmental science & technology* **2002,** *36*, (10), 2227-2235.

241. Shen, H.; Chen, Z.; Li, H.; Qian, X.; Qin, X.; Shi, W., Gas-Particle Partitioning of Carbonyl Compounds in the Ambient Atmosphere. *Environmental science & technology* **2018,** *52*, (19), 10997-11006.

242. Okochi, H.; Brimblecombe, P., Potential trace metal–organic complexation in the atmosphere. *The Scientific World Journal* **2002,** *2,* 767-786.

243. Beeby, A.; Mohammed, D. b. H.; Sodeau, J. R., Photochemistry and photophysics of glycolaldehyde in solution. *Journal of the American Chemical Society* **1987,** *109*, (3), 857-861.

244. Guillén-Sans, R.; Vicario, I.; Guzmán-Chozas, M., Further studies and observations on 2-thiobarbituric acid assay (fat autoxidtion) and 2-thiobarbituric acid-aldehyde reactions. *Food/Nahrung* **1997,** *41*, (3), 162-166.

245. Fukunaga, K.; Takama, K.; Suzuki, T., High-performance liquid chromatographic determination of plasma malondialdehyde level without a solvent extraction procedure. *Analytical biochemistry* **1995,** *230*, (1), 20-23.

246. Ho, K.; Huang, R.-J.; Kawamura, K.; Tachibana, E.; Lee, S.; Ho, S.; Zhu, T.; Tian, L., Dicarboxylic acids, ketocarboxylic acids, α-dicarbonyls, fatty acids and benzoic acid in PM 2.5 aerosol collected during CAREBeijing-2007: an effect of traffic restriction on air quality. *Atmospheric Chemistry and Physics* **2015,** *15*, (6), 3111-3123.

247. Ho, K.; Lee, S.; Ho, S. S. H.; Kawamura, K.; Tachibana, E.; Cheng, Y.; Zhu, T., Dicarboxylic acids, ketocarboxylic acids, α-dicarbonyls, fatty acids, and benzoic acid in urban aerosols collected during the 2006 Campaign of Air Quality Research in Beijing (CAREBeijing-2006). *Journal of geophysical research: atmospheres* **2010,** *115*, (D19).

248. Kawamura, K.; Okuzawa, K.; Aggarwal, S.; Irie, H.; Kanaya, Y.; Wang, Z., Determination of gaseous and particulate carbonyls (glycolaldehyde, hydroxyacetone, glyoxal, methylglyoxal, nonanal and decanal) in the atmosphere at Mt. Tai. *Atmospheric Chemistry and Physics* **2013,** *13*, (10), 5369-5380.

249. He, N.; Kawamura, K.; Okuzawa, K.; Pochanart, P.; Liu, Y.; Kanaya, Y.; Wang, Z., Diurnal and temporal variations of water-soluble dicarboxylic acids and related compounds in aerosols from the northern vicinity of Beijing: Implication for photochemical aging during atmospheric transport. *Science of the Total Environment* **2014,** *499*, 154-165.

250. Campadelli, F.; Tosi, C.; Santoro, E.; Roberti, L., Spectroscopic investigation on the acrolein hydration. *Spectroscopy letters* **1983,** *16*, (8), 601-611.

251. Pressman, D.; Lucas, H., Hydration of Unsaturated Compounds. XI. Acrolein and Acrylic Acid1. *Journal of the American Chemical Society* **1942,** *64*, (8), 1953-1957.

252. Melicherčík, M.; Treindl, Ľ., Kinetics and mechanism of the oxidation of acrolein, crotonaldehyde, and methacrolein with cerium (IV) sulfate. *Chemical Papers* **1981,** *35*, (2), 153-163.

253. Fu, T. M.; Jacob, D. J.; Wittrock, F.; Burrows, J. P.; Vrekoussis, M.; Henze, D. K., Global budgets of atmospheric glyoxal and methylglyoxal, and implications for formation of secondary organic aerosols. *Journal of geophysical research: atmospheres* **2008,** *113*, (D15).

254. Mochida, M.; Kitamori, Y.; Kawamura, K.; Nojiri, Y.; Suzuki, K., Fatty acids in the marine atmosphere: Factors governing their concentrations and evaluation of organic films on sea-salt particles. *Journal of Geophysical Research: Atmospheres* **2002,** *107*, (D17), AAC 1-1-AAC 1-10.

255. Ghio, A. J.; Tong, H.; Soukup, J. M.; Dailey, L. A.; Cheng, W.-Y.; Samet, J. M.; Kesic, M. J.; Bromberg, P. A.; Turi, J. L.; Upadhyay, D., Sequestration of mitochondrial iron by silica particle initiates a biological effect. *American Journal of Physiology-Lung Cellular and Molecular Physiology* **2013,** *305*, (10), L712-L724.

256. LoPachin, R. M.; Gavin, T., Molecular mechanisms of aldehyde toxicity: a chemical perspective. *Chemical research in toxicology* **2014,** *27*, (7), 1081-1091.